uOttawa

L'Université canadienne
Canada's university

FACULTÉ DES ÉTUDES SUPÉRIEURES ET POSTOCTORALES

uOttawa

L'Université canadienne
Canada's university

FACULTY OF GRADUATE AND POSDOCTORAL STUDIES

Danny G. Hill

AUTEUR DE LA THÈSE / AUTHOR OF THESIS

M.Sc. (Biochemistry)

GRADE / DEGREE

Department of Biochemistry, Microbiology and Immunology

FACULTÉ, ÉCOLE, DÉPARTEMENT / FACULTY, SCHOOL, DEPARTMENT

Transmembrane Domain Orientation and Neurotransmitter Binding in the Nicotinic Acetylcholine Receptor

TITRE DE LA THÈSE / TITLE OF THESIS

John Baenziger

DIRECTEUR (DIRECTRICE) DE LA THÈSE / THESIS SUPERVISOR

CO-DIRECTEUR (CO-DIRECTRICE) DE LA THÈSE / THESIS CO-SUPERVISOR

EXAMINATEURS (EXAMINATRICES) DE LA THÈSE / THESIS EXAMINERS

Natalie Goto

Mary Hefford

Gary W. Slater

LE DOYEN DE LA FACULTÉ DES ÉTUDES SUPÉRIEURES ET POSTDOCTORALES /
DEAN OF THE FACULTY OF GRADUATE AND POSTDOCORAL STUDIES

TRANSMEMBRANE DOMAIN ORIENTATION AND NEUROTRANSMITTER BINDING IN THE NICOTINIC ACETYLCHOLINE RECEPTOR

Danny G. Hill

Thesis submitted to the Department of Biochemistry in partial fulfillment of the requirements for the degree of Master of Science

University of Ottawa
Ottawa, Ontario, Canada
May, 2005

Your file Votre référence
ISBN: 0-494-11291-3
Our file Notre référence
ISBN: 0-494-11291-3

To my wife Veronique Hill, my parents, Linda and David Hill, for supporting and encouraging me in all my pursuits, and reminding me to enjoy the small pleasures in life.

ABSTRACT

The orientation of the hydrogen-deuterium exchange resistant "core" of the of the intact nicotinic acetylcholine receptor from *Torpedo* was studied using linear dichroism attenuated total reflectance infrared spectroscopy both in the presence and absence of the agonist Carb. Our results show that the hydrogen exchange resistant α-helical peptide hydrogens in the nAChR are preferentially oriented parallel to the bilayer normal, therefore, providing evidence for a predominantly α-helical transmembrane domain, and that there are no detectable net changes in orientation upon agonist-induced desensitization. We also examined the linear dichroism of lipid bands in spectra recorded from membranes both with and without the nAChR in order to accurately assess the effects of membrane film mosaic spread on the interpretation of the linear dichroism data. Our data also show that the mosaic spread of the reconstituted membrane films is greater than the mosaic spread observed with pure lipid films. Our work illustrates the importance of mosaic spread characterization when interpreting experimental order parameters in terms of molecular structure orientation.

The physical interactions that occur between the nicotinic acetylcholine receptor from Torpedo and the agonists carbamylcholine and tetramethylamine have been studied using both conventional infrared difference spectroscopy and a novel double-ligand difference technique. The latter was developed to isolate vibrational bands from residues in a membrane receptor that interact with individual functional groups on a small molecule ligand. The binding of either agonist leads to an increase in vibrational intensity at frequencies centered near 1663, 1655, 1547, 1430, and 1059 cm^{-1} indicating that both induce a conformational change from the resting to the desensitized state. Vibrational shifts near 1580, 1516, 1455, 1334, and between 1300 and 1400 cm^{-1} are assigned to

structural perturbations of tyrosine and possibly both tryptophan and charged carboxylic acid residues upon the formation of receptor-quaternary amine interactions, with the relatively intense feature near 1516 cm^{-1} indicating a key role for tyrosine. Other vibrational bands suggest the involvement of additional side chains in agonist binding. Two side-chain vibrational shifts from 1668 and 1605 cm^{-1} to 1690 and 1620 cm^{-1}, respectively, could reflect the formation of a hydrogen bond between the ester carbonyl of carbamylcholine and an arginine residue. The results demonstrate the potential of the double-ligand difference technique for dissecting the chemistry of membrane receptor-ligand interactions and provide new insight into the nature of nicotinic receptor-agonist interactions.

ACKNOWLEDGMENTS

At this point I would like to express my sincere gratitude to some of the many people who have assisted and befriended me over the course of my studies.

* I would like to thank Corrie daCosta for his assistance with the figures, for taking time to review my thesis drafts, for his patience with my endless litany of questions in the lab, for all his helpful discussions, and for sharing his enthusiasm for science with me.

* I would like to thank my wife for encouraging and enduring me.

* I would like to express my gratitude to Lisa Belivaqua. I will always remember and value your friendship and kindness.

* I would like to thank Dan Kaiser, Bridget Thompson, Anna Jasinska, and Nadine Levine for assisting me with the more banal laboratory duties, and for ensuring I was never in need of nAChR.

* I would like to thank my past and present labmates who have made my sojourn here more enjoyable: Dr. Andrei Ogrel, Marlene McKay, Emile Chartrand, Ming Yu, Sarah Medaglia, Mike Goodried, Ian Wagg, Dave Houtman, Michel Sturgeon, Ngoc Vuongand Prateek Khatri.

PREFACE

The work presented in this thesis has either been previously published or will be submitted for publication as described below:

CHAPTER 3

Hill, D.G., and Baenziger, J.E. Orientation of the Transmembrane α-Helices of the Nicotinic Acetylcholine Receptor. Manuscript in preparation.

CHAPTER 4

Ryan, S.E., Hill, D.G., and Baenziger, J.E. Dissecting the Chemistry of the Nicotinic Acetylcholine Receptor. J. Biol. Chem. 277(12), 10420-10426.

TABLE OF CONTENTS

LIST OF FIGURES AND TABLES

CHAPTER 1

CHAPTER 2

CHAPTER 3

CHAPTER 4

GENERAL CONCLUSIONS

LIST OF ABBREVIATIONS

A	Absorbance
A_w	Absorbance at wavenumber ω
$A_{\|\|}$	Absorption of parallel polarized light
$A\perp$	Absorption of perpendicular polarized light
$\mathring{A}$	Angstrom
ACh	Acetylcholine
AChBP	Acetylcholine Binding Protein
ATR	Attenuated total reflectance
BAC	Bromoacetylcholine chloride
c	Velocity of light
Ca^{2+}	Calcium ion
$CaCl_2$	Calcium chloride
Carb	Carbamylcholine
Chol	Cholesterol
Cl^-	Chlorine ion
$C{=}O$	Carbonyl group
C	Cysteine
χ	Angle of incidence
Cys	Cysteine
⊕-π	Cation-pi electron
d	Depth
D	Aspartate
Da	Dalton
$D \rightarrow D$	Desensitized to desensitized
DDF	p-(N,N-Dimethyl)aminobenzenediazonium
DGTS	Deuterated triglycine sulfate
d_p	Penetration depth
DTT	Dithiothreitol

dTC	d-turbocurarine
$\Delta E_{0\rightarrow 1}$	Energy difference between vibrational levels 0 and 1
$EC50$	Effective concentration at 50% efficacy
$EDTA$	Ethylenediaminetetraacetic acid
$EGTA$	Ethylene Glycol-bis(β-aminoethyl ether)- N,N,N′,N′-Tetraacetic acid
E_x	Electric field vector along the x axis
E_y	Electric field vector along the y axis
E_z	Electric field vector along the z axis
E_v	Vibrational level energy
E_w	Energy of a wave
ε_ω	Molar absorption coefficient
F	Phenylalanine
F_o	Force constant
f	Frequency
f_v	Vibrational frequency
f_w	Frequency of a wave
$FTIR$	Fourier transform infrared
$^3H\text{-}ACh$	Tritiated acetylcholine
$H\text{-}^2H$	Hydrogen-Deuterium
h	Planck's constant
^2H_2O	Deuterium oxide
I	Intensity
I_o	Initial intensity
IR	Infrared radiation
IRE	Internal reflection element
K^+	Potassium ion
KCl	Potassium chloride
kDa	KiloDalton

L	Length
l	Sample thickness
λ	Wavelength
M	Molarity
m	Mass
M_c	Molar concentration
$MgCl_2$	Magnesium chloride
M_{red}	Reduced mass
N	Number of atoms in a molecule
n	Quantum number
n_1	Refractive index of a dense medium
n_2	Refractive index of a rarer medium
n_3	Refractive index of a biological sample
Na^+	Sodium ion
nAChR	Nicotinic acetylcholine receptor
NaCl	Sodium Chloride
$NaHCO_3$	Sodium bicarbonate
NaH_2PO_4	Sodium dihydrogen phosphate
Na_2HPO_4	Disodium phosphate
NaN_3	Sodium azide
NMR	Nuclear magnetic resonance
N_r	Number of internal reflections
P	Probability
POPC	1-Palmitoyl-2-Oleoyl-*sn*-Glycero-3-Phosphocholine
POPA	1-Palmitoyl-2-Oleoyl-*sn*-Glycero-3-Phosphate
PMSF	Phenylmethylsulphonyl fluoride
ϕ	Polar angle along the xz plane
Q	Magnitude of charge
R_{ATR}	Measured Dichroic Ratio

R	Arginine
r	Distance between two charges
$R \rightarrow D$	Resting to desensitized
rpm	Rotations per minute
S	Order parameter
S_{acyl}	Order parameter for lipid acyl chains
S_{Exp}	Experimentally determined order parameter
$S_{Bilayer}$	Order parameter for the mosaic spread
S_{MA}	Order parameter for a molecular axis
S_{motion}	Order parameter for lipid acyl chain motion
S_{SS}	Order parameter for a protein secondary structure
S_{tilt}	Order parameter for lipid acyl chain tilting relative to membrane surface normal
S_{TDM}	Order parameter for a transition dipole moment
SCAM	Substituted cysteine accessibility method
θ	Average angle between the molecular axis/transition dipole moment and the z axis in the xy plane
θ_o	Angle between the molecuar axis and the z axis in the xy plane
TID	3-Trifluoromethyl-3-(*m*-[^{125}I]iodophenyl)diazirine
TID-BE	3-Trifluoromethyl-3-(*m*-[^{125}I]iodophenyl)diazirine benzoate ester
T_m	Phase transition temperature
TMA	Tetramethylammonium
Tris	Tris(hydroxymethyl)aminomethane
Γ	Angle between the electric field and the transition dipole moment
W	Tryptophan
Y	Tyrosine
μ	Dipole moment
v	Velocity
cm^{-1}	Wavenumber

ω	Wavenumber
z	Distance from interface
ψ	Angle of refraction
ψ_c	Critical angle

General Introduction

The human brain is the ultimate product of biological evolution. Its intricate network of neurons rapidly acquire, integrate and transmit information, providing the biological basis for perception, learning, memory, and behaviour. To understand how the brain functions requires intimate knowledge of how information is conveyed both within and between neurons, and how changes in the efficiency of these processes influence human behaviour.

Considerable research into brain function has focussed on identifying and characterizing the molecular agents that facilitate intra and inter neuronal communication. The neurotransmitter-gated ion channels, located at specialized junctions between neurons, called synapses, are of particular interest as they mediate rapid inter-neuronal communication by converting the chemical signals that are released from the surface of one neuron into electrical signals at another. Since the activity of these receptors can be modulated by various endogenous factors, including phosphorylation and membrane lipid composition, it is believed that these proteins perform an essential role in higher brain functions such as thought, memory and learning. An understanding of neurotransmitter-gated ion channel structure and function is believed to have important implications for our understanding of the brain.

The research described in this thesis is centred on one neurotransmitter-gated ion channel, the nicotinic acetylcholine receptor (nAChR) from *Torpedo*. Since Claude Bernard investigated the action of a Central American arrow poison (curare), the nicotinic acetylcholine receptors have been the objects of attention (1). The 'nicotinic receptive substance' in the neuromuscular junction was the first receptor to be recognized and named, the first to be studied electrophysiologically, and the first to be characterized biochemically (1).

The aim of this work has been to employ the Fourier transform infrared (FTIR) spectroscopy to examine the structural and orientational changes in the receptor and the nature of the physical interactions that form between the nAChR and the neurotransmitter analog carbamylcholine (Carb) as it undergoes the resting to desensitized conformational change. It is hoped that this information would lead to a greater understanding of how neurotransmitter binding elicits both channel activation and receptor desensitization and how conformational change in the receptor is achieved.

CHAPTER 1
THE NICOTINIC ACETYLCHOLINE RECEPTOR

CYS-LOOP RECEPTORS

Nicotinic acetylcholine receptors belong to a superfamily of ligand-gated ion channels, know as the Cys-loop receptors. Members of this family mediate the transfer of information throughout the central and peripheral nervous systems as well as at neuromuscular junctions; they comprise both the major excitatory, cation-conducting, receptors, such as the neuronal nAChRs, the neuromuscular nAChRs, the serotonin receptors and the major inhibitory, anion-conducting, neuronal receptors, such as the γ-aminobutyric acid and the glycine receptors. The nAChR from Torpedo is the best characterized member of this superfamily of genetically and structurally related neurotransmitter-gated ion channels.

nAChRs are large, integral membrane glycoproteins (~290 kDa) composed of five homologous subunits. There are five classes of muscle-type nAChR subunits: α1, β1, γ, ϵ and δ. In electrocytes, muscle-like cells from the electric organs of sting rays, and fetal muscle, the nAChR composition is $\alpha 1_2\beta 1\gamma\delta$, whereas in adult muscle, the composition is $\alpha 1_2\beta 1\epsilon\delta$ (2, 3). Neuronal-type nAChR subunits are designated α or β. To date there are 12 known types of vertebrate neuronal nAChR subunits: α2-α10 and β2-β4. The neuronal nAChR is also a pentameric receptor, but depending on the tissue involved, these chains can be arranged in several heteromeric or homomeric combinations. For instance, α9- and α10- subunits form homopentamers by themselves and heteropentamers with each other. Similarly, α7- and α8-subunits make homopentamers by themselves and heteropentamers with each other. The α2-α6 and β2-β4 are included in a range of complex heteropentamers (4-8).

THE *TORPEDO* NACHR

In *Torpedo*, the pentameric structure of the nAChR is created from four distinct gene products, designated α (52.4 kDa), β (56.2 kDa), γ (63.2 kDa), and δ (65.9 kDa), that assemble with a stoichiometry of $\alpha_2\beta\gamma\delta$ (2, 9, 10). The high degree of sequence homology, both between subunits and between species, suggests the nAChR subunits have been well conserved throughout evolution. Molecular cloning and protein sequencing of α, β, δ and γ subunits from *Torpedo* reveals ~19% sequence identity and ~54% homology between subunits (9-16). The different muscle nAChR subunits share between 31- 49% sequence homology; whereas the neuronal nAChR subunits share between 37-68% sequence homology; the corresponding *Torpedo* and mammalian muscle nAChR subunits share approximately 60-70% sequence homology. Thus the *Torpedo* nAChR provides a good model for human muscle-type nAChR.

Electron microscopy has aided in elucidating the overall structure of the mucle-type nAChR. When viewed from the synaptic cleft, the receptor appears as a rosette, ~80 Å in diameter with a central pore with diameter of ~ 25 Å wide at the synaptic entry, which becomes narrower, ~10 Å, at the transmembrane level; when viewed from the side the receptor appears ~125 Å in height (Fig. 1.1) (17-19). Approximately 55% of the receptor's mass is found within the synaptic cleft, ~25% within the lipid bilayer and ~20% within the cytoplasm (17-19). The synaptic portion extends ~60 Å above the lipid head groups of the postsynaptic membrane and the cytoplasmic portion extends ~20 Å below (17-19). The five subunits are arranged pseudo-symmetrically around an axis that passes through the ion pore, perpendicular to the plane of the lipid membrane. The nAChR subunits are arranged around the ion channel in a clockwise αγαβδ order (20). Based on primary sequence analysis, electron microscopy, and hydrophobicity profiles, the nAChR subunits can be divided into

Figure 1.1

Schematic diagram illustrating the quaternary organization of the nAChR. The nAChR is a large integral membrane protein composed of five subunits ($\alpha_2\beta\gamma\delta$) arranged with pseudo five-fold symmetry around a central ion pore that facilitates ion translocation across the postsynaptic membrane. Each receptor pentamer contains two neurotransmitter binding sites, one on each of the two subunits. Modified from Changeux (60).

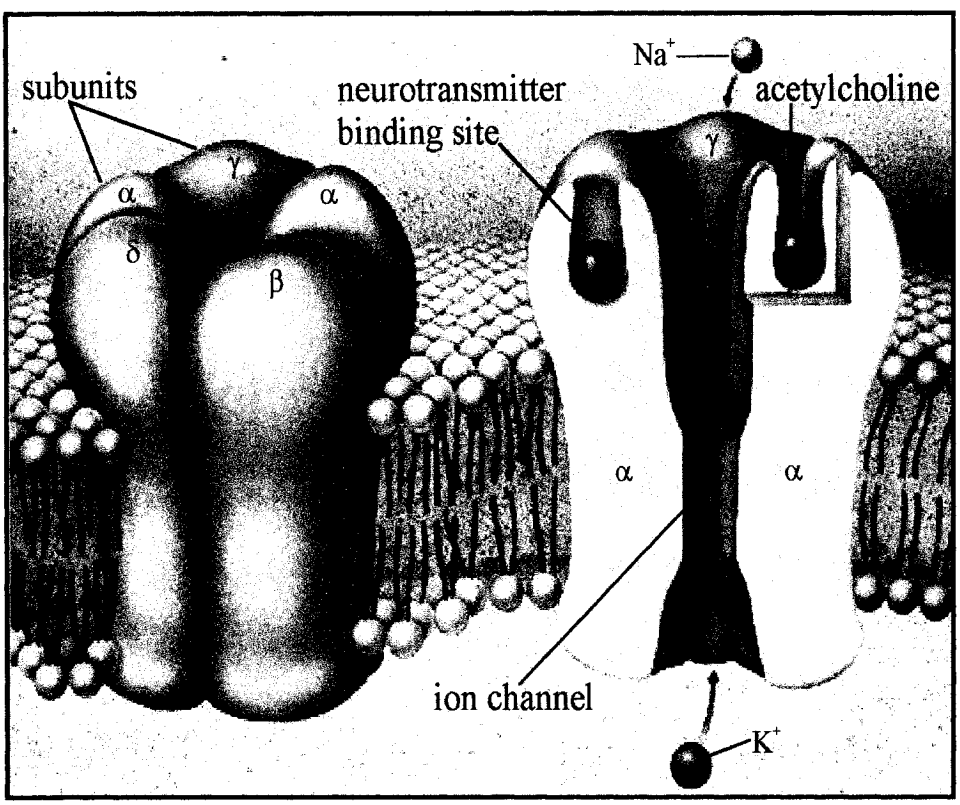
subunits
neurotransmitter
binding site
Na+
acetylcholine
α
γ
α
δ
β
γ
α
α
ion channel
K+

three structural domains: the extracellular domain, the transmembrane domain, and the intracellular domain.

THE EXTRACELLULAR DOMAIN AND THE NEUROTRANSMITTER BINDING SITES

The extracellular domain is believed to be composed largely of β-sheet structures. Structure prediction algorithms proposed that the extracellular domain contains 31.7% β-sheet, and 13.7% α-helix (21). These algorithms have depicted two α-helices at the N-terminus followed by a large core of β-strands that extends to the first transmembrane segment (21). These predictions are supported by circular dichroism measurements of the soluble α1 extracellular portion that reveal an abundance of β-strands [51% β-strand, 12% α-helix, (22)]. Additionally, electron micrographs of *Torpedo* nAChR at 4.6Å resolution have also suggested a large seven-stranded β-sheet structure (18).

Our knowledge of the structure of the extracellular domain of the nAChR took a leap forward with the solution of the three dimensional structure of the Acetylcholine Binding Protein (AChBP) from Lymnaea stagnalis [protein database 1I9B, (20)]. AChBP is a soluble protein that is secreted by snail glial cells into cholinergic synapses where it modulates the synaptic transmission by binding acetylcholine [ACh, (23)]. Structurally, AChBP is a cylinder with an 80 Å diameter and a 62 Å height (20). Each of the five subunits occupies a sector of the cylinder and together the subunits line a channel that is 18 Å in diameter (20). Each subunit begins with a three-turn α-helix, and thereafter form ten β-strands with connecting loops, including two short 3_{10} helices (20). The β-strands are arranged in a twisted immunoglobulin-like fold (20). Recent efforts comparing cryo-electron micrographs of the *Torpedo* nAChR with the crystal structure of AChBP have illustrated the similarities in size and shape between the extracellular domain of *Torpedo* nAChRs and AChBP, and

have suggested that the extracellular domain of the nAChR contains the same twisted immunoglobulin fold (18, 24).

Initially it was believed that the two ligand binding sites in *Torpedo* nAChR were located in the two α subunits. However, it is now understood that the ligand-binding site is not confined to the α subunit; there are contributions, both direct and indirect, from the neighboring subunits. In both the *Torpedo* and muscle-type nAChR, experimental evidence indicates that the binding site for nicotinic agonists and competitive antagonists is located at the αγ and the αδ subunit interface (Fig. 1.2). For instance, affinity labeling experiments performed with an array of structurally different competitive antagonists - such as the aryl-cation p-(dimethylamino) benzenediazonium fluoroborate [DDF, (25, 26)], the alkaloid d-turbocurarine [dTC, (27)] the polypeptide α-bungarotoxin (28) and with the agonist nicotine (29) - demonstrate that all probes primarily label the α1 subunit, and to a lesser extent the γ and δ subunits [typically 10%-25% of the α1 subunit labeling, (21, 25, 29-33)]. Moreover, expression of the α1 subunit with either the γ or δ subunits yields an ACh binding pocket with native pharmacology, whereas all other paired subunit combinations fail to give acetylcholine binding sites (34).

Significant insight into the primary structure of the *Torpedo* nAChR neurotransmitter binding site has been gleaned via sequential affinity labeling, proteolysis, and Edman degradation experiments. Most binding site amino acid residues localize to the α subunit (Fig. 1.2): The sulfhydryl-directed affinity ligand, 4-(N-maleimido) benzyltrimethyl ammonium, labelled two adjacent cysteine residues, αC192 and αC193 (30). In the native receptor these cysteines form an unusual gem disulphide bridge that are only found in the α subunits (35). DDF, labels αY93, αW149, αY190, αC192, and αC193, and weakly labels αY198 (26, 31). Within the γ and δ

Figure 1.2

Current model of the neurotransmitter binding sites of the nAChR. The binding sites consist primarily of aromatic residues that have been highly conserved throughout evolution. Those residues identified as being in or near the neurotransmitter binding site are shown (numbers refer to their position within the primary sequence of the subunit from *Torpedo*). Amino acid residues from neighboring and subunits are also believed to contribute to agonist/competitive antagonist binding (identified as *x*). Modified from Changeux (60).

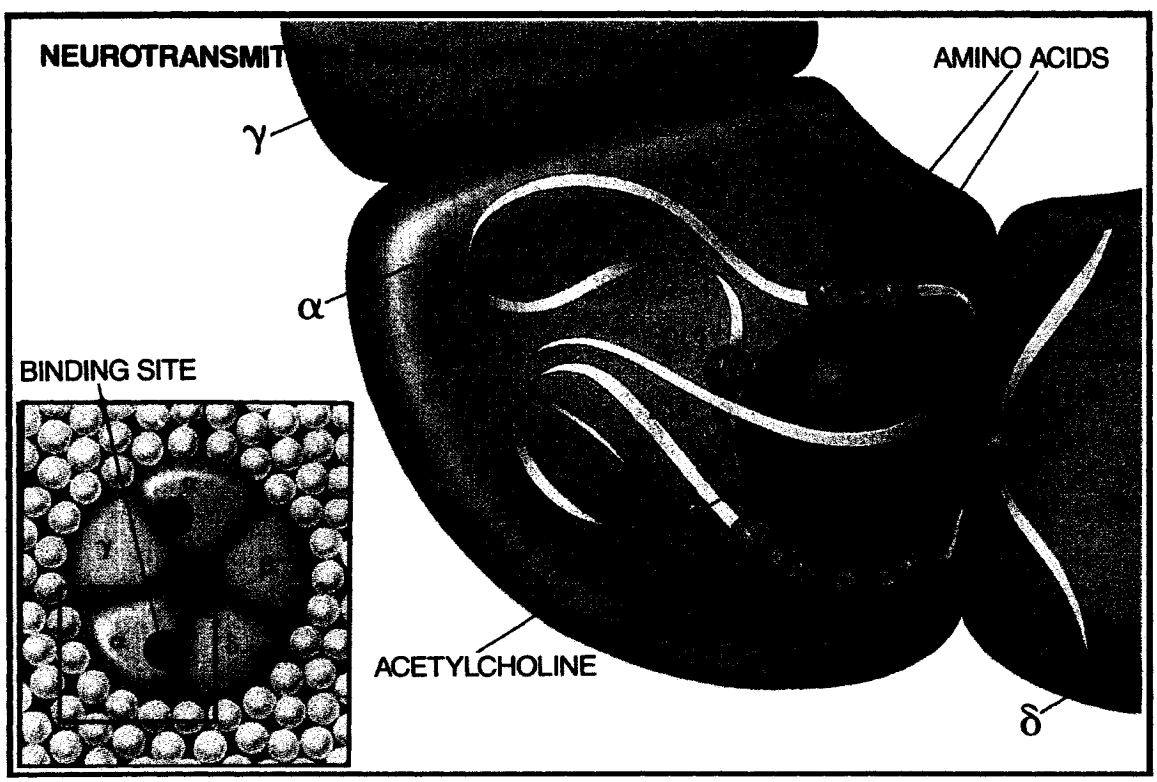
NEUROTRANSMIT
AMINO ACIDS
γ
α
BINDING SITE
ACETYLCHOLINE
δ

subunits, the homologous γW55 and δW57 were labelled by nicotine and dTC, and the homologous γY111 and δR113 were also labelled by dTC (32). To identify negatively charged residues believed to be contributing to the stabilization of the cationic ligands, a probe that specifically labels aspartates and glutamates was grafted onto the reduced αC192 – αC193 disulphide bridge and was found to label δD180 (33).

With the exception of the neuronal α5 subunit, which does not contain amino acids homologous to αY93 and αY190, and does not form functional receptors when expressed in Xenopus oocytes (36), these four aromatic residues, αY93, αW149, αY190 and αY198, along with αC192 and αC193 are highly conserved among Cys-loop receptors and appear essential to agonist binding. They are present in the α2-, 3-, 4-, 6-, 7-, and 8-subunits (37). The homologous γW55 / δW57 is present in the β2-, β4- and α7-, α8-subunits and δD180 is conserved in all γ-, ϵ-, and α7-subunits (37). Unlike this conserved core of amino acids, the γY111 / δR113 appears highly variable.

NEUROTRANSMITTER BINDING

Historically it was believed that the ACh binding site consisted of both an anionic subsite and an esterophilic subsite. The anionic subsite was thought to contain one or more carboxylate anions, such as aspartate and glutamates side chains, that would stabilize ACh's quaternary ammonium group through the formation of one or more salt bridges, while the esterophilic subsite was thought to interact with ACh's highly polar ester group probably through a hydrogen bond. Discovering a preponderance of aromatic residues within the ACh binding site came as a surprise. But when Dougherty and Stauffer demonstrated that a synthetic receptor composed primarily of aromatic residues binds ACh with a dissociation constant similar to that of the native nAChR, and that this

binding occurs through a stabilizing interaction between the aromatic π-electrons and ACh's positively charged quaternary ammonium group the experimental data was reconciled with a new model of ACh binding (38). It is now believed that the conserved core of electron-rich aromatic residues provide stabilizing interactions with cationic ligands.

Several studies have noted the importance of αW149 to ACh binding. For instance, the 50% effective concentration (EC50) for ACh correlates with the cation-π electron (⊕-π) binding capability for a series of fluorinated tryptophan derivatives (39). Moreover, incorporation of a modified tyrosine residue with a linked quaternary ammonium group [Tyr-O-$(CH_2)_3$-$N(CH_3)_3^+$], presumably mimicking a bound agonist close to αW149 at this position produces some constitutive activity (40). Furthermore, the ACh affinity for the α7 receptor is particularly sensitive to mutation at this position: with a 100-fold increase in EC50 for αW149F compared with a 10-fold increase for αY93F and αY190F (41). Lastly, a survey of known protein structures reveals that tryptophan is the most potent ⊕-π binding site, and in the X-ray crystallographic structure of acetylcholine esterase, the quaternary ammonium group of ACh makes van der Waals contact with W84 (39). Based on these observations, it is believed that the indole ring of αW149 makes van der Waals contact with the quaternary ammonium group of ACh, and ACh binding is primarily mediated by a ⊕-π interaction.

While most attention in recent years has focussed on the aromatic residues of the α-subunit, the binding contribution from the γ- and δ- subunits have also been examined via mutagenesis studies. Mutation of the homologous γD174 and δD180 to asparagine decreased the receptor affinities for agonists by 100-200 fold, and for competitive antagonists by 10-15 fold (42). Interestingly, mutating two other aspartates, αD152 and αD200 (43), located outside the ACh

binding site, to asparagine will also reduce ACh binding affinity, whereas mutating ϵD174 of $\alpha 1_2\beta 1\epsilon\delta$ compromised channel gating but not agonist binding (44). Following these observations, it was suggested that aspartates may provide additional stabilization of the ammonium ion through long-range electrostatic interactions, and that their movement towards a bound quaternary ammonium group of agonist may represent part of the activation cascade (45-47). Finally, mutations such as γY111R and δR113Y alter primarily the apparent affinities for dTC and α-conotoxin M1, but not for ACh, indicating the specific contribution of this residue to the binding of these large antagonists but not contributing to the binding of agonist (32).

THE TRANSMEMBRANE DOMAIN AND THE ION CHANNEL

The transmembrane domain was first identified, chemically, using the photoaffinity labeling agent, and channel blocker, chlorpromazine. Since then the primary structure of the hydrophobic transmembrane domain has been steadily defined and assigned to approximately 90 residues that can be further subdivided into four membrane spanning segments designated M1 (27 residues), M2 (20 residues), M3 (20 residues) and M4 (19 residues, Fig. 1.3). These hydrophobic segments display the greatest degree of sequence homology both between subunits and between species (13-15). Originally, the four membrane spanning segments were predicted to be all α-helical (13-15), but early electron micrographs of Torpedo nAChR suggested that only the ion channel-lining segment is α-helical, while the remaining segments form transmembrane β-strands (17). Subsequent FTIR secondary structural analyses, covalent modification, and chemical labelling studies have challenged the largely β-sheet hypothesis, and instead supported the original largely α-helical prediction (48-55). Recent electron micrographs of the nAChR collected at 4 Å resolution also support an all α-helical transmembrane domain (56).

Figure 1.3

Schematic diagram illustrating the transmembrane topology of the nAChR subunits. Each subunit contains (i) a large hydrophilic amino-terminal domain oriented towards the synaptic cleft, (ii) four hydrophobic segments designated M1-M4 that span the lipid bilayer as -helices, and (iii) a small hydrophilic domain between segments M3 and M4 oriented towards the cytoplasm. The M2 segment from each of the five subunits is believed to form the lining of the ion channel. Modified from Changeux (60).

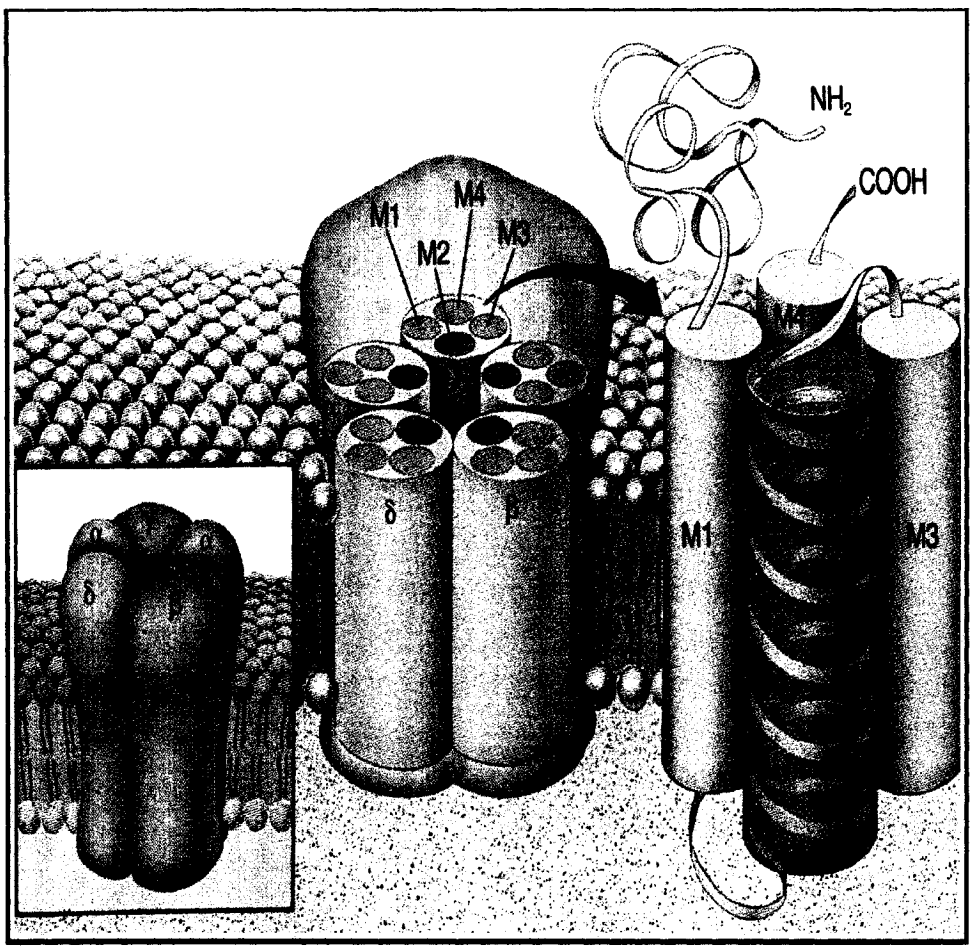
NH2
COOH
M1
M4
M2
M3
δ
β
M1
M3
δ
β

The nAChR ion channel is formed primarily from the M2 segments from each of the five subunits. Chemical labelling of the M2 segment with photoaffinity agents such as chlorpromazine (57-60), Meproadifen mustard (61), 3-trifluoromethyl-3-(m-[^{125}I]iodophenyl) diazirine [TID, (62)], and others (63-66), as well as by the substituted cysteine accessibility method [SCAM, (54, 67)], suggest that each M2 segment assumes a predominantly α-helical secondary structure and that these five helices arrange pseudo-symmetrically around the central axis of the receptor to form the walls of the ion channel. The ion channel is funnel-shaped: at the upper face, the channel diameter is 36Å, whereas at the lower face, the diameter is 23Å across (19). The ion channel pore is 10Å wide in the open state (19). Electron micrographs of the transmembrane helices, however, indicate that they do not traverse the lipid bilayer as straight rods, instead they are bent, or 'kinked' inwards near the middle of the bilayer [Fig. 1.4, (17)]. This kink produces a constriction in the circumference of the ion channel and is believed to represent the location of the ion channel gate. In the closed conformation, this gate presents an impenetrable barrier to ions.

The significant sequence homology of the M2 segment, both between subunits and between species, and the observation that mutation of M2 segment residues at analogous positions produces similar functional consequences imply a stratified structure of the ion channel, ie. side chains at homologous positions form rings of distinct physical properties that determine the various ion conductance properties of the ion channel (58, 59, 63, 68-70). In order from the most inner ring to the most outer ring, relative to the cell interior, there is the charged cytoplasmic ring, the intermediate ring, the threonine ring, the serine ring, the leucine ring, the valine ring, and lastly the charged extracellular ring.

ION CHANEL GATING

Figure 1.4

Schematic diagram illustrating the structural organization of both the channel-lining M2 segments and the M2 residues within the ion channel pore. The ion channel is formed from five -helical M2 segments, one from each subunit, that arrange pseudo-symmetrically around the central axis of the receptor (see inset; also Fig. 1.3). Homologous residues located at equivalent M2 positions on each subunit are thought to form a series of rings around the channel that mediate and govern ion conductance (see text for details). Identified (from top to bottom): the outer charged ring, the leucine ring, the intermediate ring and the inner charged ring. Modified from Changeux (60).

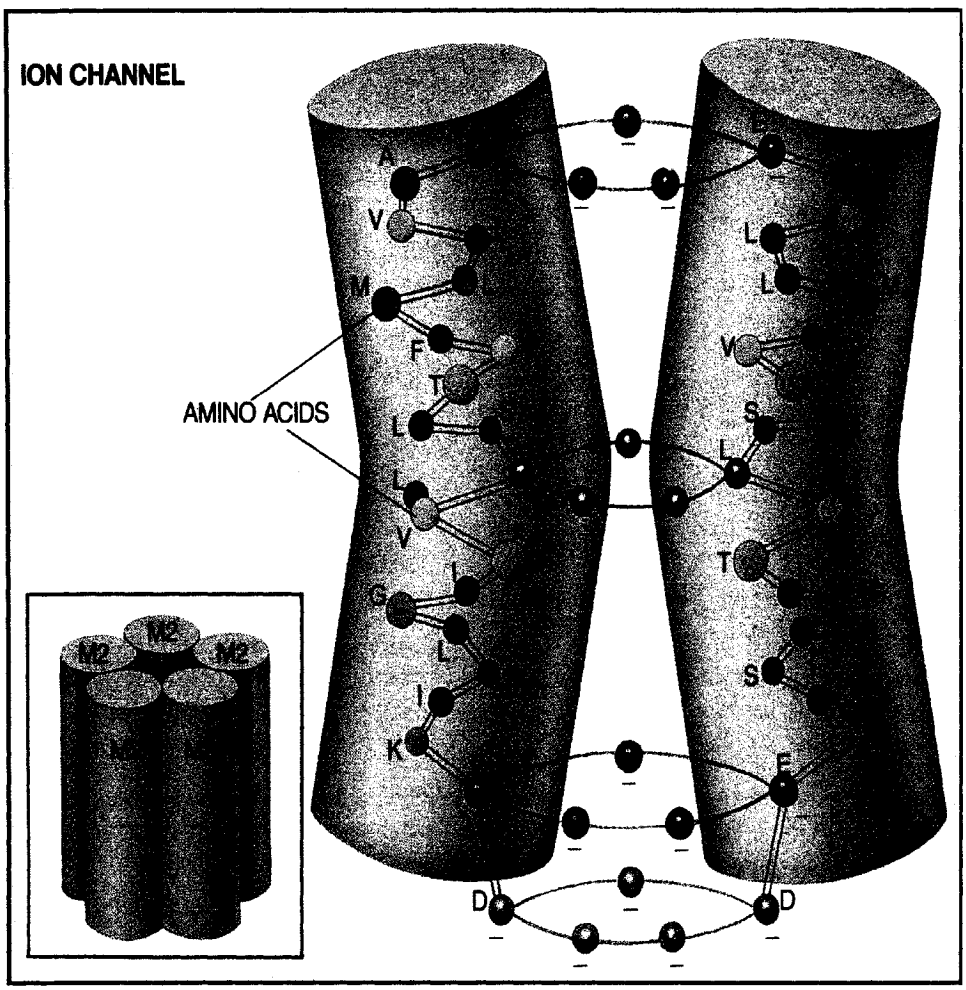
ION CHANNEL
AMINO ACIDS
M2
M2
M2
M2
A
V
M
F
T
L
L
V
I
G
L
I
K
D
L
L
V
S
L
T
S
F
D

It is generally held that there are two channel gates: a resting gate and a desensitization gate. Previously it was believed that the leucine ring of the channel M2 segment represented the resting ion channel gate (17-19). Based on electron micrographs, it was proposed that the hydrophobic side chain of leucine ring interdigitate to produce an impenetrable barrier to ion conductance in the resting state (17-19). During receptor activation, the leucine side chains were believed to twist out of the channel, and thus permit the conductance of cations into the cell. However, replacing one or more of these leucines did not significantly diminish channel gating (71, 72). Moreover, mutating all the leucines of this ring with residues with small side chains, such as serine or alanine, did not abrogate channel closure (73, 74). Furthermore, SCAM studies suggest the resting channel gate resides below the leucine ring (54, 75). Currently, the resting ion channel gate is believed to reside between the serine/threonine rings and the intermediate ring (75). When the receptor is in the resting state, SCAM studies localize the channel gate to the serine/threonine rings and the intermediate ring.

The desensitization gate, on the other hand, is believed to be an extension of the resting gate. SCAM studies have also shown that, when the receptor is in the slow-onset desensitized state (defined below), the channel gate extends from the intermediate ring to include the leucine ring (76). Other experiments have also suggested the leucine ring comprises the desensitization gate, as opposed to the resting gate (73). Pharmacological studies of leucine ring and valine ring mutants, found that these residues are located in a hydrophobic environment when the receptor is in the resting state, and move into a more hydrophilic environment during receptor activation (54, 73, 77, 78).

THE CYTOPLASMIC DOMAIN

The cytoplasmic domain is approximately four-fold smaller than the extracellular domain, and is intercalated between segments M3 and M4. The cytoplasmic domain contains several serine and tyrosine phosphorylation sites. Phosphorylation-dephosphorylation has been found to participate in receptor modulation (79-84). The cytoplasmic domain also bears the binding site for Rapsyn, a 43 kDa membrane-associated protein believed to participate in nAChR clustering at the neuromuscular junction and receptor-cytoskeleton communication (85).

NICOTINIC ACETYLCHOLINE RECEPTOR ALLOSTERY

The nAChR is an allosteric protein and fluorescence studies and ^{3}H-ACh binding assays are consistent with a four-state allosteric model (Fig. 1.5): a low-affinity resting state, an active open-channel state, a fast-onset desensitized, state and a slow-onset desensitized state. The resting state is the most stable in the absence of agonist, and the slow-onset desensitized state (abbreviated to desensitized) is the most stable in the presence of agonist. Kinetic experiments indicate that a conformational equilibrium exists between a channel-competent resting (~80%) and channel-inactive desensitized state [~20%, (86)].

RECEPTOR ACTIVATION

The binding of ACh to the resting state induces a conformational change in the receptor to the open state precipitating the translocation of ~10^4 Na^+ ions/msec across the postsynaptic membrane (87). Electron micrographs of the *Torpedo* nAChR at 4.6Å resolution, interpreted in light of the AChBP structure, suggest that the α subunits undergo a conformational change upon activation such that they come to resemble the non-α subunits. The inner set of β-strands twisted about 15° in a clockwise direction about an axis running through the channel, and the outer set of β-strands tilted outward about 11° about an axis normal to the axis through the channel (24). Based

Figure 1.5

Schematic diagram illustrating the known conformational states of the nAChR. In the absence of agonist, the nAChR exists within a conformational equilibrium between a channel-competent resting and channel-inactive desensitized state. The binding of agonist to the resting state induces a conformational change in the receptor to an open state, precipitating the conductance of cations across the postsynaptic membrane through the receptor's membrane-spanning ion channel. Prolonged or repeated exposure to agonist, induces a further conformational change to the desensitized state. Modified from Ryan (126).

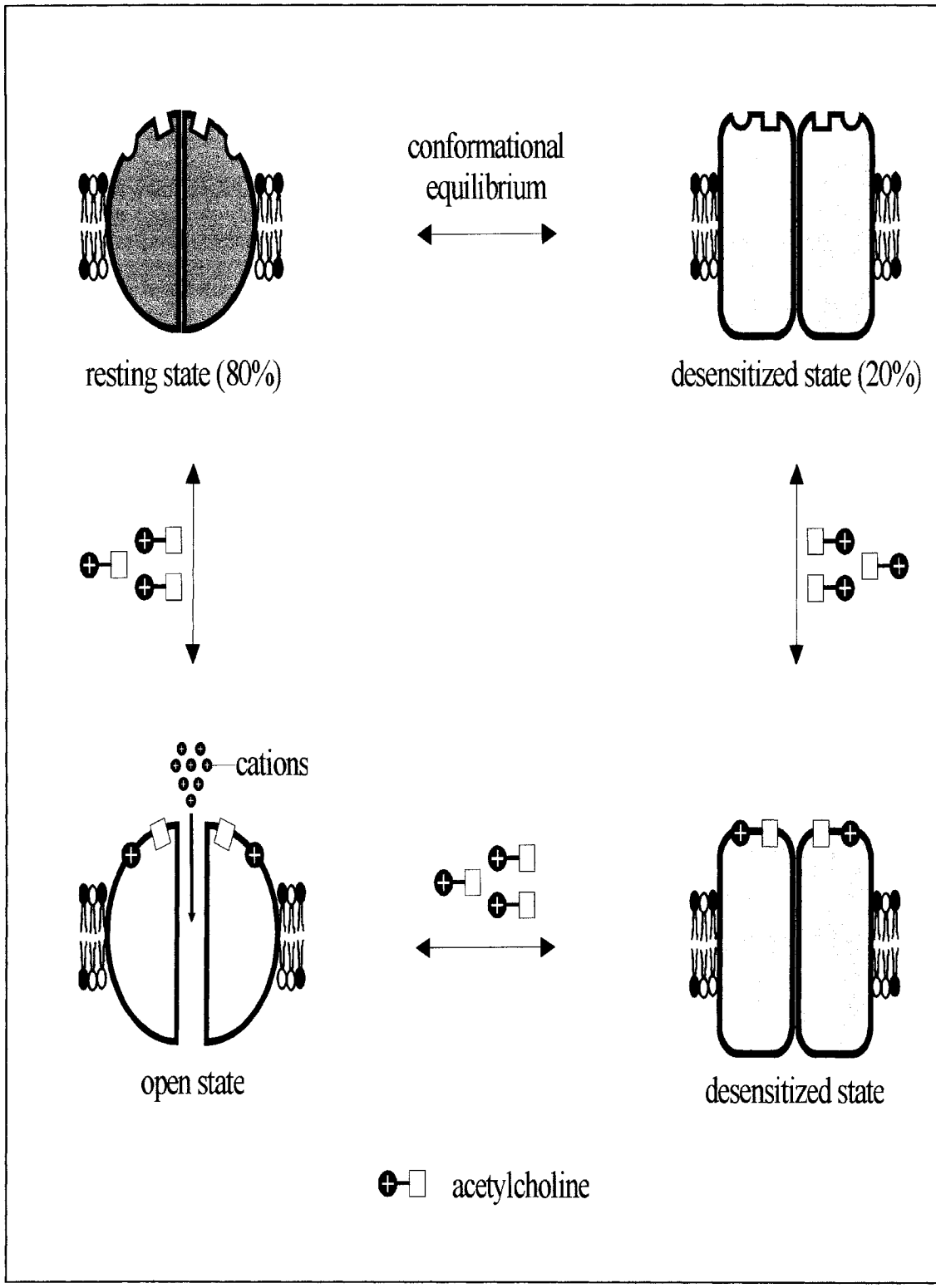
conformational
equilibrium
resting state (80%)
desensitized state (20%)
cations
open state
desensitized state
acetylcholine

on these observations, it is now believed that upon activation of the receptor, conformational changes in the inner and outer β-sheets convert from the α to non-α conformation, and these changes likely underlie the state changes from low to high affinity for ACh.

RECEPTOR DESENSITIZATION

The open state is transient, lasting for only ~1 msec, and prolonged exposure to ACh initiates an additional conformational change in the nAChR to the desensitized state. This state is characterized both by its inability to conduct cations, even though ACh remains bound, and by an approximate 1000-fold increase in ACh affinity (86, 88, 89). In the course of the resting-to-desensitized-state transition, photoaffinity labelling of the agonist binding site with DDF demonstrates a six-fold increase in contributions from the α-subunit to the neurotransmitter binding site in the desensitized state, an increase in the contribution of the γ-subunit, but a decrease in the contribution of the δ-subunit (41). It has been proposed that during nAChR activation and desensitization, the amino acid residues of the neurotransmitter binding site contract around the agonist producing a cage-like structure. This model is supported by photoaffinity labelling and disulfide reduction susceptibility studies. For instance, affinity labels attached to reduced α C192/193, behaving as tethered agonists were at most 9Å in length, whereas affinity labels behaving as tethered antagonists were at least 12Å in length, suggesting that the ACh binding site contracts around a bound agonist during activation, but cannot around an antagonist (90). Moreover, the αC192-αC193 disulphide bond is less susceptible to reduction by dithiothreitol in the presence of agonists than in the presence of competitive antagonists (91). It has been noted that in the AChBP, the disulphide projects into the binding site crevice at the tip of a loop that acts as a flexible lid on the binding site (20). This loop would have to move for large antagonists to enter the site. It is

believed that when the binding site is unoccupied, or when it is occupied by antagonist, the loop, and therefore the disulphide bond, is mobile and accessible. However, when an agonist occupies the site, the loop might be immobilized, capping the binding site, rendering the disulphide inaccessible, even to a small molecules such as dithiothreitol (92).

During desensitization, the labeling by channel blockers known to stabilize the resting state [TID (62), TID-BE (64), tetracaine (66), and diaminofluorescein (65)] shifts in the presence of a desensitizing agonist to a more expanded pattern that includes additional intracellular residues, a finding consistent with a widening of this region of the ionic pathway in the course of desensitization. Still, the same face of the helix is labeled both in the presence and in the absence of agonist.

CONCLUSIONS

It was nearly a century ago when British scientist T.R. Elliot observed the discontinuity in electrical signal propagation during neurotransmission, and postulated the existence of chemical compounds that mediated transmission between neurons and effector cells. Since then, we have continuously refined our knowledge of synaptic transmission and neurotransmitter receptor function. While a molecular snapshot of the nAChR continues to elude us, a picture of the receptor is slowly emerging.

The ambition of this project has been to better understand ligand binding, the mechanism of ion channel opening and receptor desensitization. Specifically we examined the orientation of the nAChR transmembrane domain in the resting and desensitized states and the physical interactions mediating ACh binding.

CHAPTER 2

FOURIER TRANSMISSION INFRARED SPECTROSCOPY

INTRODUCTION

One of the greatest challenges facing structural biochemistry involves unravelling the intricate relationship between protein structure and function. Typically, protein structural information is gathered using either x-ray crystallography or NMR spectroscopy, as both techniques are capable of solving protein structures at or near atomic resolution. Unfortunately, neither technique is readily amenable to the study of large integral membrane proteins, such as the nAChR. Infrared spectroscopy, however, has become an increasingly useful technique that uses molecular vibrations to gather protein structural information, as these vibrations are extremely sensitive to chemical structure, conformation and local environment. The most significant advantages of infrared spectroscopy are that it is neither limited by the size of a protein nor the nature of its environment. More importantly, infrared spectroscopy remains one of the few techniques capable of providing detailed structural information of large integral membrane proteins.

ELECTROMAGNETIC RADIATION

Many properties of electromagnetic radiation, such as reflection, refraction, and diffraction, can be described by treating the radiation as of two mutually perpendicular electric and magnetic waves that both oscillate in planes perpendicular to the plane of propagation through space. Unfortunately, the wave model of light fails to account for all behaviors of electromagnetic radiation, and does not account for phenomena associated with the absorption or emission of radiant energy. For these processes, electromagnetic radiation must be treated as a stream of discrete particles or packets of energy called photons or quanta. The energy of a photon (E_w) is given by:

$$E_w = hf_w \qquad \text{(equation 2.1)}$$

where h is Planck's constant (6.6256×10^{-34} J/s), and f_w describes the frequency of the wave. The Planck equation unifies the wave and particle nature of electromagnetic radiation by specifying the relationship between the energy of a photon, its particle property, and its frequency.

MOLECULAR VIBRATIONS

All molecules in nature consist of atoms connected by chemical bonds. These molecules are not static structures, however, and at any temperature, even absolute zero, these bonded atoms will vibrate. The simplest vibration a molecule may execute is a simple harmonic oscillation about its equilibrium position, and a plot of each atom's displacement as a function of time produces a sinusoidal wave (Fig. 2.1a). Moreover all atoms vibrate in phase and with the same frequency, although the relative amplitude and direction of each atom's displacement may differ, while the molecule's centre of gravity remains fixed. Such vibrations are described as normal modes of vibration.

For a linear polyatomic molecule, there are 3N-5 distinct normal modes of vibration, where N represents the number of atoms in the molecule; if the molecule is non-linear, there are 3N-6 distinct normal modes of vibration. In general, each normal mode of vibration can be classified as either stretching or bending, depending on the effect of the vibration on the molecule's chemical bonds. Stretching vibrations induce either symmetric or antisymmetric changes in bond length whereas bending vibrations induce either in-plane or out-of-plane changes in bond angle (Fig. 2.1b).

According to quantum mechanics, every normal mode of vibration possesses a unique set of vibration levels, the lowest vibration level is termed the ground state. These vibration levels are quantized, ie. each vibration level is separated by a discrete amount of energy. The energy of each normal mode of vibration (E_v) is given by:

Figure 2.1

Schematic diagram illustrating (**A**) a diatomic molecule executing a simple harmonic oscillation and (**B**) several independent modes of vibration of both a linear (i) and non-linear (ii) polyatomic molecule. (A) In a simple harmonic oscillation, each of a molecule's atoms move in phase with the same frequency while the molecule's center of gravity remains constant, and a plot of each atom's nuclear displacement as a function of time yields a sinusoidal wave whose amplitude is proportional to the magnitude of each atom's displacement from equilibrium. (B) In general, each of a molecule's normal modes of vibration can be classified as either stretching (change in bond length) or bending (change in bond angle). Arrows indicate the movement of atoms along the plane of the page while positive (+) and negative (-) signs indicate the movement of atoms into or out of the page, respectively. Modified from Ryan (126).

A

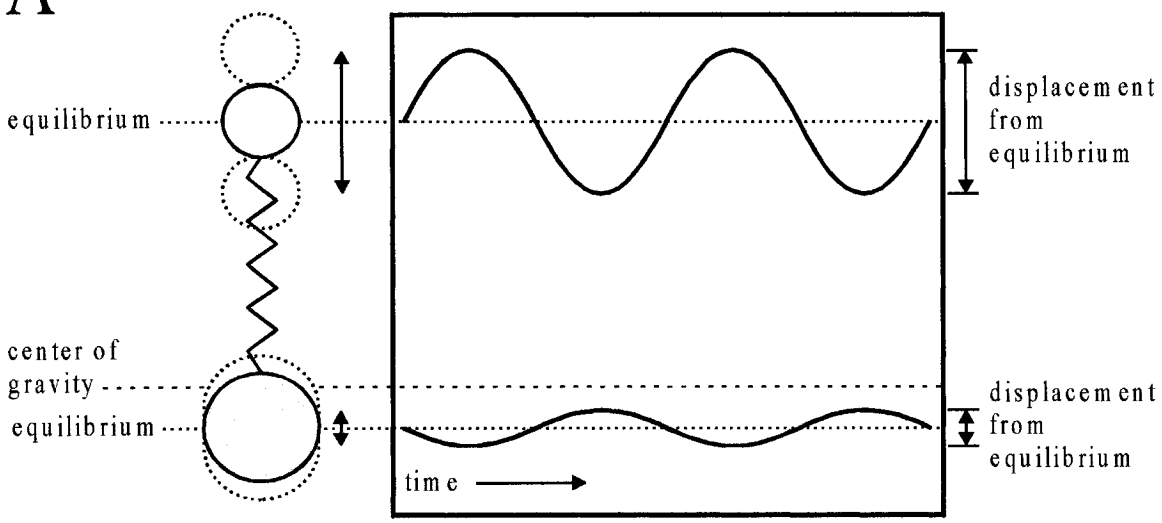
equilibrium
center of
gravity
equilibrium
displacement
from
equilibrium
displacement
from
equilibrium
time

B

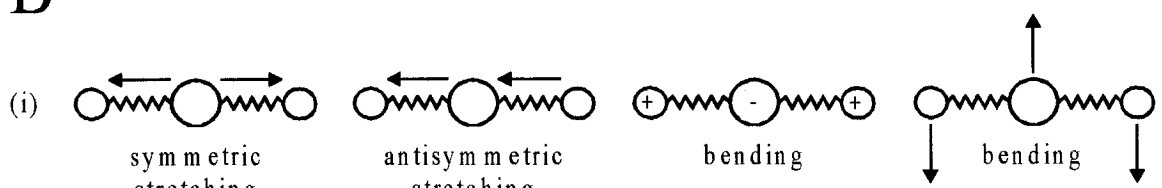
(i)
symmetric
stretching
antisymmetric
stretching
bending
bending

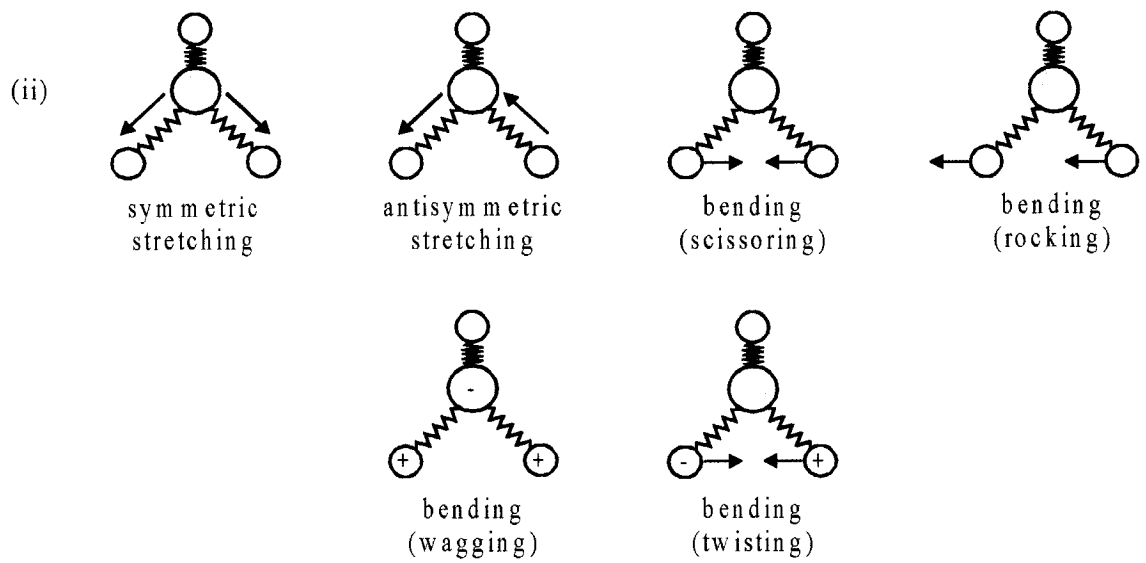
(ii)
symmetric
stretching
antisymmetric
stretching
bending
(scissoring)
bending
(rocking)
bending
(wagging)
bending
(twisting)

$$E_v = \left(n + \tfrac{1}{2}\right)hf_v \qquad \text{(equation 2.2)}$$

where f_v is the frequency of the normal mode of vibration and n is the vibrational quantum number, which only assumes integer values (i.e. 0, 1, 2, 3...). As indicated in equation 2.2, even the lowest possible vibrational level retains a vibrational energy of $\frac{1}{2}hf_v$. Moreover, the energy difference between each successive vibration level is equivalent to hf_v. Thus, the vibration levels for each normal mode of vibration are arranged in an array of increasing energy.

ABSORPTION OF RADIATION

At any given temperature, the molecules that comprise a system of harmonic oscillators are in a state of dynamic equilibrium determined by the Boltzmann energy distribution. Under normal conditions, the population distribution of vibration levels is steady. However, incident radiation can stimulate transitions between vibrational energy levels. For instance, for a diatomic molecule possessing one atom with a net positive charge and one atom with an equivalent net negative charge, the dipole moment (μ) is defined as:

$$\mu = Qr \qquad \text{(equation 2.3)}$$

where Q is the magnitude of either charge and r is the distance between the two charges. The probability (P) of a transition from the ground state (n=0) to the first excited vibrational level (n=1), is defined by:

$$P = \frac{\pi}{3hf_v M_{red}}\left(\frac{\partial \mu}{\partial Q}\right)^2 \qquad \text{(equation 2.4)}$$

where $\partial\mu/\partial Q$ is a measure of the change in the dipole, ie. the transition dipole moment and M_{red} is the reduced mass of the two atoms (m_1 and m_2) given by:

$$M_{red} = \frac{m_1 m_2}{m_1 + m_2} \qquad \text{(equation 2.5)}$$

As indicated in equation 2.4, the probability of transition is proportional to the square of the change in the dipole moment during the normal vibration. Accordingly, if $d\mu/dQ$ is zero during the vibration then the incident radiation can not be absorbed by the oscillator and the vibration is said to be infrared inactive.

Since a molecule's vibration levels are quantized, the molecule will only absorb the energy of an incident photon if the energy of the photon exactly matches the energy difference between the molecule's successive vibration levels. Incidently, this means that the frequency of the incident photon must match the frequency of the molecule's normal mode of vibration. Consider a diatomic molecule, possessing a permanent dipole moment, in the path of electromagnetic radiation. For a transition from the ground state (n=0) to the first excited vibrational level (n=1), the energy difference between these vibrational states ($\Delta E_{0\to 1}$) is given by

$$E_w = \Delta E_{o\to 1} \qquad \text{(equation 2.6)}$$

which after substituting in equations 2.1 and 2.2, reduces to the following:

$$f_w = f_v \qquad \text{(equation 2.7)}$$

again, where f_w is the frequency of the incident radiation and f_v is the frequency of the normal mode of vibration.

Schematically, the relationship between the frequency of the electromagnetic radiation absorbed by a molecule and the frequency of its normal mode of vibration is depicted in Figure 2.2. Since the wavelength of the incident radiation is significantly greater than the size of the molecule, the electric field of the incident photon can be considered uniform over the entire molecule. When the frequency of the incident photon matches the vibrational frequency of the molecule, the oscillating electric field will exert a force on the molecule's dipole. Since the force exerted on opposite charges acts in opposite directions, the molecule will absorb energy from the incident photon and increase its vibrational energy by vibrating with a greater amplitude. When the frequency of the incident radiation does not exactly match the vibration frequency, the molecule does not effectively absorb the energy of the photon.

We have now encountered two of the three principal rules governing the absorption of radiation by a vibrating molecule: First, the dipole moment of a molecule must change during a vibration. Second, the frequency of the incident radiation must exactly match the frequency of the molecule's normal mode of vibration. We will encounter the third later.

Note that though the absorption frequency is determined by the molecular vibrational frequency, the absorption intensity is determined by the magnitude of the change in the dipole moment. The effective change in a molecular bond's dipole moment, which varies with the frequency of the incident radiation, is often described by the molecular bond's molar absorption coefficient (e_w). If radiation with wavenumber ω and initial intensity I_o is passed through a sample of thickness l and molar concentration M_c, such that the transmitted light has an intensity I, then the intensity of the absorbance of the sample (A_w) will obey the Beer-Lambert law:

Figure 2.2

Schematic diagram illustrating the interaction of electromagnetic radiation with a diatomic molecule. (**A**) When a polychromatic beam strikes a diatomic molecule possessing a permanent dipole moment, the component of the radiation oscillating at the same frequency as the molecule's normal mode of vibration will be absorbed, (**B**) because the oscillating electric field alternately increases and decreases the length of the molecule's chemical bond resulting in an increase in the molecule's vibrational energy. This does not alter the frequency of the molecule's vibration, but rather the amplitude of each atom's displacement from equilibrium. Modified from Ryan (126).

A

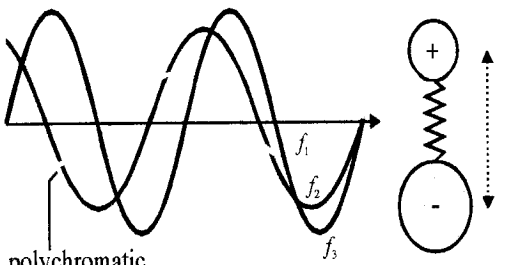

polychromatic radiation with component waves of frequency f_1, f_2 and f_3.

diatomic molecule possessing permanent dipole moment

① Vibrational energy before absorption.

② Vibrational energy after absorption of radiation with frequency f_3.

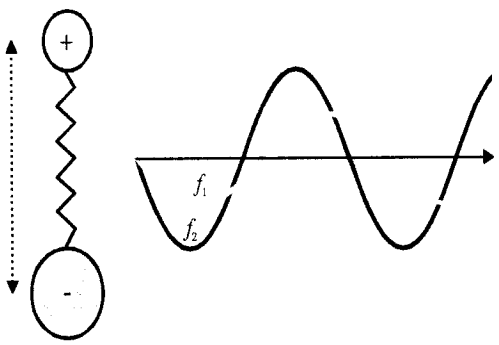

B

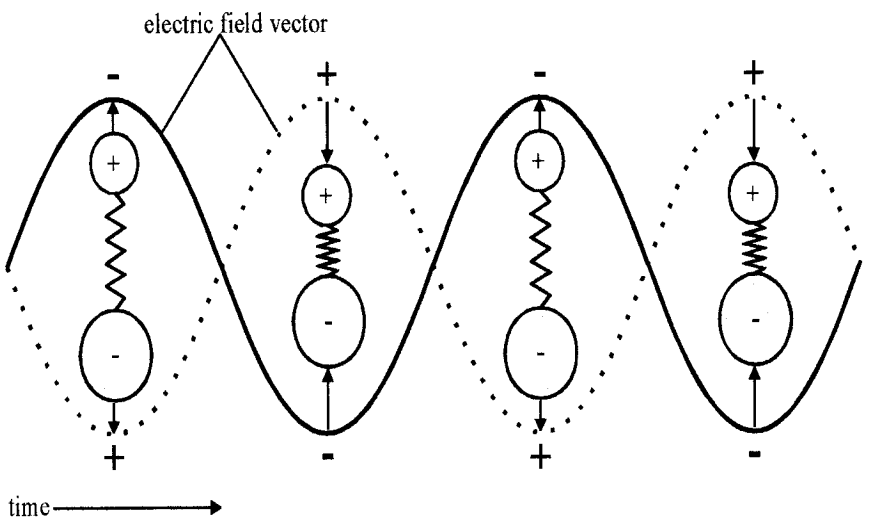

$$A_w = \log\left(\frac{I_o}{I}\right) = \varepsilon_w l M_c \qquad \text{(equation 2.8)}$$

ATR-FTIR SPECTROSCOPY

Attenuated total reflectance (ATR) spectroscopy is based on the behavior of light as it strikes the interface between two media of different refractive indices (n_1 and n_2). According to Snell's law, when electromagnetic radiation propagates through a dense medium (n_1), such as an internal reflection element (IRE), and strikes the interface between the prism surface and a medium of lower refractive index (n_2), such as a lipid membrane, then the incident radiation will be partially reflected and partially transmitted (Fig. 2.3). For the reflected radiation, the angle of reflection is equal to the angle of incidence; for the transmitted radiation the angle of refraction is defined by:

$$\sin \chi = \frac{n_1 \sin \psi}{n_2} \qquad \text{(equation 2.9)}$$

where χ is the angle of incidence and ψ is the angle of refraction. The extent to which the incident radiation is either reflected or refracted at the interface depends on how the radiation's angle of incidence relates to the prism's critical angle (ψ_c), defined by $\sin^{-1}(n_2/n_1)$. Radiation with an angle of incidence less than ψ_c is partially reflected and partially refracted; radiation with an angle of incidence greater than ψ_c is entirely reflected back into the denser medium. This phenomenon is known as total internal reflection.

Both experimental and theoretical studies have demonstrated that during total internal reflection, an evanescent wave is generated that penetrates beyond the interface and into the rarer

Figure 2.3

Schematic diagram illustrating ATR spectroscopy. In ATR, a thin layer of the sample is placed on the surface of an IRE. A sample spectrum is then recorded by passing the infrared beam through the IRE at an angle, such that the beam undergoes multiple internal reflections. Each time the beam strikes the interface between the sample and the IRE, a portion of the infrared radiation is absorbed by the sample. The effective penetration depth of the beam into the sample, however, is restricted to only a few microns, thus significantly reducing the contribution of water absorption to the sample spectrum. Modified from Ryan (126).

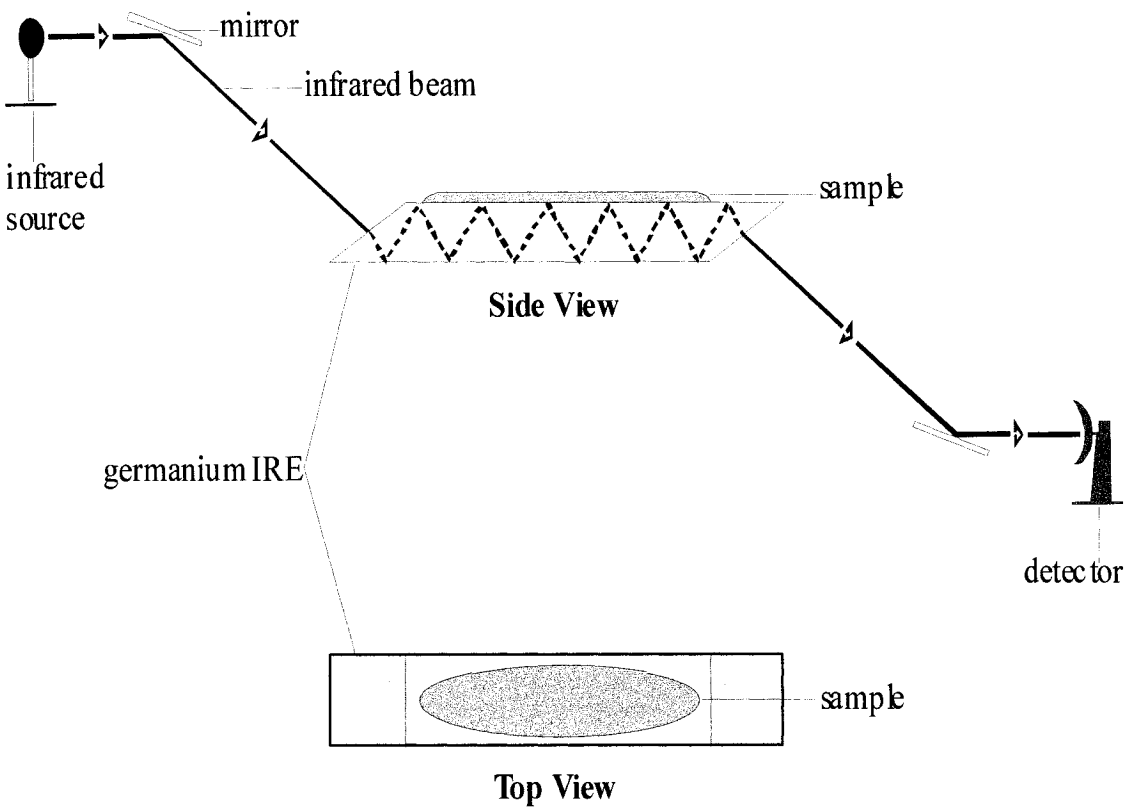
mirror
infrared beam
infrared
source
sample
Side View
germanium IRE
detector
sample
Top View

medium. If the rarer medium is an absorbing sample, it will interact with and absorb energy from the evanescent wave just as with ordinary electromagnetic energy.

An evanescent wave is an electromagnetic field that oscillates with the same frequency as the incident radiation. It is not a stationary wave, but is rather one component of a mode that exists simultaneously in both phases. There are no evanescent photons, instead merely an oscillating energy flux about the interface. The amplitude of the evanescent wave decays exponentially with the distance from the interface according to:

$$I = I_o e^{-zdp} \qquad \text{(equation 2.10)}$$

where I_o is the electric field intensity at the interface, in the rarer medium, I is the field intensity at a distance, z, from the interface, and d_p represents the effective penetration depth, which is defined as the distance required for the intensity of the evanescent wave to fall to e^{-1} of its value at the interface. It is given by:

$$d_p = \frac{\lambda}{2\pi n_1 \sqrt{\sin^2 \chi - \left(\frac{n_2}{n_1}\right)}} \qquad \text{(equation 2.11)}$$

where λ is the wavelength. Equation 2.11 illustrates that the effective penetration depth of the evanescent wave into the rarer medium is directly proportional to the wavelength of the incident beam. Consequently, for incident radiation arising from a polychromatic light source, the penetration depth of its higher component wavelengths will be greater than that of its lower

component wavelengths. Over the entire infrared spectrum, however, the effective penetration depth never exceeds a few micrometers.

In ATR spectroscopic studies, the sample may be dispersed throughout the sparser phase, but it is a more common to distribute it as a continuous film on the IRE as the penetration depth is very small. The end faces of the IRE are cut at an angle, defining the angle of incidence (χ), allowing for multiple internal reflections within the IRE to be produced, and leading to multiple interactions with the sample. For example, all spectra presented in this thesis were acquired using a germanium IRE with the dimensions of 50 x 20 x 2 mm (length x width x depth) and an angle of incidence of 45°. The number of internal reflections (N_r) that occur as an infrared beam passes through this IRE is given by:

$$N_r = Ld \cot \chi \qquad \text{(equation 2.12)}$$

where L is the length of the IRE and d is its depth. For the germanium IRE employed in this research, this translates into ~25 internal reflections.

INFRARED SPECTROSCOPY AND PROTEIN STRUCTURE

Infrared spectroscopy is an excellent tool for the study of protein structure because the frequency of a molecule's many normal modes of vibration, and thus the frequency of the radiation that it absorbs, is extremely sensitive to molecular structure and local environment. For a linear diatomic molecule, for instance, the number of independent normal modes of vibration is equal to 3N-5 = 3(2) - 5 = 1. According the frequency (f) of this vibration is given by:

$$f = \tfrac{1}{2}\pi\sqrt{\frac{F_o}{M_{red}}} \qquad \text{(equation 2.13)}$$

where F_o is the force constant binding the two atoms together. Equation 2.13, indicates that the frequency of this normal mode of vibration is directly proportional to the strength of the chemical bond. As a result, external factors that enhance the strength of this bond will increase the molecule's vibrational frequency, while factors that diminish its strength will decrease the molecule's vibrational frequency.

In the context of a protein, consider a carbonyl group located along the protein's polypeptide backbone. The frequency of this groups stretching vibration can be approximated by equation 2.13. If the carbonyl oxygen is involved in a hydrogen bond, the oxygen will donate electron density to the adjacent proton, and the strength of the carbonyl bond will be reduced, resulting in a decrease in its stretching vibration frequency and hence, a decrease in the frequency of the absorbed radiation. Similarly, dipole-ion or dipole-dipole interactions between the carbonyl group and neighboring amino acid side chains will also increase or decrease the strength of the carbonyl bond and consequently increase or decrease the stretching vibration frequency.

Note that since the region of the electromagnetic spectrum responsible for inducing vibrational transitions lies within the infrared, and since the frequencies of infrared radiation are inconveniently large numbers (between 10^{11} to 10^{14} sec^{-1}), when referring to infrared radiation, the term wavenumber is substituted for frequency. The relationship between frequency and wavenumber (ω) is given by:

$$\omega = \frac{f}{c} \qquad \text{(equation 2.14)}$$

where c is the velocity of light in a vacuum.

LINEAR DICHROISM SPECTROSCOPY AND ORIENTATIONAL DISTRIBUTION

The use of linear dichroism Fourier-transform infrared spectroscopy to study molecular orientation is widespread and continuing to increase in popularity, especially in laboratories researching the biophysics of lipid-protein interactions. When combined with internal reflection techniques, it provides detailed structural information about the orientation of protein secondary structures, amino acid side chains, and functional groups relative to the membrane normal, presently unavailable by X-ray diffraction, nuclear magnetic resonance, circular dichroism, and Raman spectroscopy.

In three dimensional space, the position of a diatomic molecule may be described according to two sets of Cartesian coordinates with respect to the x, y, and z axes. The orientation of the diatomic molecule may be described according to two polar angles: in the xz plane, θ_o describes the angle between the molecular axis and the z-axis, and in the xy plane, ϕ describes the angle between the molecular axis and the x axis (Fig. 2.4). In a population of diatomic molecules with uniaxial symmetry about the z-axis, ie. all sharing the same θ_o, all values for ϕ are equally probable, and a uniform distribution of molecules about the z axis is created. In a lipid bilayer the complete rotational disorder of the constituent molecules also creates a relatively uniform distribution of molecular axes about the membrane surface normal.

As mentioned earlier, when incident radiation impinges upon a diatomic molecule it will absorb the energy of the radiation and vibrate with a greater amplitude provided two conditions are met. First, the frequency of the incident radiation must exactly match the vibrational frequency of the diatomic molecule. Second, the molecule's dipole moment must change during the course of the vibration. But there is a third requirement as well: the plane of the oscillating electric field of the

Figure 2.4

Schematic diagram illustrating the coordinate system used in polarized ATR-FTIR spectroscopy. The position of a molecule's axis may be described according to two sets of Cartesian coordinates with respect to the x, y, and z axes; the orientation of the molecule's axis may be described by two polar angles with respect to the xz plane and the xy plane.

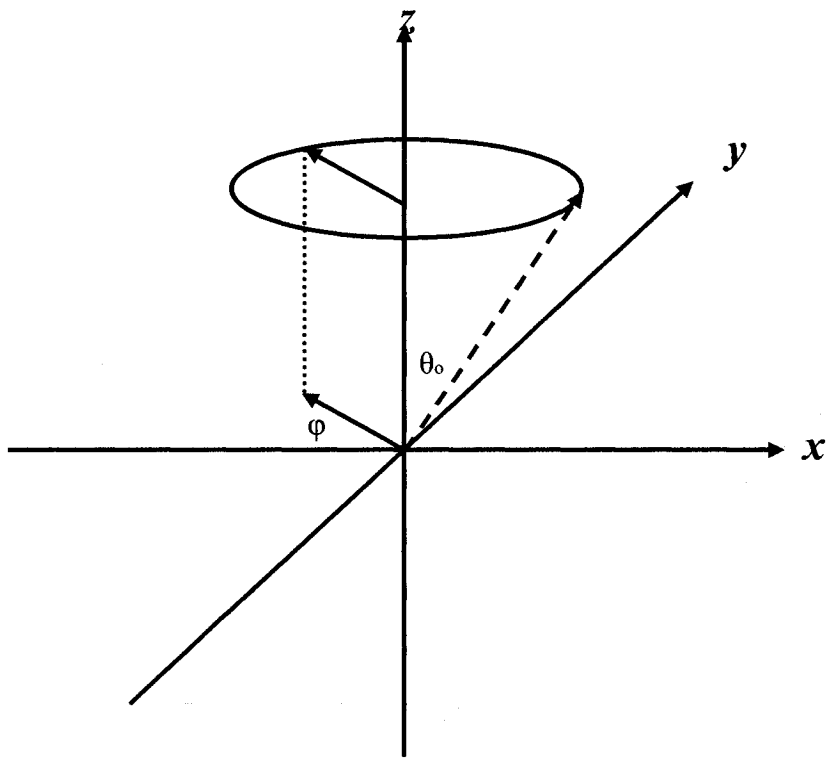
z
y
θo
φ
x

incident radiation must not be perpendicular to the vibrational path of the diatomic molecule, because the absorption of IR by an IR active molecule is dependent upon the angle between incident radiation and the transition dipole moment:

$$A = E^2 \frac{\partial \mu}{\partial Q} \cos \Gamma \qquad \text{(equation 2.15)}$$

where A is absorbance, E is the electric field component of the incident radiation, and Γ is the angle between the electric field and the transition dipole moment. The absorption of IR by an IR active molecule will vary from zero, for E perpendicular to $\partial\mu/\partial Q$, to a maximum, for E parallel to $\partial\mu/\partial Q$.

When using unpolarized IR, we are not concerned with the angle between the plane of the oscillating electric field and the vibrational path of the molecule of interest because all planes of oscillation are equally probable and it is assumed that all IR active groups in the system will be sampled. But when a polarizer is used, we can select for incident radiation with a desired electric field oscillation plane. Thus in a complex biological system, such as a lipid bilayer with accompanying membrane proteins, we can selectively sample IR active molecules with vibrational paths, at least partially, overlapping the controlled plane of electric field oscillation.

In linear dichroism ATR-FTIR spectroscopy, all molecular orientation information is contained in the dichroic ratio, R_{ATR}, which is defined as the ratio of the absorbance intensity measured with IR polarized parallel to the plane of incidence, $A_{\parallel}$, to the absorbance intensity measured with IR polarized perpendicular to the plane of incidence, $A\perp$:

$$R_{ATR} = \frac{\int A_{\parallel}}{\int A_{\perp}} \qquad \text{(equation 2.16)}$$

Since the electric field vector of the evanescent wave created by parallel polarized light has components in the x and z directions, where the x axis describes the length of the IRE element, and the z axis is normal to the IRE surface, and the electric field vector of the evanescent wave created by perpendicular polarized light only has components in the y direction, and the dichroic ratio becomes (Fig. 2.5):

$$R_{ATR} = \frac{E_x^{\,2} \sin^2\theta + 2E_z^{\,2} \cos^2\theta}{E_y^{\,2} \sin^2\theta} \qquad \text{(equation 2.17)}$$

where θ is the angle between the transition dipole/molecular axis and the IRE surface normal, and E_x, E_y, and E_z are the magnitudes of the electric field vectors of the evanescent wave along each axis and are given by the following:

$$E_x = 2\frac{\sqrt{\left(\sin^2\phi - n_{31}^{\,2}\right)}\cos\phi}{\sqrt{1-n_{31}^{\,2}}\sqrt{\left(1+n_{31}^{\,2}\right)\sin^2\phi - n_{31}^{\,2}}} \qquad \text{(equation 2.18)}$$

$$E_y = \frac{2\cos\phi}{\sqrt{1-n_{31}^{\,2}}} \qquad \text{(equation 2.19)}$$

$$E_z = 2\frac{2\sin\phi\cos\phi}{\sqrt{1-n_{31}^{\,2}}\sqrt{\left(1+n_{31}^{\,2}\right)\sin\phi - n_{31}^{\,2}}} \qquad \text{(equation 2.20)}$$

Figure 2.5

Schematic diagram illustrating the orientations of the polarized radiation relative to the IRE surface.

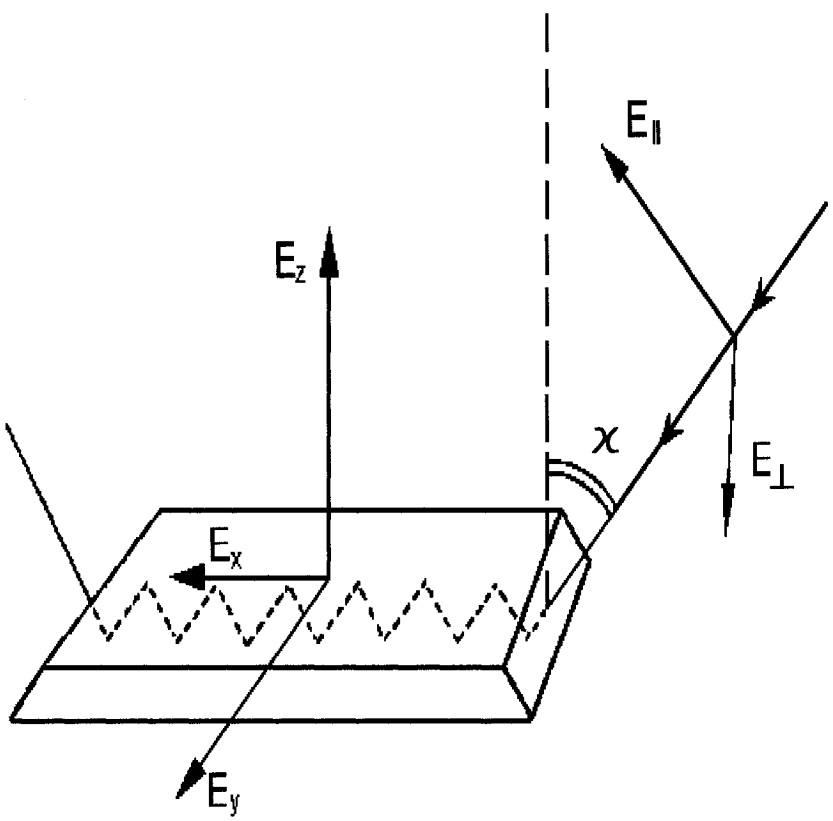
E∥
Ez
χ
E⊥
Ex
Ey

If all molecules in a population of interest were uniformly oriented at a specific angle (θ_o in figure 2.4) and evenly distributed about the z axis, then this angle of orientation could be calculated from the dichroic ratio. In practice, however, molecules are rarely uniaxially symmetric. Instead, orientational fluctuations within the molecules create a distribution of molecular orientations about θ_0 which contribute to the measured dichroic ratio. Consequently, it is customary to measure the dichroic ratio and relate it to an order parameter as follows:

$$S = \frac{E_x^{\,2} - R_{ATR}E_y^{\,2} + E_z^{\,2}}{E_x^{\,2} - R_{ATR}E_y^{\,2} - 2E_z^{\,2}} \qquad \text{(equation 2.21)}$$

The order parameter (S) is a scalar projection of the distribution of molecular orientations in the sample, and is related to θ by the following

$$S = \tfrac{3}{2}\cos^2\theta - \tfrac{1}{2} \qquad \text{(equation 2.22)}$$

It is important to note that in FTIR spectroscopy, θ describes the angle between the molecule's transition dipole moment and the z axis and not the angle between the molecule's molecular axis and the z axis. This affects the interpretation of θ as the orientation of the molecule, relative to the z axis because the transition dipole moment is not always coincident with the molecular axis. Consequently, before a molecule can be said to possess a certain orientation, relative to the z axis, it is necessary to correct for the angle between the molecule's transition dipole moment and the molecular axis. Moreover, θ describes the average angle of orientation of a population of molecules that are assumed to be evenly distributed about θ.

The interpretation of S and its relationship to θ merits further discussion, as misinterpretations are easily made. The order parameter can assume values between 1.0 and -0.5, and the interpretation of S will depend on the value S assumes. When S equals 1.0 every transition dipole moment in the population of interest are perfectly oriented parallel to the z axis, and θ equals 0. When S equals -0.5 every transition dipole moment in the population of interest is perfectly oriented perpendicular to the z axis, and θ equals 90°. Intermediate values of S, on the other hand, incorporate not only molecular orientations between 0° and 90°, but disordering within the population of interest as well. Thus, unlike the situation in which the order parameter equals either 1.0 or -0.5, intermediate values of S are subject to more than one interpretation. Moreover, the greater the disordering, the broader the distribution of molecules about θ, and the more the value of S approaches that of a completely isotropic distribution - being a value of 0. For instance, when S equals 0 the population of molecular transition dipole moments may be perfectly oriented at the magic angle of 54.7°, or they may be distributed randomly, in which all angles of orientation are equally probable, or they may be uniformly and rather tightly distributed about an average angle of orientation of 54.7°. Which interpretation is ultimately chosen will depend on the extent of disordering the population of interest is known, or believed to possess.

ORIENTATION DETERMINATION IN MEMBRANE PROTEINS

Although the measured order parameter allows one to determine the average angle of orientation between a molecular transition dipole moment and the IRE surface normal, when investigating the orientation of structural elements that comprise a membrane protein embedded in a lipid bilayer, it is often more desirable to determine the orientation of the structural elements that comprise the membrane protein, relative to the membrane normal. For instance, it is preferable to

know the orientation of a membrane protein's transmembrane helices, relative to the membrane normal, than to know the orientation of a peptide amine's transition dipole moment relative to the z axis. Consequently, it is customary to treat the different structural elements of a membrane protein system as a series of nested symmetrical distributions, each with its own order parameter (Fig. 2.6). The measured order parameter, in turn, is decomposed into a set of order parameters.

$$S_{Exp} = S_{Bilayer} S_{SS} S_{MA} S_{TDM} \qquad \text{(equation 2.23)}$$

$S_{Bilayer}$ describes the mosaic spread of the membranes on the IRE surface, relative to the z axis, and has values between 0, complete disorder, and 1, perfect order. The mosaic spread of the membranes is affected by imperfections in the surface of the IRE, and by contamination of membrane multilayer formation by dust particles and other airborne contaminants. Every contamination of the system disrupts the even layering of lipid bilayers on top of each other, introduces disorder in the system, and increases the mosaic spread of the membrane film. S_{SS} describes the orientation of a secondary structural element within the protein, relative to the membrane normal. It is generally assumed that the secondary structures which comprise a protein are relatively fixed structures, tightly distributed about an average orientation, relative to the membrane normal. Depending on the system of interest, S_{MA} describes either the angle between the molecular axis and the membrane normal, or the angle between the molecular axis and the main axis of the secondary structure to which it is fixed (as illustrated in figure 2.6) Disordering of the molecular axis will often depend on the type of secondary structure it is a component of. When part of a regular secondary structure, such as an α-helix or β-sheet, the molecular axis is assumed to be tightly distributed about an average orientation. But when part of a loop structure, the molecular axis will possess greater rotational freedom, and the

Figure 2.6

Schematic diagram illustrating the organization of membrane and protein structures of interest in ATR-FTIR spectroscopy. The different structural elements in a membrane protein system can be divided into a series of nested symmetrical distributions.

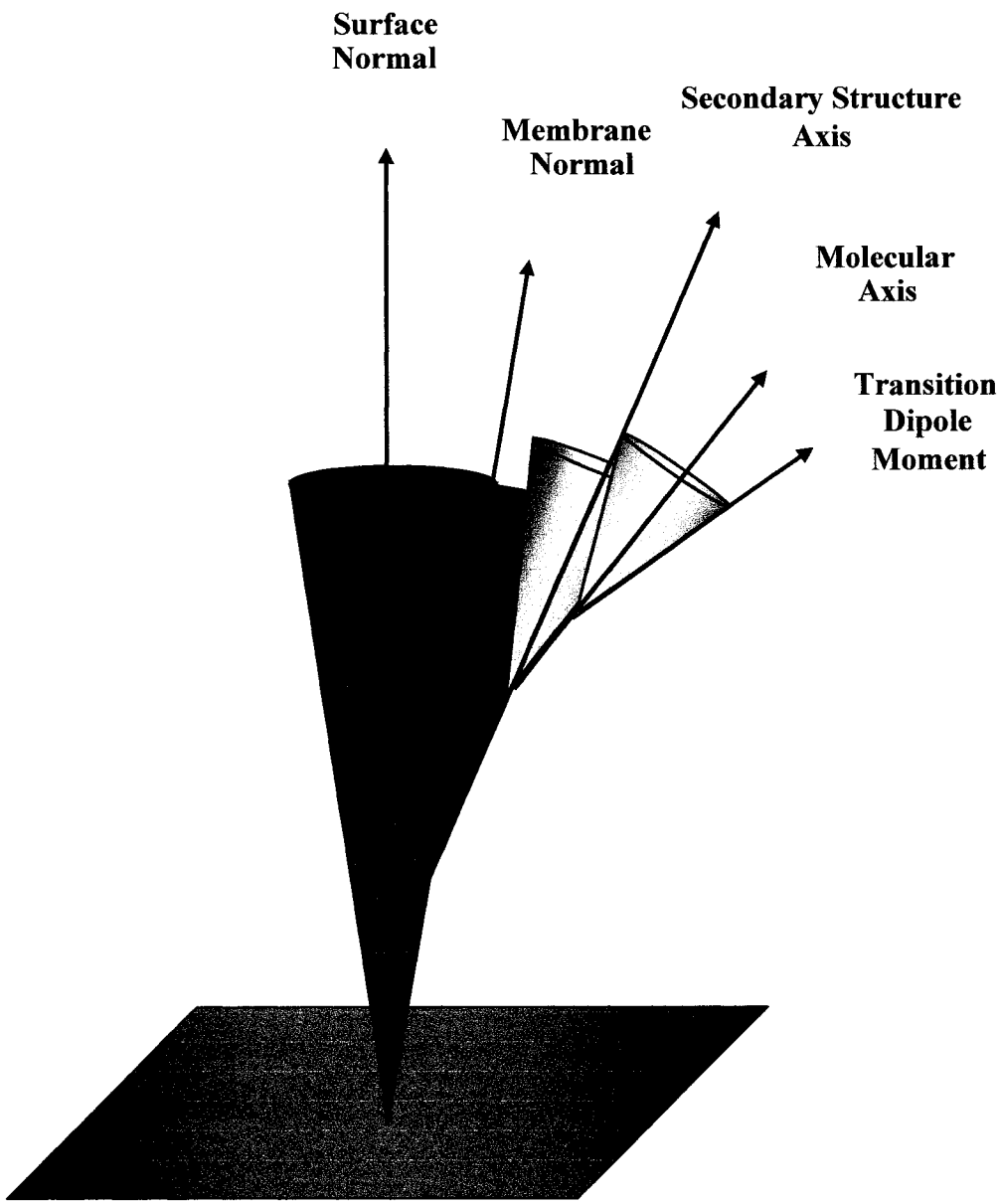
Surface
Normal
Membrane
Normal
Secondary Structure
Axis
Molecular
Axis
Transition
Dipole
Moment

distribution will be broader. The flexibility of the loop structure will, ultimately, determine the distribution of the molecular axis. Lastly, S_{TDM} describes the angle between the transition dipole moment and the molecular axis, although it is more frequently determined relative to the main axis of a specific secondary structure. The transition dipole moment is assumed to be tightly distributed about a specific angle.

FINAL NOTE

In order to estimate the magnitudes of the electric field vectors, E_x, E_y, and E_z, of the evanescent field, it was necessary to assume the membrane films were of a uniform composition and exceed the penetration depth of the evanescent field. In the context of this thesis the refractive index of the membrane film was estimated at 1.44, the refractive index the germanium IRE is 4.0, and the electric field vectors were estimated at 1.398, 1.516, and 1.625, respectively, as determined elsewhere (93).

CHAPTER 3

ORIENATATION OF THE TRANSMEMBRANE DOMAIN OF THE NICOTINIC ACETYLCHOLINE RECEPTOR IN THE RESTING AND DESENSITIZED STATES

INTRODUCTION

With the solution of the three dimensional structure of the acetylcholine binding protein - a snail glial protein with significant homology to the extracellular domain of the nAChR - increasing attention has focused on the structure of the transmembrane domain (20). Based on hydrophobicity plots, the four membrane spanning segments were origianlly predicted to be α-helical, however low resolution electron micrographs of native nAChR membranes suggested the existence of transmembrane β-strands (14, 15, 94-96). In contrast, both the pattern of chemical labelling of the transmembrane segments with the hydrophobic probe, 3-Trifluoromethyl-3-(*m*-[^{125}I]iodophenyl)diazirine and FTIR/circular dichroism studies all support the original α-helical predictions (52, 55, 60, 97). A recent model of the nAChR transmembrane domain based on higher resolution electron micrograhs of native membranes also suggests an essentially α-helical transmembrane domain (56).

FTIR spectroscopy has been used extensively to examine the structure of the nAChR and other integral membrane proteins (48, 98, 99). Our FTIR studies have shown that the nAChR is a mixed α-helical/β-sheet protein with an α-helical transmembrane domain (100). The latter conclusion is based the strong α-helical character of the amide I band observed in FTIR spectra of nicotinic receptors treated with proteinase K to remove the extramembranous domains. In addition, we found that 20-30% of the nAChR peptide hydrogens are resistant to hydrogen-deuterium exchange even after 72 hours exposure of the nAChR to $^{2}H_{2}O$ at 4 °C (48). These unexchanged peptides give rise to a strong amide I component band near 1655 cm^{-1} characteristic of α-helical peptide hydrogens. As the exchange resistant core is likely made up of peptides located in the

transmembrane domain, the spectroscopic data suggest that the transmembrane domain of the nAChR is composed of α-helical peptides.

The ability to isolate features in the infrared spectrum of the nAChR that are due predominantly to unexchanged peptides located within the transmembrane domain provides a means for assessing the structural features of this domain under varying conditions. In this study, we probe the orientational properties of the hydrogen-deuterium exchange resistant core of the intact nAChR using linear dichroism attenuated total reflectance infrared spectroscopy both in the presence and absence of the agonist Carb. To avoid ambiguities in the interpretation of the linear dichroism data, thick films of reconstituted nAChR membranes that extend beyond the penetration depth of the evanescent wave were studied. We also examined the linear dichroism of lipid bands in spectra recorded from membranes both with and without the nAChR in order to accurately assess the effects of membrane film mosaic spread on the interpretation of the linear dichrosm data. Our data also show that the mosaic spread of the reconstituted membrane films is greater than the mosaic spread observed with pure lipid films. Additionally, our results show that the hydrogen exchange resistant α-helical peptide hydrogens in the nAChR are preferentially oriented parallel to the bilayer normal and that there are no detectable net changes in orientation upon agonist-induced desensitization.

EXPERIMENTAL PROCEDURES

PREPARATION OF CRUDE NACHR-ENRICHED MEMBRANE FRACTION

A crude nAChR-enriched membrane fraction was prepared from *Torpedo californica* electroplaques (Marinus; Long Beach, CA or Aquatic Research Consultants; San Pedro, CA) as described by Ochoa *et al.* (101) with modifications (102). All steps were performed at 4 °C. Approximately 100 g of frozen electroplaques were partially thawed, sliced into 2-4 cm^2 portions

and added to 500 ml of homogenization buffer (10 mM Na_2HPO_4, 5 mM EDTA, 5 mM EGTA, 0.25 mM PMSF, 11 mM iodoacetamide and 0.2% NaN_3, pH 7.4). The electroplaques were then homogenized in a Waring blender using 3 x 30 second bursts. The resulting homogenate was centrifuged for 10 minutes at 5000 rpm in a Sorvall (model RC2-B) centrifuge and the supernatant collected after filtering through two layers of cheesecloth. The pellets were re-homogenized in 250 ml of homogenization buffer using a Brinkman Polytron and centrifuged as described above. The pooled supernatants were then centrifuged for 3.5 hours at 14000 rpm and the supernatant discarded. The crudely purified nAChR pellets were re-suspended in dialysis buffer (1 mM NaCl, 50 mM Na_2HPO_4, 1 mM EDTA and 0.2% NaN_3, pH 7.8) to a final volume of 50 ml, further dispersed using a 55 ml Wheaton hand homogenizer, and stored at –80 °C.

SYNTHESIS OF BROMOACETYLCHOLINE CHLORIDE

For the affinity purification of the nAChR, bromoacetylcholine chloride (BAC) was used to derivatize Bio-Rad Affi-Gel 102 (Bio-Rad, Richmond, CA). BAC was synthesized according to Damle *et al.* (103). Over a period of 40 minutes, 0.15 moles of bromoacetyl chloride was added dropwise to 0.1 moles of choline bromide and the resulting mixture cooled in an ice bath for 1.5 hours. 75 ml of absolute ethanol was then added slowly over a period of 30 minutes and the resulting white precipitate (BAC) filtered using a Buchner funnel. BAC was re-crystallized twice using 200 ml of isopropanol, dried under vacuum overnight and stored at –20 °C.

PREPARATION OF BROMOACETYLCHOLINE AFFINITY COLUMN

The nAChR was affinity purified using a bromoacetylcholine column prepared as described by Ellena *et al.* (104). 20 ml (packed volume) of Affi-Gel 102 was added to 20 ml of thiolactone solution (1.44 M N-acetyl-DL-homocysteine thiolactone and 1 M $NaHCO_3$) and the pH adjusted to

9.7. This mixture was then left to stir overnight at 4 °C. The following morning, the gel was washed with 1 L of cold 0.1 M NaCl solution and re-suspended in 20 ml of DTT solution [0.2 M dithiothreitol and 0.2 mM tris(hydroxymethyl)aminomethane (Tris), pH 8.0]. The gel was stirred gently for 30 minutes, transferred to a 2.5 x 40 cm glass column (Amersham Pharmacia Biotech, Piscataway, NJ) and the DTT solution drained. 20 ml of fresh DTT solution was then added to the gel and the column agitated for 30 minutes. The DTT solution was again drained and the gel washed with 140 ml of buffer B (100 mM NaCl, 20 mM Na_2HPO_4, 0.02% NaN_3, pH 7.0). After re-suspending the gel in 15 ml of 50 mM Na_2HPO_4 buffer (pH 7.0), 0.4 g of BAC was added and the column agitated for 1 hour. The gel was then washed with 80 ml of buffer B, re-suspended in 15 ml of buffer B containing 0.14 g of iodoacetamide and the column again agitated for 20 minutes. The column was drained and the gel washed with 60 ml of unbuffered 0.2% NaN_3 solution. The column was then stored at 4°C until use.

AFFINITY PURIFICATION AND RECONSTITUTION OF THE NACHR

All steps were carried out at 4 °C. 20 mL of the crude nAChR-enriched membrane fraction was thawed and diluted with dialysis buffer (100 mM NaCl, 10 mM Na_2PO_4, 0.1 mM EDTA, 0.02% w/v NaN_3, pH 7.8) to a final protein concentration of 4 mg/ml. To this was added an equal volume of dialysis buffer containing 1% cholate. The mixture was gently stirred for 1 hour and then centrifuged at 87,000 rpm for 30 min using a Beckman (model L8-55M) ultracentrifuge. The supernatant, comprising cholate-solubilized nAChR, was applied to the bromoacetylcholine affinity column following a pre-wash of 60 ml of dialysis buffer. The column flow rate during this and all remaining steps was ~1 ml/minute.

To reconstitute the nAChR into different lipid mixtures, the affinity column was washed with the lipids of choice (Avanti Polar Lipids, Alabaster, AL). First, the column was washed with lipid solution B (32.5 ml dialysis buffer, 1.3 mM lipids and 1% cholate) to remove contaminating proteins. The column was then washed with lipid solution A (60 ml dialysis buffer, 3.2 mM lipids and 1% cholate) to exchange native lipids with defined lipids. Following this, the column was washed with lipid solution C (50 ml dialysis buffer, 0.13 mM lipids and 1% cholate) to lower the final lipid-to-protein ratio.

The nAChR was eluted from the affinity column using lipid solution D (10 mM Carb, 10 mM Na_2HPO_4, 50 mM NaCl, 0.1 mM EDTA, 0.02% NaN_3, 0.13 mM lipids and 0.5% cholate, pH 7.8). 3 ml fractions were collected and those with an absorbance greater than 0.05 a.u. at 280 nm were combined. The affinity purified nAChR solution was then placed in membrane tubing (molecular weight cut-off 12-14 kDa; Spectrum Laboratories, Gardena, CA) and dialyzed against 2 L of dialysis buffer. The dialysis buffer was changed four times, once every 12 hours, to ensure complete removal of both Carb and cholate and to reconstitute the nAChR into the defined lipids. Following dialysis, the purified nAChR was centrifuged for 2 hours at 120,000 rpm, again using the Beckman (model L8-55M) ultracentrifuge. The pellet was re-suspended in 1 ml phosphate buffer (1.2 mM NaH_2PO_4, 0.8 mM Na_2HPO_4, 0.02% NaN_3, pH 8.0) and further dispersed using a small glass hand homogenizer. Protein concentration was estimated by BCA assay (Pierce; Rockford, Il) using bovine serum albumin as the standard and lipid solution D as the blank. The reconstituted nAChR was then separated into 250 μg aliquots and stored at –80 °C. The purity of all nAChR samples were analyzed by 12 % SDS PAGE with Coomassie Blue staining. Lipid-protein molar ratios were calculated by FTIR (105) and were generally found to be in the 150:1 molar range. Note that the slight variations

in lipid to protein ratio between reproduced preparations had unappreciable effects on the results described here.

SAMPLE PREPARATION

The nAChR from frozen *Torpedo californica* electric tissue was affinity-purified and reconstituted into membranes composed of 1-palmitoyl-2-oleoyl-*sn*-glycero-3-phosphocholine/1-palmitoyl-2-oleoyl-*sn*-glycero-3-phosphate/cholesterol (PC/PA/Chol) 3:1:1 (mol:mol:mol) as described above. 250 μg aliquots of reconsitituted nAChR protein were centrifuged and resuspended in 2 mM phosphate ^2H_2O buffer (pH 7.8) two times. Samples were left for 72 hours at 4 °C to allow peptide hydrogen-deuterium exchange and then frozen at -80 °C until use. nAChR membrane films were prepared by drying the 50 μl aliquot on the surface of a germanium 50 x 20 x 20 mm germanium internal reflection element (IRE, Harrick, Ossining, NY). Pure lipid samples were first mixed in chloroform (300μg total of lipid) and then deposited from chloroform onto the IRE. After evaporating the bulk solvent with a gentle stream of N_2 gas, the germanium IRE was installed in an ATR liquid sample cell (also from Harrick) both the reconsistuted and pure membrane lipid films were hydrated in ^2H_2O *Torpedo* ringer buffer (5 mM Tris, 250 mM NaCl, 5 mM KCl, 3mM $CaCl_2$, and 2 mM $MgCl_2$, pH 7.0).

POLARIZED FTIR MEASUREMENTS

FTIR spectra were recorded using the attenuated total reflection (ATR) technique on an FTS-575 spectrometer (Bio-Rad), equipped with a deuterated triglycine sulfate detector (DTGS) detector. Linear dichroism spectra were recorded using a computer controlled wire grid polarizer (Pike Technologies; Madison, WI). Spectra of the pure lipid multilayers were derived from 256 single beam scans taken at 2 cm^{-1} resolution. Spectra of the nAChR-membrane films were derived

from 4000 single beam scans taken at 2 cm^{-1} resolution. The polarized single beam spectra were ratioed against a corresponding background recorded using polarized light. Polarized spectra of the pure lipid films were recorded at 2°C intervals as the sample was cooled from 35°C to -10°C using the software program DeltaTemp from Neslab. A 30 minute time interval was allowed for the water bath to equilibrate at each temperature and for sample equilibration.

ORDER PARAMETER DETERMINATION FROM ATR-FTIR DICHROISM OF THICK MEMBRANE FILMS

The dichroic ratio, R_{ATR}, for a given infrared absorption band is defined as the ratio of the absorption intensities obtained with infrared radiation polarized parallel versus perpendicular to the plane of incidence.

$$R_{ATR} = \frac{\int A_{\parallel}}{\int A_{\perp}} \qquad \text{(equation 3.1)}$$

where $A_{\parallel}$, and $A_{\perp}$ are the integrated absportion intensities of a certain vibrational band in the frequency range. From the dichroic ratio, and an estimation of the electric field amplitudes of the evanescent wave at the surface of the internal reflectance element (E_x, E_y, and E_z; xy-plane is parallel to the surface of the Ge element), an order parameter S is calculated for the orientation of the transition dipole moment relative to the internal reflection element (IRE) surface normal:

$$S = \frac{E_x^{\,2} - R_{ATR}E_y^{\,2} + E_z^{\,2}}{E_x^{\,2} - R_{ATR}E_y^{\,2} - 2E_z^{\,2}} \qquad \text{(equation 3.2)}$$

As described in Hubner and Mantsch (93), for a uniaxially oriented fiber normal to the IRE surface, under the experimental conditions used here (45° angle of incidence, thick film

approximation, refractive index for the lipid film, n_2=1.44, refractive index for the germanium IRE is 4.0, and the electric field vectors, E_x, E_y, E_z estimated at 1.398, 1.516, and 1.625, respectively), the order parameter for the lipid ester carbonyl stretching vibration, can be simplified as follows:

$$S_{C=O} = \frac{R_{ATR} - 2}{R_{ATR} + 1.45} \qquad \text{(equation 3.3)}$$

Moreover, the order parameter for the lipid acyl C-H symmetric stretching vibration can be simplified as follows:

$$S_{acyl} = -2\frac{R_{ATR} - 2}{R_{ATR} + 1.45} \qquad \text{(equation 3.4)}$$

In the context of a lipid bilayer, S_{acyl} can be broken down into four additional order parameters:

$$S_{acyl} = S_{tilt} S_{motion} S_{bilayer} S_{distortion} \qquad \text{(equation 3.5)}$$

where S_{tilt} describes the average angle between the acyl chain axis and the bilayer normal, and can assume values between 1 and -0.5, however, it is generally assumed to take a value of 1, implying acyl chain axes are perpendicular to the membrane normal. S_{motion} describes the amplitudes of the molecular motions (trans-gauche isomerization, etc.) of the acyl chain, and $S_{bilayer}$ describes the mosaic spread of the membrane film on the IRE surface. Whereas S_{tilt} describes an average angle, $S_{distortion}$, S_{motion}, and $S_{bilayer}$ are correction factors, and therefore assume values between 1, for a perfectly ordered system, and 0, for a randomly oriented system.

Lastly, in the determination of the transmembrane helix orientation, assuming the helix peptide carbonyl transition dipole moments are oriented 35° to the helix fiber axis, as described elsewhere (106), the order parameter for the transmembrane helices can be simplified as follows:

$$S_{TMD} = 1.97\frac{R_{ATR} - 2}{R_{ATR} + 1.45} \qquad \text{(equation 3.6)}$$

which can also be broken down in an analogous fashion as follows:

$$S_{TMD} = S_{helix}S_{bilayer} \qquad \text{(equation 3.7)}$$

where S_{helix} describes the average angle between the transmembrane helix axis and the bilayer, normal. In this case S_{helix} assumes values between 1 and -0.5.

The average angle, θ, between the transmembrane fiber axis and the IRE surface normal is related to S_{helix} as follows:

$$S_{helix} = \tfrac{3}{2}\cos^2\theta - \tfrac{1}{2} \qquad \text{(equation 3.8)}$$

Note that all spectral analyses were performed using the GRAMS/AI Spectral Notebase program suite (Thermo Galactic, Salem, NH, USA). Dichroic ratios were determined from either the integrated intensities and/or the peak heights of the bands using baselines calculated between data points, limiting the integrating intervals. Integrating intervals were chosen such that only one dichroic band fell in that region, thus minimizing interference from overlapping bands.

RESULTS AND INTERPRETATION

A rigorous interpretation of linear dichroism FTIR spectra in terms of the orientation of protein transmembrane segments requires knowledge of the orientational uniformity or mosaic spread of the membrane film on the surface of the planar internal reflection element. The mosaic spread can be described by an order parameter, $S_{bilayer}$, which varies from 1, for uniformly oriented membranes parallel to the IRE surface, to 0, for randomly oriented membranes. To quantify the

mosaic spread of reconstituted nAChR membranes, we recorded linear dichroism spectra from both pure and reconstituted PC/PA/Chol 3:1:1 (mol:mol:mol) membrane films. The pure lipid membranes were deposited on the IRE from chloroform, whereas the reconstituted nAChR membranes were deposited as unilamellar vesicles from aqueous solution. In both cases, the samples were dried under N_2 and the membranes hydrated with excess *Torpedo* Ringer buffer. Note that PC/PA/Chol 3:1:1 membranes are particularly effective at stabilizing the nAChR in a functional resting state that fluxes cations upon agonist binding (102). We have shown previously that this method of film formation on a planar surface yields fully functional receptors (99).

Linear dichroism spectra of PC/PA/Chol 3:1:1 membranes exhibit several lipid vibrations that provide insight into both the orientational properties of the membranes on the IRE surface and the motional properties of the lipids themselves. The most useful is the acyl chain symmetric C-H stretching vibration centered near 2850 cm^{-1}. The dichroic ratio of this vibration can be interpreted in terms of a molecular order parameter, S_{acyl}, that is sensitive to the average orientation of methylene C-H bonds relative to the bilayer, the amplitudes of local acyl chain *trans-guache* isomerizations, and the mosaic spread of the membrane film. The dichroic ratio for the C-H stretching vibration reaches a minimum of 0.85 corresponding to an $S_{acyl} = 1.0$ for a perfectly ordered all-*trans* saturated chain oriented parallel to the bilayer normal in a membrane film with no mosaic spread. The value of S_{acyl} will decrease with an increasing deviation of the C-H bond vector away from the all-trans configuration (such as is the case near a double bond), with increasing acyl chain motion, and with increasing mosaic spread. Note that the symmetric stretching vibration is also of interest because it undergoes a shift up in frequency with increasing acyl chain disorder (i.e. increasing *trans-guache* isomerizations). The C-H stretching frequency provides a sensitive probe of the transition from the

ordered gel to the relatively disordered liquid crystalline phase. Previous studies have shown that incorporation of the nAChR into PC/PA/Chol 3:1:1 leads to a shift up in the gel-to-liquid crystal phase transition temperature from roughly 3.8 to 12.6 °C (107).

The lipid ester carbonyl stretching vibrations centered near ~1750 cm^{-1} is also of interest to the discussion presented here. This band is composed of two underlying components centered near 1740 and 1730 cm^{-1} that reflect non-hydrogen bonded and hydrogen bonded lipid ester carbonyls, respectively. A membrane with a tighter lateral packing has less water penetration into the bilayer interfacial region and thus a greater proportion of ester carbonyls vibrating near 1740 cm^{-1}. For example, tightly packed gel phase membranes composed of PC/PA/Chol 3:1:1 membranes exhibit a much higher proportion of non-hydrogen bonded ester carbonyls near 1740 cm^{-1} than is observed in the same membranes in the liquid crystalline phase. Note that incorporation of the nAChR into the PC/PA/Chol 3:1:1 membrane leads to an increase in the proportion of non-hydrogen bonded lipid ester carbonyls suggesting a lateral tightening of the lipid bilayer, as noted previously (107).

Membrane films composed of PC/PA/Chol 3:1:1.

Spectra of the PC/PA/Chol 3:1:1 membrane films at 22.5 °C exhibit a relatively high C-H stretching frequency near 2852 cm^{-1} and a relatively large proportion of hydrogen bonded lipid ester carbonyls, as expected for a bilayer above its gel-to-liquid crystalline phase transition (compare Fig. 3.1a and 3.1b, middle traces). At this temperature, the average dichroic ratio for the C-H symmetric stretching and the ester carbonyl stretching vibrations are 1.18 and 1.34, respectively, which compare well with the values of 1.30 and 1.4, respectively, obtained by Hubner and Mantsch for DPPC membrane films in the liquid crystalline phase (93). The dichroic ratio of the C-H stretching

Figure 3.1

A comparison between polarized FTIR spectra of PC/PA/Chol 3:1:1 membranes collected at -5°C (top traces) and at 22.5°C (middle traces) and reconstituted nAChR PC/PA/Chol 3:1:1 membranes (bottom traces). FTIR spectra of the membranes were recorded with either perpendicular polarized light (dashed lines) or parallel polarized light (solid lines). The spectra collected with perpendicular polarized light were scaled by a factor of two to account for differences in the evanescent field strength. The acyl chain C-H stretching bands are illustrated in panel A, the lipid ester carbonyl stretching band is illustrated in panel B, and the deconvolved lipid ester carbonyl stretching band is illustrated in panel C. Spectra were deconvolved between 1800 - 1600 cm^{-1} using gamma factor 10 and smoothing 80%.

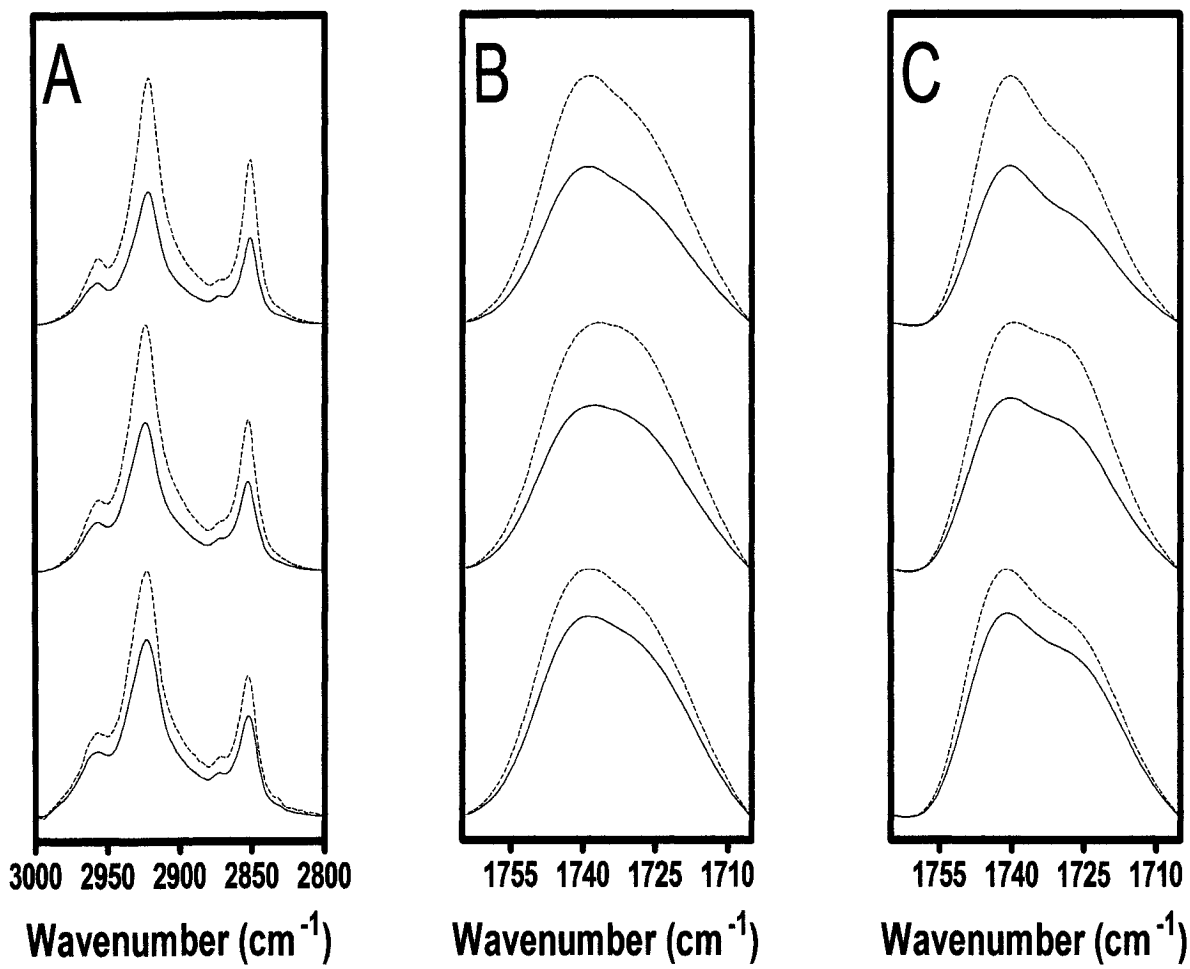
A
B
C
3000 2950 2900 2850 2800
1755 1740 1725 1710
1755 1740 1725 1710
Wavenumber (cm-1)
Wavenumber (cm-1)
Wavenumber (cm-1)

vibration corresponds to an order parameter, $S_{acyl} = 0.64$, which is lower than the value expected for an ordered saturated chain in a membrane film with no mosaic spread. It is possible that the drop in S_{acyl} is due mainly to the mosaic spread of the lipid film. As noted, however, the molecular order parameter, S_{acyl}, also reflects local acyl chain motions in the liquid crystalline phase and any deviation of the average C-H bond angle away from perpendicular to the bilayer normal, as should occur near the unsaturated bond in the oleoyl chain.

To estimate the contributions of local acyl chain motions to both the observed dihroic ratio and the resulting order parameter, S_{acyl}, we collected linear dichroism spectra from the PC/PA/Chol 3:1:1 membranes as the temperature was lowered from 35 °C down to -10 °C. As the PC/PA/Chol 3:1:1 membrane film is cooled below the gel-to-liquid crystalline phase transition, the peak absorption frequency of the C-H stretching vibration decreases by roughly 2 cm^{-1} and the lipid ester carbonyl band changes shape in manner indicative of an increase in the proportion of non-hydrogen bonded lipid ester carbonyls (Fig. 3.1a and 3.1b, upper traces). The latter reflects a lateral tightening of the lipid bilayer and a consequent decrease in the degree of water penetration into the bilayer interfacial region.

In the gel phase, the dichroic ratio for the acyl chain C-H symmetric stretching vibration decreases from 1.18 down to a value of 1.00, which corresponds to an increase in the order parameter from 0.64 to 0.82 (Fig. 3.2). This value is close to the value of 1.1 reported by Hubner and Mantsch for DPPC in the gel phase (93). A molecular order parameter of 0.82 is closer to the order parameter expected for a perfectly ordered saturated membrane with C-H transition dipoles oriented perpendicular to the bilayer normal. Our results show that the pure lipid films are highly

Figure 3.2

The dependence of the PC/PA/Chol 3:1:1 membrane acyl chain C-H symmetric stretching vibration dichroic ratio (**A**) and order parameter (**B**) on temperature.

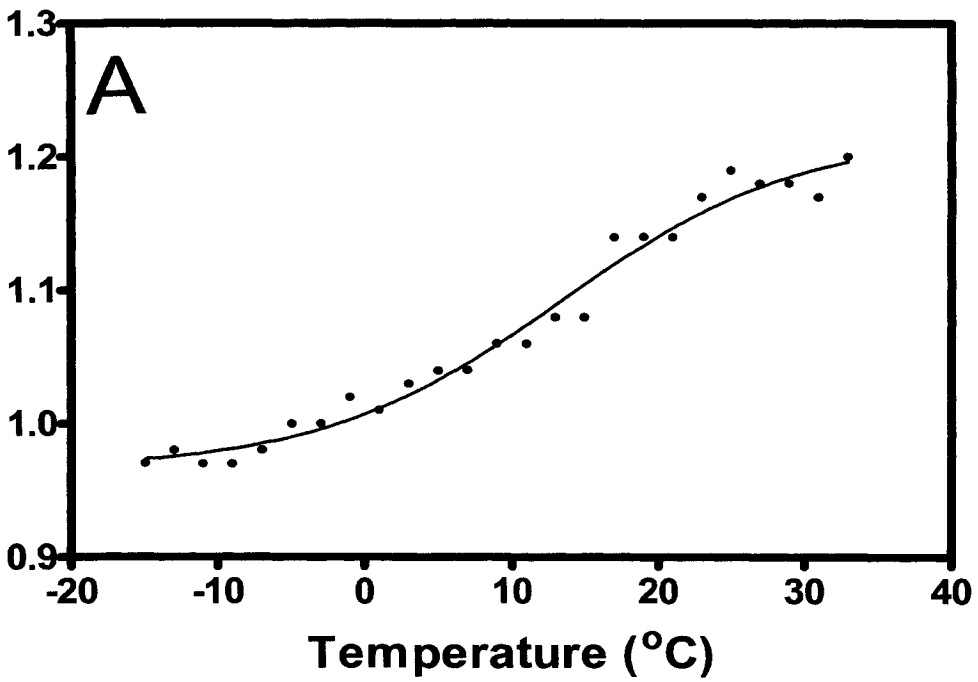
A
1.3
1.2
1.1
1.0
0.9
-20
-10
0
10
20
30
40
Temperature (°C)

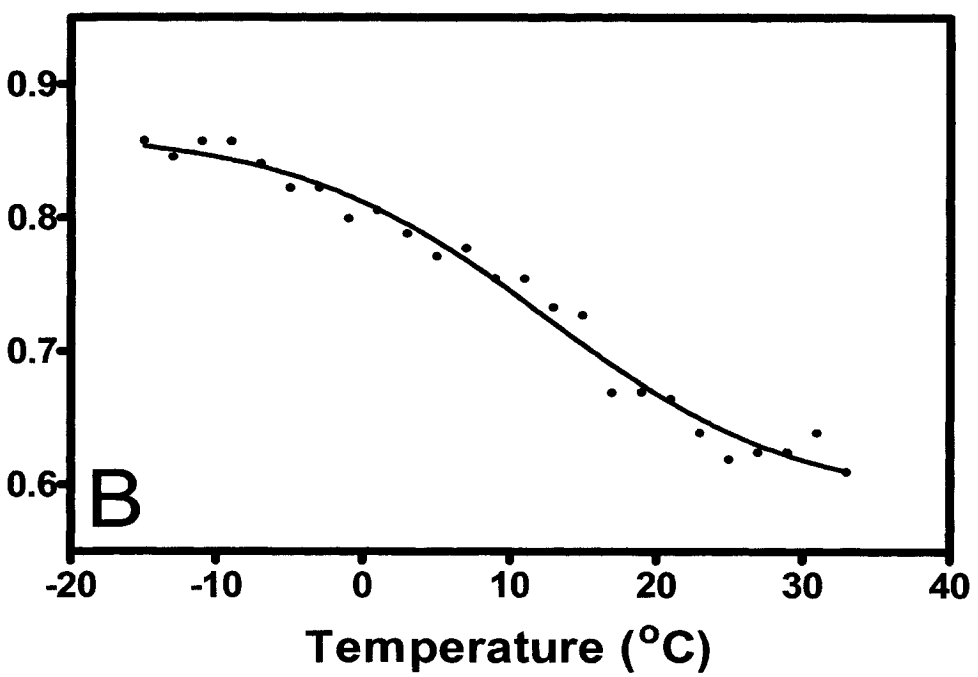
B
0.9
0.8
0.7
0.6
-20
-10
0
10
20
30
40
Temperature (°C)

ordered on the germanium IRE, and that mosaic spread contributes an order parameter of at most $S_{bilayer} = 0.82$. Although a value of 0.82 likely represents an overestimate of the contribution of $S_{bilayer}$ to S_{acyl} due to the acyl chain unsaturation (see above), the similarity of the values obtained for saturated DPPC lipids may suggest that mosaic spread contributes substantially to the disordering reflected in the molecular order parameter.

Reconstituted nAChR Membranes composed of PC/PA/Chol 3:1:1.

The dichroic ratios observed for the pure lipid bilayer films were next compared to those obtained from membrane films formed using reconstituted nAChR membranes (Table 3.1). At room temperature, the dichroic ratio for the C-H symmetric stretching vibration is 1.30, which is comparable to values observed for lipids in other reconstituted membranes (linear dichroism ATR-FTIR spectra collected of rhodopsin measured an C-H symmetric stretching vibration dichroic ratio of 1.34 (108), but higher than observed for the pure PC/PA/Chol 3:1:1 membranes. A dichroic ratio of 1.30 corresponds to a molecular order parameter, $S_{acyl} = 0.51$. In the gel phase, the dichroic ratio of the C-H stretching vibration drops to 1.15, which corresponds to a molecular order parameter of 0.66. As in the case of the liquid crystalline bilayers, the value of S_{acyl} obtained for the reconstituted membranes in the gel phase is greater than the S_{acyl} obtained for the pure PC/PA/Chol 3:1:1 membrane films under the same conditions (Table 3.1).

The difference in molecular order parameters observed for the pure and reconstituted PC/PA/Chol 3:1:1 membranes could reflect either an increase in the mosaic spread of the reconstituted bilayer films or an increase in the local motions (*trans-gauche* isomerizations) of the fatty acyl chains in the presence of the nAChR, or a combination of both. While the dichroic ratios do not allow us to distinguish between the various possibilities, previous studies have shown that

Table 3.1

Comparison between dichroic ratios and order parameters for the lipid ester carbonyl stretching vibration and acyl chain symmetric stretching vibration between PC/PA/Chol 3:1:1 membranes and reconstituted nAChR PC/PA/Chol 31:1 membranes at temperatures above and below the phase transition temperature.

- nAChR

Assignment	-5 °C			22.5 °C		
	Wavenumber (cm^{-1})	R_{ATR}	S	Wavenumber (cm^{-1})	R_{ATR}	S
$\nu CH_{2\ sym}$	2852.09	1.00	0.82	2853.13	1.18	0.64
$\nu C=O$	1733.07	1.27	-0.268	1732.79	1.34	-0.239

+ nAChR

Assignment	-5 °C			22.5 °C		
	Wavenumber (cm^{-1})	R_{ATR}	S	Wavenumber (cm^{-1})	R_{ATR}	S
$\nu CH_{2\ sym}$	2851.61	1.15	0.66	2852.60	1.30	0.51
$\nu C=O$	1733.06	1.33	-0.24	1733.22	1.45	-0.19

incorporation of the nAChR into bilayers, such as PC/PA/Chol 3:1:1, that contain the anionic lipid PA leads to a lateral tightening of the bilayer and an increase in the gel-to-liquid crystalline phase transition (107). Indeed, the carbonyl stretching vibrations recorded here show that incorporation of the nAChR into the PC/PA/Chol 3:1:1 membranes leads to an increase in non-hydrogen bonded ester carbonyls likely due to a lateral tightening of the lipid bilayer (Fig. 3.1, bottom traces). Based on these observations, it is likely that the increased dichroic ratio of the C-H stretching vibration and consequent decrease in molecular order parameter of the acyl chain in the presence of the nAChR are due to an increased mosaic spread of the reconstituted nAChR membranes relative to the pure lipid bilayers. A slight increase in mosaic spread is not surprising given that the reconstituted membrane films were prepared from unilamellar lipid vesicles, as opposed to the pure lipid films that were prepared after drying lipids from chloroform on the IRE surface. In addition, the nAChR extends beyond the surface of the bilayer, possibly contributing to the mosaic spread (17, 56).

Based on the above data, it is possible to calculate the mathematical limits for the contribution of mosaic spread to the molecular order parameter obtained for the reconstituted lipid membrane films. If the deviation in the molecular order parameter, S_{acyl}, from 1 down to 0.66 for the reconstituted membranes in the gel phase is due entirely to mosaic spread, then we can calculate a *maximal* mosaic spread corresponding to an $S_{bilayer} = 0.66$, although as noted this is not entirely likely due to acyl chain unsaturation. Alternatively, if we assume that the films formed using the lipid alone exhibit no mosaic spread (i.e. are perfectly oriented perpendicular to the IRE surface), then we can attribute the deviation of the molecular order parameter in the pure bilayer system from 1.0 down to 0.82 to the distortion of the acyl chains and thus the C-H stretching transition dipole away from the bilayer planar surface as a result of acyl chain unsaturation. As similar orientational

effects of the unsaturated bond on the oleoyl chain would likely occur in the reconstituted membranes, we can mathematically remove the average orientational effects from S_{acyl}. In this case, the drop in S_{acyl} for the reconstituted membranes that is due to mosaic spread, $S_{bilayer}$, is equivalent to 0.66/0.82. The *minimal* mosaic spread for the reconstituted membrane film is thus $S_{bilayer} = 0.81$. The true mosaic spread lies somewhere between these two limits, i.e. $0.66 < S_{bilayer} < 0.81$.

Orientation of the nAChR.

Infrared spectra recorded from the reconstituted membranes exhibit two main protein bands that are sensitive to the structure and orientation of secondary structural features in the nAChR. The amide I vibration (1600 – 1700 cm^{-1}) is due mainly to peptide C=O stretching and is highly sensitive to both hydrogen bonding and protein secondary structure. The amide II vibration (1620 – 1580 cm^{-1}) is due mainly to peptide N-^{1}H bending. This vibration shifts down in frequency to near 1450 cm^{-1} upon the exchange of peptide N-^{1}H for N-^{2}H. The residual amide II vibration intensity in spectra of the nAChR recorded in ^2H_2O is a measure of the number of peptide hydrogens that remain in the protiated form (109, 110).

After 72 hours exposure of the nAChR to ^2H_2O at 4 °C, the amide I band shape is relatively broad and symmetric with a maximum around 1640 cm^{-1} (48, 109, 111). Deconvolution shows that this broad band is composed of two main peaks centered near 1655 and 1630 cm^{-1} due to peptides in α-helical and β-sheet secondary structures, respectively. The residual amide II band intensity indicates that roughly 25% of the peptide hydrogens remain unexchanged for deuterium after 72 hours in ^2H_2O (48). Further exchange of these exchange resistant peptide hydrogens for deuterium under conditions, such as alkaline pH, that enhance peptide hydrogen-deuterium exchange leads to a consequent downshift in frequency of the amide I component band near 1655 cm^{-1}, suggesting that

the exchange resistant peptides in the nAChR are predominantly α-helical (48). The exchange resistant α-helical peptide hydrogens likely reside within the transmembrane domain of the nAChR. We therefore assign the 1655 cm^{-1} amide I component band to α-helical transmembrane peptides.

We probed the orientation of this exchange resistant "core" by recording linear dichroism spectra of the nAChR after 72 hours exposure to ^2H_2O at 4 °C. In an α-helical peptide, the amide I and amide II transition dipoles are preferentially oriented parallel and perpendicular, respectively, to the long axis of the α-helix. An α-helix with a net preferential orientation parallel to the bilayer normal will give rise to a dichroic ratio greater than 2 for the amide I vibration and a dichroic ratio less than 2 for the amide II band. In contrast, an α-helix with a net orientation parallel to the bilayer surface will exhibit the opposite dichroism for the two vibrations, whereas an α-helix oriented at the magic angle of 54.7° should exhibit a dichroic ratio of 2 for both bands.

The linear dichroism spectra clearly show that the α-helical peptides in the exchange resistant core of the nAChR exhibit a preferential orientation parallel to the bilayer normal (Fig. 3.3). As expected the dichroism of the amide I and amide II bands are clearly greater and less than 2, respectively. Although a precise mathematical measure of this dichroism is difficult due to the presence of overlapping vibrations, we estimate the amide I dichroism near 1655 cm^{-1} be 2.37. Taking into account the possible contributions of mosaic spread to this value, the dichroic ratio suggests an average tilt of the transmembrane α-helices of between 44° and 46° relative to the bilayer normal.

Average tilt in the presence of Carb.

The effect of desensitization on the average orientation of the transmembrane α-helices was determined by recording linear dichroism spectra in the presence and absence of the agonist

Figure 3.3

Polarized FTIR spectra of reconstituted nAChR PC/PA/Chol 3:1:1 membrane films. FTIR spectra collected with perpendicular polarized light (dashed lines) were scaled by a factor of two to account for differences in the evanescent field strength. FTIR spectra collected with parallel polarized light are illustrated by the solid lines.

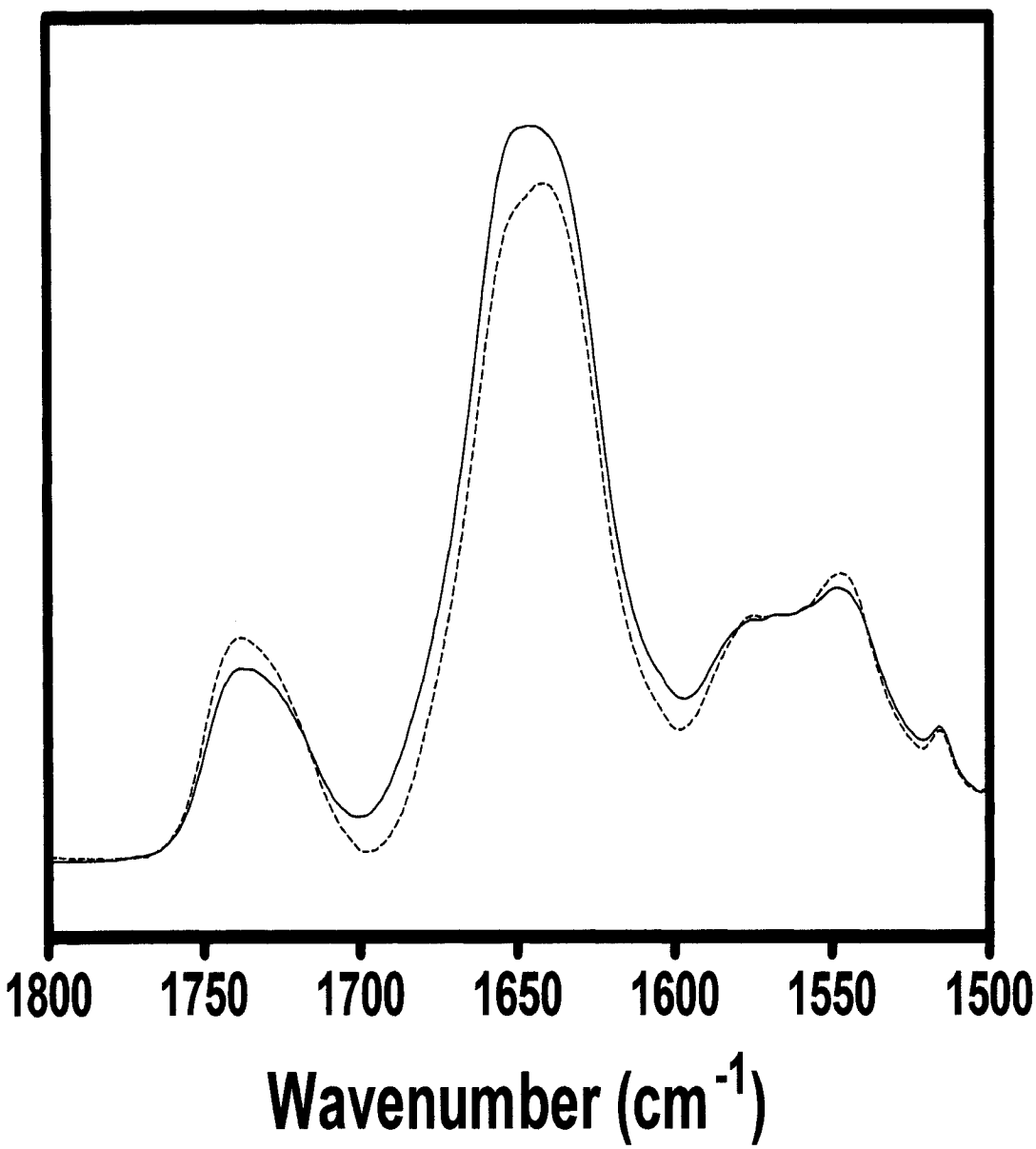
1800
1750
1700
1650
1600
1550
1500
Wavenumber (cm-1)

carbamylcholine (Carb). In the absence of Carb, the nAChR adopts predominantly a low affinity acetylcholine binding resting conformation (86). After prolonged exposure to Carb, the nAChR adopts a relatively high affinity acetylcholine binding desensitized state. The linear dichroism spectra recorded from the nAChR in the presence of Carb are virtually identical to those recorded in its absence (Fig 3.4). These results show that the nAChR does not undergo substantial net changes in the orientation of transmembrane α-helices upon agonist binding and desensitization. This result is consistent with FTIR difference spectra, which show that there are only subtle changes in the structure of the nAChR upon desensitization (111, 112).

SUMMARY AND DISCUSSION

In the absence of a complete crystal structure ATR-FTIR spectroscopy remains one of the best tools available to investigate the structural composition and organization of such large membrane proteins such as the nAChR. While the thickness of the membrane film, the extent of disorder within the lipid bilayer, and the presence of contaminants in the system are o little importance in conventional ATR-FTIR spectroscopy, they are of critical importance in polarized ATR-FTIR spectroscopy (see below). It is therefore paramount to carefully characterize one's membrane system before meaningful conclusions may be drawn. We began our study of the orientational arrangement of the nAChR transmembrane helices by carefully examining the mosaic spread of our membrane films.

Although it is customary to assume a perfect mosaic spread of one's membranes on the IRE surface, this is rarely true, especially of reconstituted films. Comparing the acyl chain order parameters calculated from polarized spectra of nAChR-reconstituted PC/PA/Chol 3:1:1 membranes and pure PC/PA/Chol 3:1:1 membranes revealed that neither system achieved a perfect mosaic

Figure 3.4

Deconvolved polarized FTIR spectra of reconstituted nAChR PC/PA/Chol 3:1:1 membrane films in the absence (**A**) and presence (**B**) of 1 mM Carb. Spectra were deconvolved between 1900 - 1300 cm^{-1} using gamma factor 7 and smoothing 80%. Deconvolved FTIR spectra collected with perpendicular polarized light (dashed lines) were scaled by a factor of two to account for differences in the evanescent field strength. FTIR spectra collected with parallel polarized light are illustrated by the solid lines.

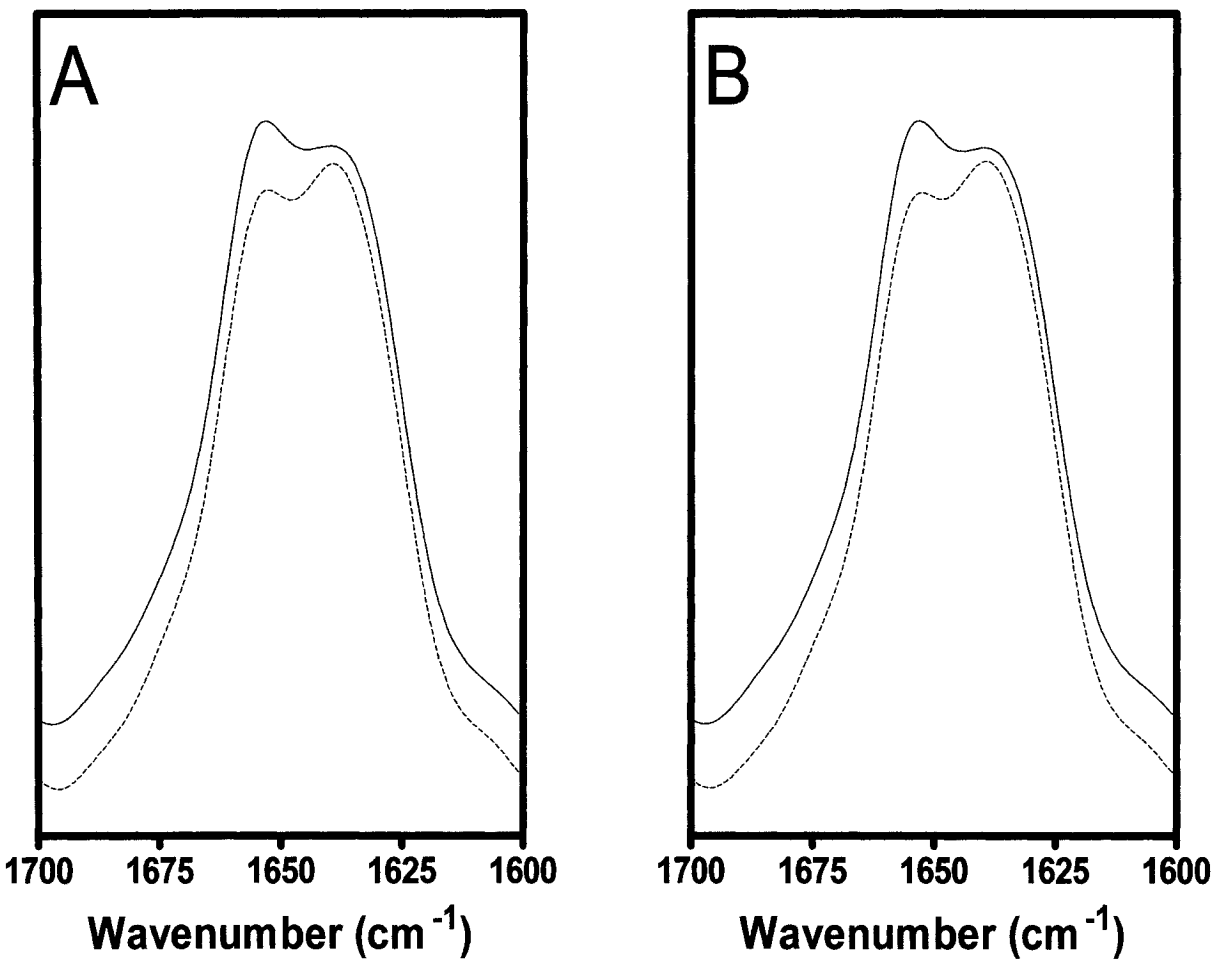
A
1700
1675
1650
1625
1600
Wavenumber (cm -1)
B
1700
1675
1650
1625
1600
Wavenumber (cm -1)

spread, even in the more ordered gel state. Moreover, the order parameters calculated from the reconstituted films were consistently less than the order parameters calculated from the pure PC/PA/Chol 3:1:1 membrane films. It is difficult to discriminate between an increase in chain distortion within and an increase in film mosaic spread in the nAChR reconstituted films, relative to the pure PC/PA/Chol 3:1:1 membrane films. However, previous studies in our laboratory have shown that incorporation of the nAChR into bilayers, such as PC/PA/Chol 3:1:1, that contain the anionic lipid PA leads to a lateral tightening of the bilayer (107). Therefore the decrease in molecular order parameter of the acyl chain in the presence of the nAChR can be attributed to an increased mosaic spread of the reconstituted nAChR membranes, rather than an increase in chain tilt or chain disordering. This apparent disordering of the nAChR reconstituted films is not surprising since the pure PC/PA/Chol 3:1:1 membrane films were prepared from chloroform solutions, whereas the reconstituted films were prepared from plated membrane vesicles.

Additionally, by minimizing the contribution arising from the molecular motions and gauche conformers in the acyl chains to the order parameter, the contribution of the nAChR-induced increase in mosaic spread in the membrane films was quantified. The *maximal* contribution from the mosaic spread was determined to be 0.66, whereas the *minimal* contribution from the mosaic spread was determined to be 0.81, with the true mosaic spread somewhere between these two limits.

With the organization and behaviour of the nAChR reconstituted PC/PA/Chol 3:1:1 membrane films more clearly characterized, the orientation of the nAChR transmembrane α-helices were examined. Polarized ATR-FTIR spectra collected of the nAChR reconstituted into PC/PA/Chol membranes identified dichroism in both the amide I and amide II bands. The dichroism in the amide I band was focused at the 1652 cm^{-1} peak and indicates a preferential orientation parallel

to the membrane surface normal, whereas the dichroism in the amide II band was focused on the 1545 cm^{-1} peak, and indicates a preferential orientation perpendicular to the membrane surface normal. Previous studies have found that 25% of the nAChR peptide hydrogens are resistant to hydrogen-deuterium exchange, even after 72 hours exposure of the nAChR to ^2H_2O at 4 °C (48), and that these unexchanged peptides give rise to a strong amide I component band near 1655 cm^{-1}, characteristic of α-helical peptide hydrogens. Since this exchange resistant core is likely made up of peptides located in the transmembrane domain, we assign the 1652 cm^{-1}peak of the amide I band to α-helical transmembrane peptides. Based on our characterization of the contribution of the mosaic spread to the order parameter, the dichroism in the 1652 cm^{-1}peak suggests an average tilt of the α-helix axis of between 44° and 46° relative to the bilayer normal.

Lastly, the orientation changes in the nAChR transmembrane domain, as it undergoes the resting to desensitized conformational change, were examined. Polarized FTIR spectra of the nAChR reconstituted into PC/PA/Chol membranes in the presence and absence of carbamylcholine were collected and no significant differences between spectra were observed. The absence of any discernable difference between the absolute absorbance spectra collected of the receptor in the absence (mostly resting state) and in the presence (desensitized state) of the desensitizing ligand Carb suggests the orientational changes upon desensitization are small. This result is consistent with FTIR difference spectra which show that there are only subtle changes in the structure of the nAChR upon desensitization (111, 112).

To our knowledge this work represents the first quantification of a membrane film's mosaic spread on an IRE surface. Although it is customary to assume a perfect mosaic spread of one's membranes on an IRE surface, this approach may be flawed. Since the angle of orientation for the

molecular structure of interest will be determined from the measured order parameter, inaccuracies in the order parameter may manifest as inaccurate angles of orientation and erroneous conclusions. The extent of contamination within the membrane films and the distortion within the membrane bilayers and multilayers, created by plating reconstituted membrane vesicles, will contribute to the membrane system mosaic spread which contributes to the measured order parameter. The greater the mosaic spread of the films, the greater the error in the angle of interest may be, if ignored. A careful characterization of one's membrane system, as described in this work, can help reduce such errors and improve the quality of the work.

Given the ability for polarized FTIR spectroscopy to be combined with time-resolved and difference techniques, it has the unique potential to examine the subtle changes in protein structure and environment as it moves from resting to active to inactive conformational states. A careful characterization of one's membrane system can help reduce errors, improve accuracy, and may aid in the elucidation of protein mechanisms of action.

CONCLUSIONS

The orientation of the hydrogen-deuterium exchange resistant "core" of the of the intact nicotinic acetylcholine receptor from *Torpedo* was studied using linear dichroism attenuated total reflectance infrared spectroscopy both in the presence and absence of the agonist Carb. Our results show that the hydrogen exchange resistant α-helical peptide hydrogens in the nAChR are preferentially oriented parallel to the bilayer normal, therefore, providing evidence for a predominantly α-helical transmembrane domain, and that there are no detectable net changes in orientation upon agonist-induced desensitization. We also examined the linear dichroism of lipid bands in spectra recorded from membranes both with and without the nAChR in order to accurately

assess the effects of membrane film mosaic spread on the interpretation of the linear dichrosm data. Our data also show that the mosaic spread of the reconstituted membrane films is greater than the mosaic spread observed with pure lipid films. Our work illustrates the importance of mosaic spread characterization when interpreting experimental order parameters in terms of molecular structure orientation.

CHAPTER 4

PHYSICAL INTERACTIONS BETWEEN ACETYLCHOLINE AND THE NICOTINIC ACETYLCHOLINE RECEPTOR

INTRODUCTION

The binding of a signaling molecule to an integral membrane receptor is a key event in many biological processes, including cell growth, intercellular communication, sensory perception, etc. Understanding the chemistry of membrane receptor-ligand interactions is thus central to understanding many biological phenomena. Because membrane receptors are the targets of pharmaceutical products, membrane receptor-ligand interactions are also of particular interest to the pharmaceutical industry. Unfortunately, the modern physical methodologies commonly used to probe the structural features responsible for receptor-ligand interactions are still limited in their application to membrane-imbedded receptors.

The chemical nature of receptor-ligand interactions at the post-synaptic membrane have been studied intensively for the nicotinic acetylcholine receptor (nAChR) from *Torpedo*. Each of the two acetylcholine (ACh) binding sites on the nAChR consists of two subsites, an esterophilic subsite that binds the ester functional group of ACh and an anionic subsite that binds the quaternary ammonium cation (113, 114). Sequence analysis, affinity labeling, and site-directed mutagenesis identify both aromatic and negatively charged residues in the anionic subsite that likely interact with the charged nitrogen of ACh via cation-pi electron ($\oplus$-π) interactions and/or hydrogen bonding (115-121). The crystal structure of the homologous ACh binding protein confirms the essential role for tyrosine and tryptophan residues in the anionic subsite (20). The nature of the chemical interactions that occur between ACh and the esterophilic subsite, remain, remain poorly understood.

Infrared difference spectroscopy is a technique that has been used extensively to probe the subtle changes in chemical structure and/or local environment that are associated with protein conformational change [reviewed in (122)]. The difference between spectra of the nAChR recorded

in the presence and absence of the agonist carbamylcholine (Carb) exhibits a complex pattern of positive and negative bands that reflects shifts in the intensities and/or frequencies of vibrations from those amino acid residues whose structures are altered upon Carb binding (98, 112). Difference spectroscopy has been used to map the conformational states of the nAChR stabilized by both a variety of ligands and upon reconstitution into lipid bilayers of varying lipid compositions (123-126). The difference spectra also contain vibrational information pertaining to the physical interactions that occur between Carb and nAChR binding site residues. Extensive band overlap, however, has thus far limited interpretation of the latter in terms of either the types of amino acid side chains involved or the precise nature of the physical interactions that occur between protein side chains and Carb.

The ambition of this study was to elucidate the nAChR-ligand interactions by infrared difference spectroscopy. To circumvent the problems of extensive band overlap, we developed a new "double ligand difference" method that can be used to isolate the vibrational features from protein side chains that interact directly with individual functional groups on a small molecule ligand. This new double ligand approach allows one to map individual ligand-receptor contacts and simplifies the difference spectra allowing for a more detailed interpretation of the data. We show here that the frequencies of two main protein vibrations are altered when the nAChR interacts with the carbonyl oxygen of Carb. The frequencies of the detected vibrational bands suggest that an arginine residue in the esterophilic subsite forms a hydrogen bond with the ester carbonyl, likely mediated by a water molecule. The results provide new insight into the nature of nAChR-ligand interactions and demonstrate the potential of infrared difference spectroscopy for dissecting the physical interactions that occur between a membrane receptor and its bound ligand.

EXPERIMENTAL PROCEDURES

SAMPLE PREPARATION

The nAChR from frozen Torpedo californica electric tissue (Marinus) was affinity-purified as described in chapter 3, "experimental procedures", and reconstituted into membranes composed of either 3:1:1 egg phosphatidyl-choline/dioleoylphosphatidic acid/cholesterol or asolectin (102). Both lipid compositions stabilize the nAChR in a conformation that conducts cations across the membrane and undergoes agonist-induced desensitization (125).

FTIR DIFFERENCE SPECTROSCOPY

FTIR samples were prepared by spreading 250 mg of the affinity purified nAChR on the surface of a 50 x 20 x 2 mm (length x width x depth) germanium IRE (Harrick, Ossining, NY). After evaporating the bulk solvent with a gentle stream of N_2 gas, the germanium IRE was installed in an ATR liquid sample cell (also from Harrick) and the nAChR film rehydrated with excess Torpedo Ringer buffer (250 mM NaCl, 5 mM KCl, 2 mM $MgCl_2$, 3 mM $CaCl_2$ and 20 mM Tris, pH 7.0). FTIR spectra of the nAChR film were then acquired using the ATR technique on an FTS-575 spectrometer (Bio-Rad, Cambridge, MA) equipped with a DTGS detector. A schematic diagram of the attenuate total reflectance cell used to record the spectra is shown in Figure 4.1. Spectra were recorded at 8 cm^{-1} resolution using 512 scans each, which required roughly seven minutes per spectrum. For the difference measurements, two consecutive spectra of the nAChR in the resting state were recorded while flowing Torpedo Ringer buffer continuously through the sample compartment of the ATR cell at a rate of ~1.5 ml/min. The flowing buffer was then switched to an identical one containing 50 μM Carb. After one minute, a spectrum was recorded of the nAChR in the desensitized state. The difference between both the two resting state spectra (referred to as a control spectrum) and the consecutive resting and desensitized state spectra (referred to as a Carb-

Figure 4.1

Schematic diagram of the attenuated total reflectance cell used to record FTIR difference spectra. Spectra were recorded from an nAChR film deposited on the surface of a germanium internal reflection element while flowing either wash (-) or trigger (+) buffer past the film surface. All difference spectra presented in this report are the difference between spectra of the same nAChR sample recorded in the presence of the wash and trigger buffers (see "Experimental Procedures").

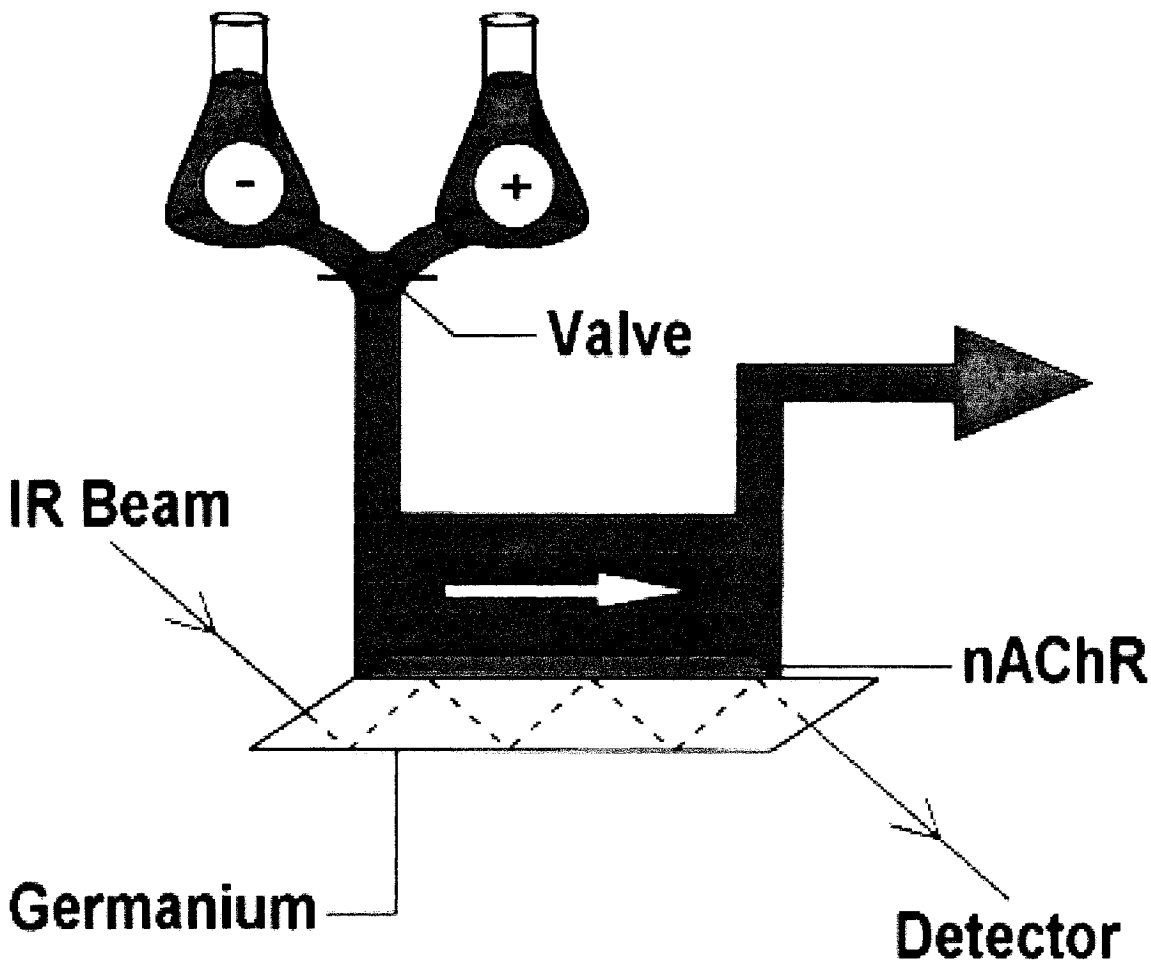
-
+
Valve
IR Beam
nAChR
Germanium
Detector

difference spectrum) were calculated, stored and the flowing solution switched back to buffer without Carb. After a 20 minute washing period to remove Carb from the film and to convert the nAChR back into the resting conformation, the process was repeated several times and the individual Carb-difference spectra averaged to increase the signal-to-noise ratio. Each Carb-difference spectrum presented is an average of 30-90 spectra recorded from at least two separate affinity purifications and reconstitutions of the nAChR. All difference spectra were baseline-corrected between 1800 and 1000 cm^{-1}, were interpolated to an effective resolution of 4 cm^{-1} and were normalized by comparing the intensity of those bands that reflect the vibrations of nAChR-bound Carb.

Tetramethylamine (TMA) R→D difference spectra were recorded as described above, except that the trigger buffer contained 1 mM TMA instead of 50 μM Carb. Carb desensitized-to-desensitized (D→D) difference spectra were recorded as described above for the Carb R→D difference spectra, except that the wash and trigger buffers both contained 200 μM dibucaine so that the nAChR was bathed continuously with dibucaine and thus maintained throughout the experiment in the desensitized state.

DOUBLE LIGAND DIFFERENCE SPECTRA

The double ligand difference spectra were recorded as described above for the Carb R→D difference spectra except that one ligand (either Carb or ACh) was included in the trigger buffer while the other ligand (either TMA or choline) was included in both the wash and trigger buffers (see Fig. 4.2 for a schematic detailing the molecular structures of agonists used in this study). In the Carb-TMA difference spectrum, for example, the trigger buffer contained 50 μM Carb and both the wash and trigger buffers contained 1 mM TMA. Two spectra of the nAChR with TMA bound to

Figure 4.2

A schematic diagram depicting the molecular structures of the agonists used in this study.

CARBAMYLCHOLINE

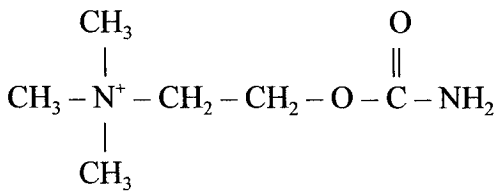

ACETYLCHOLINE

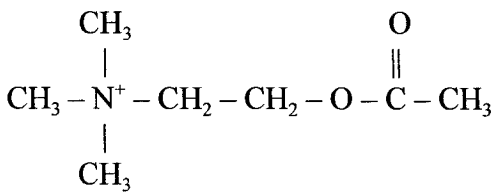

CHOLINE

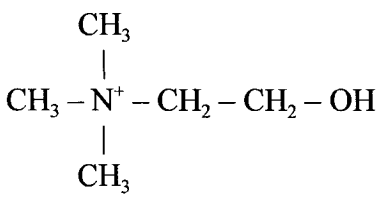

TETRAMETHYLAMMONIUM

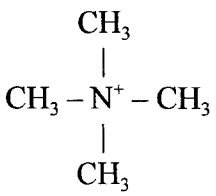

the neurotransmitter site were recorded. The flowing wash buffer was then switched to the trigger buffer, which contains sufficient Carb to displace TMA from the neurotransmitter binding site. The differences between both the two spectra recorded with TMA bound and the consecutive spectra recorded with first TMA and then Carb bound to the nAChR were calculated and stored, and the process was repeated many times. For the Carb-choline difference, the trigger buffer contained both 50 μM Carb and 10 mM choline, and the wash buffer contained 10 mM choline. For the ACh-TMA difference, the trigger buffer contained both 100 μM ACh and 1 mM TMA, and the wash buffer contained 1 mM TMA. For the ACh-minus-choline difference, the trigger buffer contained both 100 μM ACh and 10 mM choline, and the wash buffer 10 mM choline.

RESULTS AND INTERPRETATION

The difference between spectra of the nAChR recorded in the presence and absence of the agonist Carb (referred to as a Carb R→D difference spectrum) exhibits a pattern of positive and negative bands (Fig. 4.3, middle trace) that is absent in control difference spectra recorded from α-bungarotoxin-treated nAChR membranes (112). These bands reflect three related phenomena: 1) vibrations of Carb bound to the nAChR, 2) vibrational changes in the nAChR that occur upon the formation of physical interactions, such as hydrogen bonds, ⊕-π interactions, etc., between Carb and neurotransmitter binding site residues, and 3) vibrational changes in the nAChR that result from the Carb-induced R→D conformational transition.

To interpret the Carb R→D difference spectrum, bands were first assigned to each of the three related phenomena noted above. Bands due to nAChR-bound Carb were identified by comparing band frequencies in the difference spectrum with those observed in solution spectra of Carb (light

Figure 4.3

A comparison of the Carb R→D and the Carb D→D difference spectra (**A**). A Carb R→D difference spectrum (middle trace) is obtained by subtracting a spectrum recorded from the nAChR in the unliganded resting conformation from a spectrum recorded from the nAChR in the Carb-bound desensitized conformation (see accompanying schematic). Carb R→D difference spectra exhibit positive bands due to nAChR-bound Carb (identified by the dotted lines) that are evident at frequencies close to those observed for bands in the solution spectrum of Carb (top trace, the background H_2O spectrum has been subtracted). Carb R→D difference spectra also exhibit positive bands that reflect the R→D conformational change (identified by the dashed lines). These bands are absent in Carb D→D difference spectra (bottom trace). A Carb D→D difference spectrum is calculated by subtracting a spectrum of the nAChR in a Carb-free desensitized conformation from a spectrum of the nAChR in the Carb-bound desensitized conformation (see accompanying schematic). In this case, the nAChR was maintained in a desensitized state by incubating with the desensitizing local anesthetic dibucaine. Note that dibucaine binds to the two neurotransmitter sites as well as to the ion channel pore to induce desensitization. Intensity variations between the Carb D→D and Carb R→D difference spectra that are not discussed in the text reflect displacement of dibucaine from the neurotransmitter sites upon Carb binding and are discussed in detail in Ref. [126]. (**B**) A schematic diagram illustrating the events in a typical Carb R→D difference spectrum (top schematic), and the events in a typical Carb D→D difference spectrum (bottom schematic).

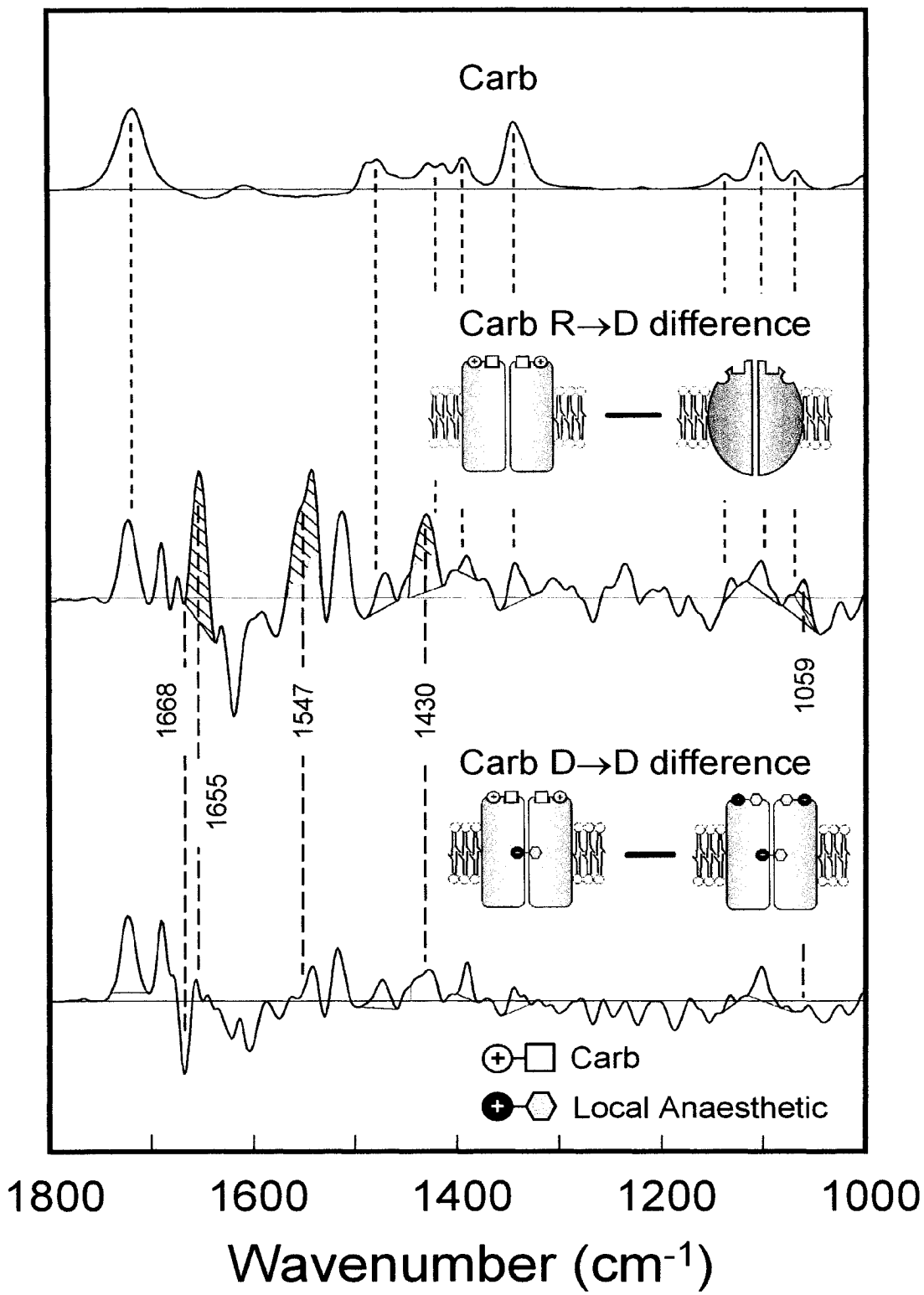
Carb
Carb R→D difference
1668
1655
1547
1430
1059
Carb D→D difference
Carb
Local Anaesthetic
1800
1600
1400
1200
1000
Wavenumber (cm-1)

shading in Fig. 4.3), as well as by similar comparisons of difference and solution spectra recorded using ACh and an isotopically labeled derivative (112). Bands that reflect the structural changes associated with the R→D conformational change were identified by recording Carb difference spectra from nAChR membranes that were maintained continuously in the desensitized state prior to (and after) Carb addition (referred to as a Carb D→D difference spectrum; Fig. 4.3, bottom trace). The resulting Carb D→D difference spectra consistently lack positive intensity centered near 1668, 1655, 1547, 1430, and 1059 cm^{-1} that is observed in the Carb R→D difference spectrum (123-126). These five positive bands in the Carb R→D difference spectrum thus reflect the main vibrational changes associated with transition of the nAChR from a resting to the desensitized state (hatched shading in Fig. 4.3, middle trace). In contrast, bands that are not affected by desensitization and that are not attributable to nAChR-bound Carb must reflect vibrational changes in protein residues that occur upon the formation of physical interactions between Carb and the desensitized nAChR. These are not shaded in Figure 4.3.

The large number of bands not attributable to either nAChR-bound Carb or the R→D conformational transition highlights the fact that the Carb R→D difference spectrum contains substantial vibrational information regarding the nature of Carb-nAChR interactions. Several vibrational features are observed at frequencies consistent with the expected frequencies of side chains known to be located in the neurotransmitter binding site. The most notable is a relatively intense band near 1516 cm^{-1} that is characteristic of tyrosine (127). In addition, weak bands are observed in regions of the spectrum normally associated with the vibrations of tryptophan (near 1334 and 1455 cm^{-1}) and carboxylate (near 1580 cm^{-1} and between 1300 and 1400 cm^{-1}) residues. A number of other vibrations, most notably near 1620 cm^{-1}, could reflect interactions between Carb and

additional binding site residues (127). The difference spectra thus suggest a rich complexity of interactions between Carb and the nAChR.

To determine which vibrational features reflect interactions that occur between binding site residues and the quaternary ammonium of Carb, the difference spectra were recorded using the agonist analog TMA, which lacks the alkyl carbamylester functional moiety (third trace from top in Fig. 4.4). The TMA difference spectrum exhibits many of the same vibrational features observed in the Carb R→D difference spectrum, including bands near 1580, 1516, 1455, 1334, and between 1300 and 1400 cm^{-1} that are potentially attributable to the aromatic side chains of tyrosine and tryptophan and the carboxylate side chains of aspartic/glutamic acid. In fact, most of the bands in the Carb R→D difference spectrum that are potentially attributable to vibrational changes in residues interacting with Carb are also present in the TMA difference spectrum. This result provides direct experimental evidence that tyrosine and possibly both tryptophan and carboxylate residues interact in some manner with the quaternary ammonium. The result also shows that the interactions between the nAChR and Carb are dominated by interactions with the quaternary ammonium functional group.

The TMA difference spectrum also exhibits positive intensity at each of the five frequencies centered near 1668, 1655, 1547, 1430, and 1059 cm^{-1} that serve as markers of the R→D conformational transition. The positive intensity at each frequency suggests that exposure to TMA leads to a shift of the nAChR from a predominantly resting to a predominantly desensitized state. The ability of TMA to desensitize the nAChR is not surprising given that TMA is an agonist of the receptor (43, 128). The desensitizing capability of TMA was also confirmed in a separate fluorescence spectroscopic study of the interactions between the conformationally sensitive probe, ethidium bromide, and the nAChR (data not shown). The difference between spectra of the nAChR

Figure 4.4

A comparison of the Carb R→D (second from top trace) and the TMA R→D (third from top trace) difference spectra. Bands due to either nAChR-bound Carb or nAChR-bound TMA (identified by the dotted lines) correspond to similar bands in the solution spectra of Carb and TMA (top and bottom traces, respectively). The vibrational features in the two difference spectra that reflect the R→D conformational transition are identfied by the solid coloured lines. Bands near 1580, 1516, 1455, 1334, and between 1300 and 1400 cm^{-1} that likely reflect structural perturbations of tyrosine, tryptophan, and charged carboxylic acid residues are noted with the dashed lines (see text). The two asterisks denote regions in the TMA R→D difference spectrum that exhibit variations in intensity relative to the Carb R→D difference spectrum resulting from differences in how Carb and TMA bind to the nAChR (see text).

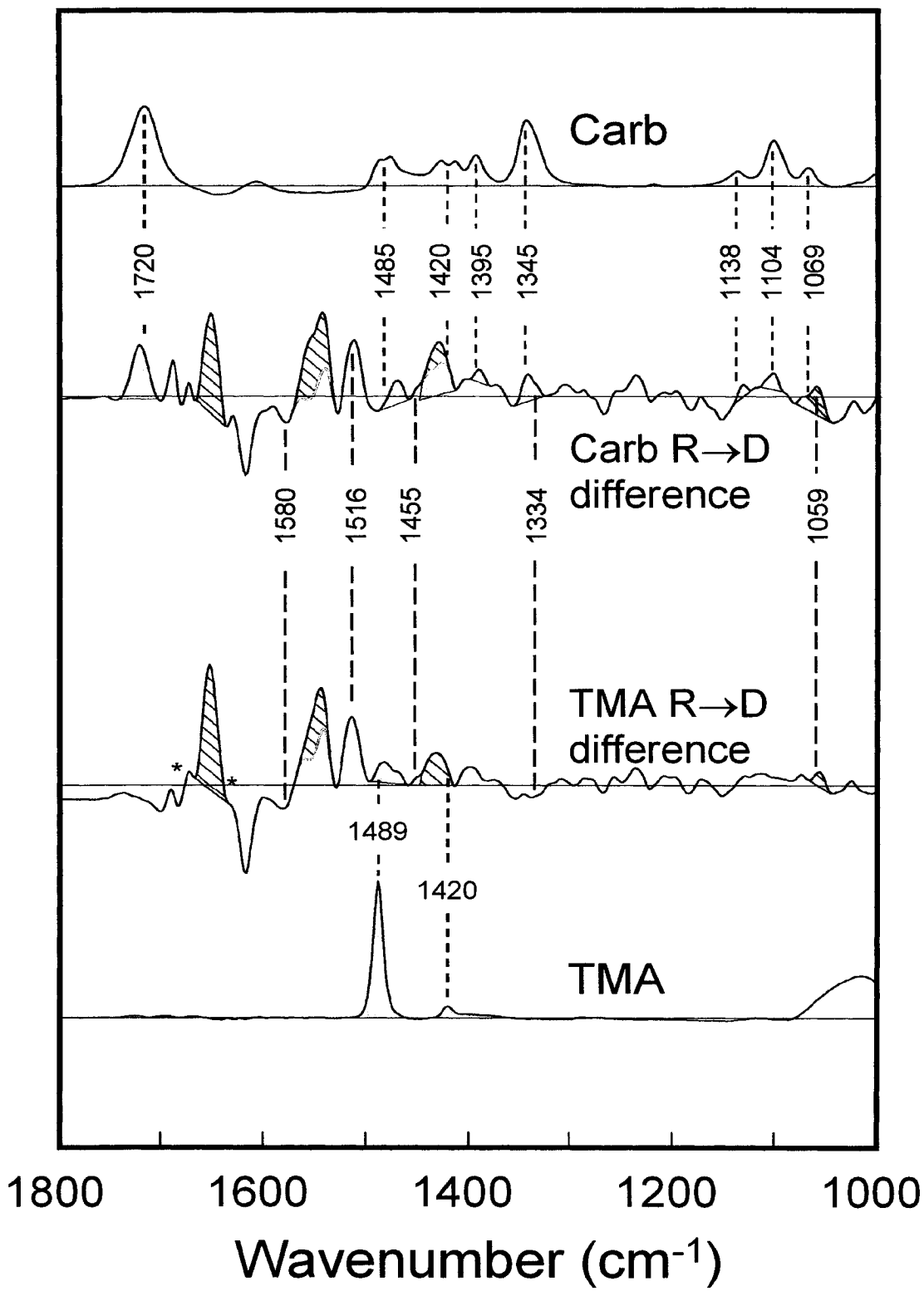
Carb
1720
1485
1420
1395
1345
1138
1104
1069
Carb R→D difference
1580
1516
1455
1334
1059
TMA R→D difference
1489
1420
TMA
1800
1600
1400
1200
1000
Wavenumber (cm-1)

recorded in the presence and absence of TMA is thus referred to as a TMA R→D difference spectrum.

In contrast to the similarities above noted, band intensity variations are evident near 1720, 1485, 1420, 1395, 1345, 1138, 1104, and 1069 cm^{-1} and between both 1690 and 1668 cm^{-1} and 1635 and 1630 cm^{-1}. The former reflect the different intrinsic vibrational frequencies and/or intensities of TMA versus Carb. The latter reflect differences in how the two ligands interact with the nAChR. Specifically, bands in the Carb R→D difference spectrum that are absent in the TMA R→D difference spectrum can be assigned to the vibrational changes that occur as a result of interactions between the alkyl carbamylester portion of Carb and residues in the esterophilic subsite.

A complete interpretation of both the Carb and TMA R→D difference spectra in terms of both the identities of the amino acids involved and the nature of the individual Carb-nAChR contacts is hampered by the extensive band overlap. Band overlap does not allow for visualization of many individual difference bands that serve as fingerprints of amino acid side chains. The downshifts in frequency of individual bands that occur upon exposure to ^2H_2O, which are diagnostic of specific side chains, are also lost in the overlapping band shifts that occur in Carb R→D difference spectra recorded in ^2H_2O versus H_2O (111). Moreover, the individual shifts in frequency that occur upon Carb binding to the nAChR, which are directly related to the nature of Carb-nAChR contacts, cannot be defined because of the spectral complexity.

To simplify the difference spectrum and thus permit a definitive interpretation of the data, we devised a novel double ligand difference method (illustrated schematically in Fig. 4.5). The idea was to calculate the difference between spectra of the nAChR recorded consecutively with TMA and then Carb bound to the neurotransmitter binding sites. Because both Carb and TMA stabilize the

Figure 4.5

Schematic diagram of the double ligand difference approach. Carb binding to the nAChR leads to interactions between Carb and the esterophilic subsite that are not present in the TMA-bound state. The difference between spectra of the nAChR recorded with either Carb or TMA-bound to the nAChR exhibits vibrational bands predominantly from the alkyl carbamylester portion of Carb as well as from side chains in the esterophilic subsite whose structures are altered upon interaction with the alkyl carbamylester portion of Carb.

Spectrum A (TMA)

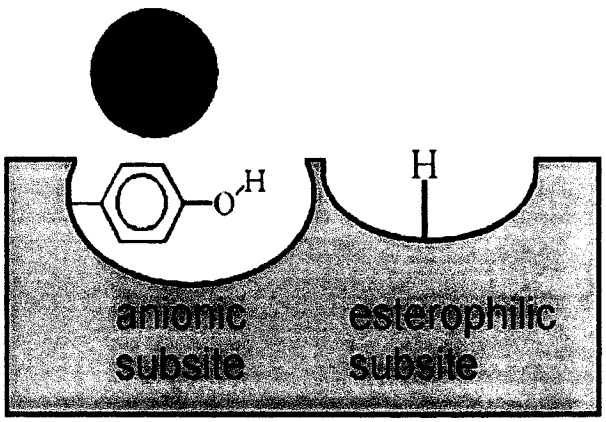

Spectrum B (Carb)

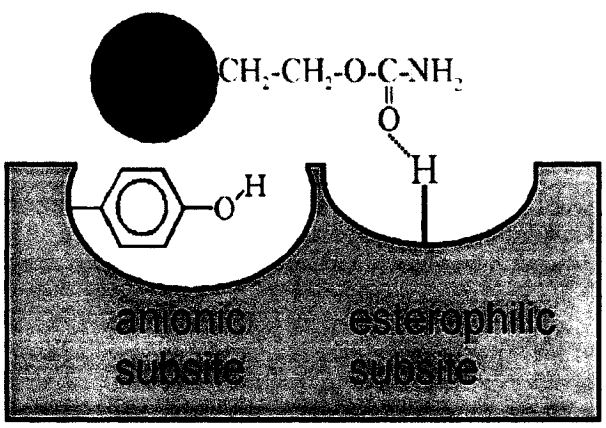

Spectrum B minus Spectrum A =

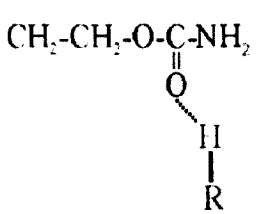

nAChR in a desensitized conformation, the difference between spectra of the nAChR recorded with either TMA or Carb bound to the neurotransmitter binding sites (referred to as a Carb-TMA difference spectrum) should not exhibit vibrational bands reflecting the R→D conformational change. The vibrational features resulting from the formation of physical interactions between the quaternary ammonium of Carb and the anionic subsite should also be absent from the Carb-TMA difference spectrum, because these interactions are already formed in the TMA-bound state. In fact, the Carb-TMA difference spectrum should only exhibit positive and negative vibrational bands due to the intrinsic vibrations of bound Carb and competitively displaced TMA, respectively, as well as bands from esterophilic subsite residues whose structures and/or environments are altered upon interaction with the alkyl carbamylester portion of Carb (Fig. 4.5).

As expected, the Carb-TMA difference spectrum exhibits very few difference bands compared with either the Carb or TMA R→D difference spectra (Fig. 4.6). Clearly defined positive and negative bands due to nAChR-bound Carb and competitively displaced TMA are observed throughout the 1800-1000 cm^{-1} region (Fig. 4.6, light shading). In contrast, relatively intense protein vibrations are only observed in the 1600-1700 cm^{-1} region near 1690, 1668, 1635, 1620, and 1605 cm^{-1}. Other weak bands are difficult to assess at the signal-to-noise ratio of these spectra. The lack of protein vibrational features attributable to tyrosine, tryptophan, and carboxylic acid containing residues, etc. confirms that the majority of the strong physical contacts that occur between Carb and the nAChR take place at the anionic subsite. This result further highlights the importance of the quaternary ammonium in agonist binding.

Two sets of positive/negative protein vibrations located near 1690/1668 cm^{-1} and 1620/1605 cm^{-1}, as well as a weak positive vibration near 1635 cm^{-1} reflect vibrational changes in esterophilic

Figure 4.6

A Carb-TMA difference spectrum (middle trace). The Carb-TMA difference spectrum is the difference between a spectrum of the desensitized nAChR recorded with bound TMA subtracted from a spectrum of the desensitized nAChR recorded with bound Carb. The solution spectra of Carb and TMA are presented for comparison (top and bottom traces, respectively).

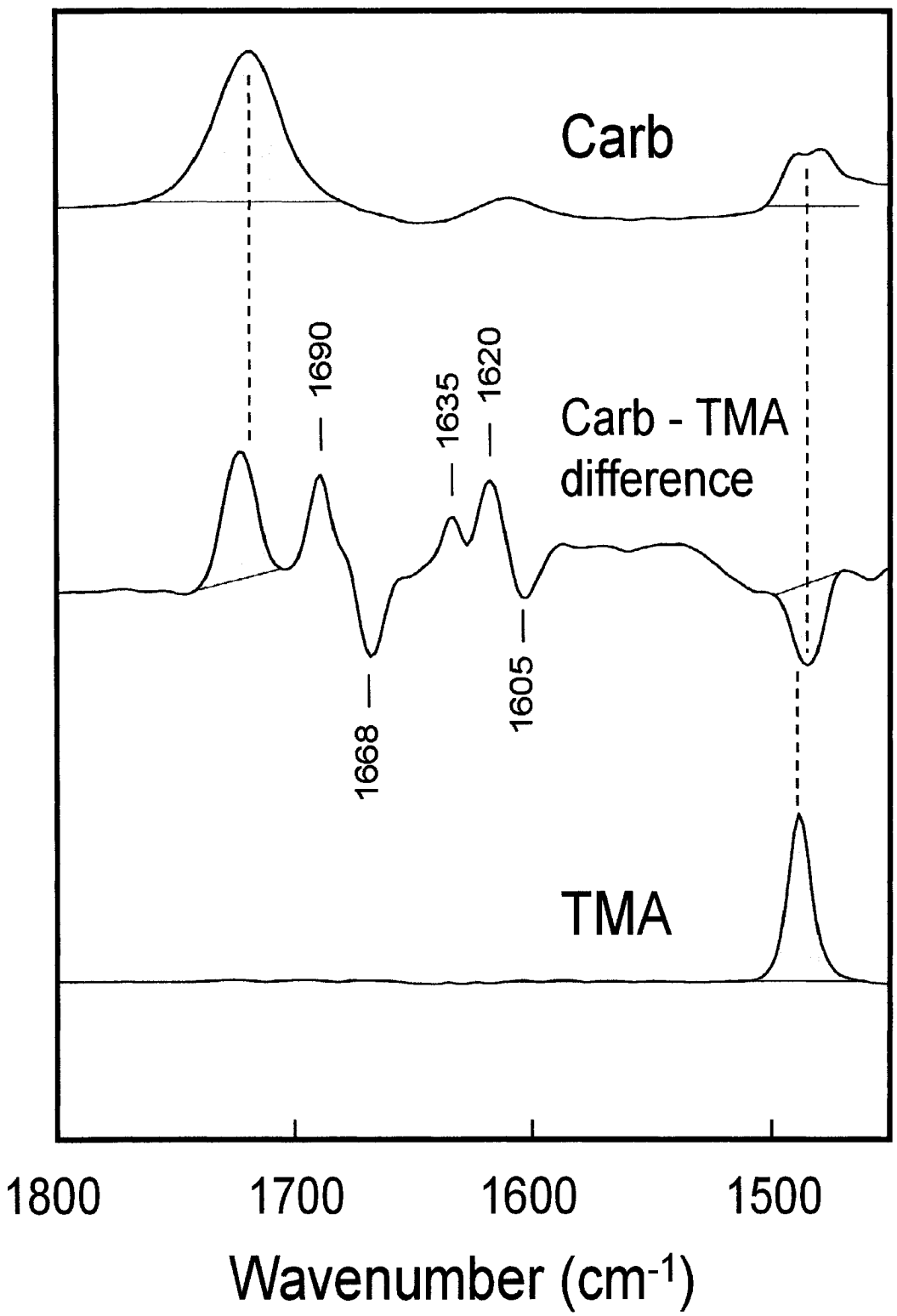
Carb
1690
1635
1620
Carb - TMA
difference
1668
1605
TMA
1800
1700
1600
1500
Wavenumber (cm-1)

subsite residues that occur upon interaction with the alkyl carbamylester portion of Carb. To further define the functional group on Carb that interacts with the esterophilic subsite residues leading to the noted band shifts, we recorded a series of double ligand difference spectra using Carb, TMA, ACh, and/or choline as ligands (Fig. 4.7). The ACh-TMA difference spectrum is similar to the Carb-TMA difference spectrum exhibiting the same difference peaks at 1690, 1668, 1635, 1620, and 1605 cm^{-1}. The similarity of the difference spectra suggests that both Carb and ACh interact with the nAChR at the esterophilic subsite in a similar manner. In other words, the NH_2 group of Carb does not appear to make strong physical contacts with residues in the esterophilic binding and is not involved in the physical interactions that lead to the vibrational shifts noted at 1690, 1668, 1635, 1620, and 1605 cm^{-1}.

Both the Carb-choline and ACh-choline also exhibit the two major positive and negative difference couples located at 1690/1668 cm^{-1} and 1620/1605 cm^{-1}. There may be a subtle change in intensity near 1635 cm^{-1}. The bands in the double ligand difference spectra located near 1690/1668 cm^{-1} and 1620/1605 cm^{-1} thus cannot be attributed to interactions between esterophilic subsite residues and either the methylene carbons or ester oxygen atom of Carb/ACh. The main vibrational changes detected in the double ligand difference spectra thus reflect interactions between esterophilic subsite residues and the carbonyl oxygen of Carb/ACh.

Although definitive assignments of the bands observed in the double ligand difference spectra is not yet possible, the frequencies of the vibrations suggest possible candidate residues for mutagenesis studies. The main vibrations detected in the double ligand difference spectra occur in the amide I (peptide C=O stretch coupled to C-N stretching) frequency region (1600-1700 cm^{-1}) of the infrared spectrum and could reflect vibrational changes resulting from the formation of hydrogen

Figure 4.7

Double ligand difference spectra reveal the protein vibrational changes that result from the formation of physical interactions between protein side chain(s) and the ester carbonyl of Carb/ACh. The top trace is the difference between spectra of the nAChR recorded with either Carb or TMA bound to the neurotransmitter site. The second from top trace is the difference between spectra of the nAChR recorded with either Carb or choline bound to the neurotransmitter site. The third from top trace is the difference between spectra of the nAChR recorded with either ACh or TMA bound to the neurotransmitter site. The bottom trace is the difference between spectra of the nAChR recorded with either ACh or choline bound to the neurotransmitter site. Protein vibrational changes are noted with the dashed lines.

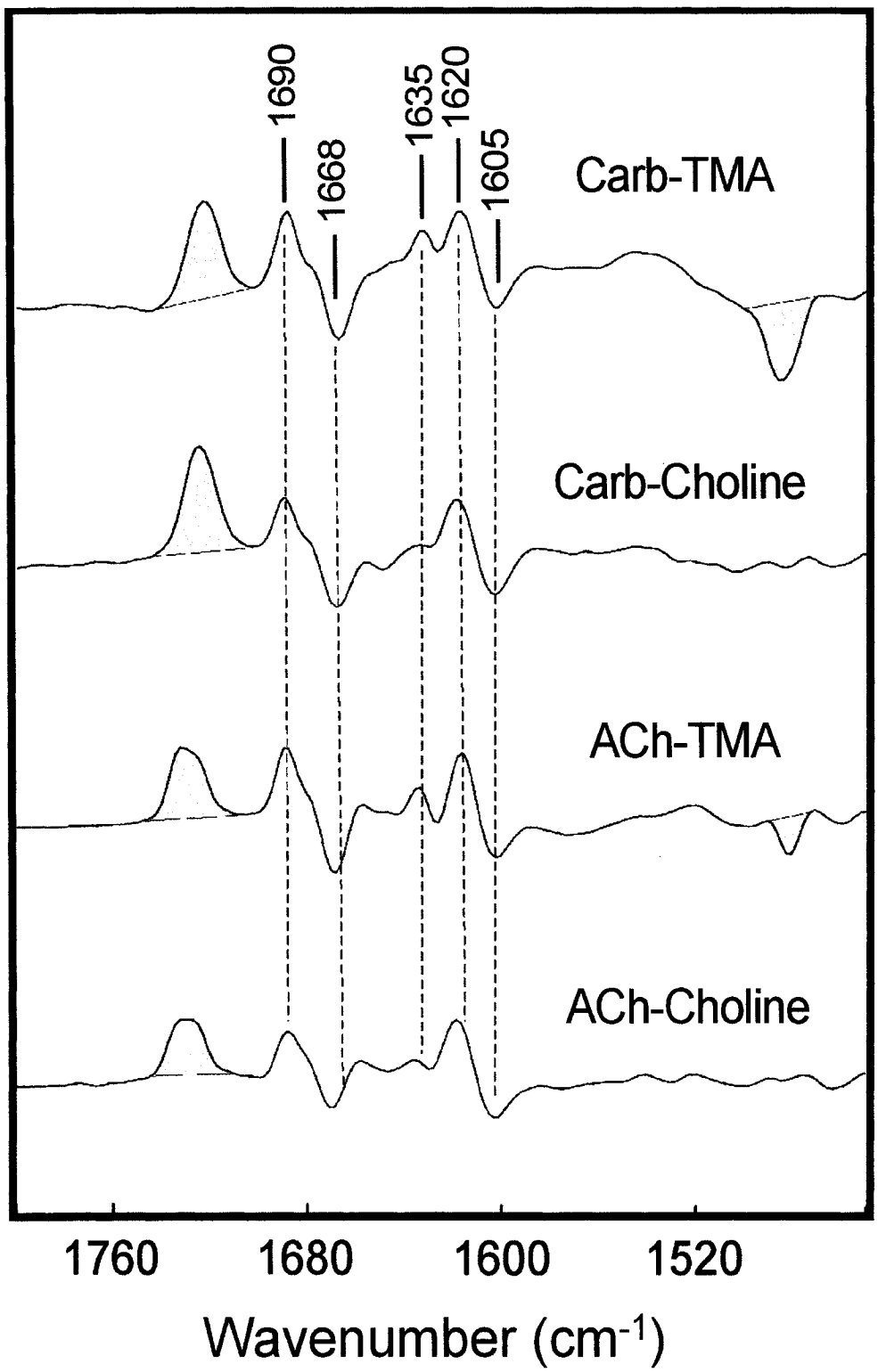
1690
1668
1635
1620
1605
Carb-TMA
Carb-Choline
ACh-TMA
ACh-Choline
1760
1680
1600
1520
Wavenumber (cm-1)

bonds with polypeptide carbonyl oxygens, possibly through a water molecule. Note that the formation of a hydrogen bond between peptide amide protons and the carbonyl oxygen seems unlikely given the absence of band shifts in the amide II (mainly N-H bending and C-N stretch) region of the spectrum (1520-1580 cm^{-1}).

Several side chains are also located in the ACh binding pocket of the homologous ACh binding protein that could interact with the carbonyl of Carb (20), although the precise location of agonist binding to the neurotransmitter site has not yet been determined. These residues in the ACh binding protein include tyrosine 192, glutamine 55, arginine 104, valine 106, leucine 112, and methionine 114. The homologous *Torpedo* nAChR residues are α tyrosine 198, γ glutamate 57 and δ aspartate 59, γ leucine 109 and δ leucine 111, γ tyrosine 111 and δ arginine 113, γ tyrosine 117 and δ threonine 119, and γ leucine 119 and δ leucine 121, respectively (12). The side chains of tyrosine, glutamate, aspartate, leucine, and threonine do not normally contribute strong vibrational intensity exclusively in the 1600-1700 cm^{-1} region of the infrared spectrum and thus are not likely responsible for the vibrations detected in the Carb-minus-TMA difference spectrum (127). In contrast, the asymmetric and symmetric CN_3H_5+ stretching vibrations of arginine are expected near 1670 and 1630 cm^{-1}, frequencies consistent with the two sets of positive and negative couples near 1690/1668 cm^{-1} and 1620/1605 cm^{-1}. Although other assignments are possible, a preliminary interpretation of our data is that the ester carbonyl of Carb interacts with an arginine side chain when binding to the desensitized state of the nAChR. Note, however, that the binding affinity of the ACh binding protein (AChBP) for ACh is 4.2 μM (23). In contrast, the desensitized nAChR binds ACh with an affinity of ~2 nM (86) suggesting conformational differences between the binding sites of the ACh binding protein and the desensitized nAChR. Additional candidate residues may thus be possible.

Shifts in vibrational band frequencies are typically observed upon a change in strength of hydrogen bonding. For a stretching vibration, an increase in hydrogen bond strength typically leads to a downshift in vibrational frequency to lower wavenumbers. Surprisingly, the interaction of Carb with the esterophilic subsite leads to shifts from 1668 and 1605 cm^{-1} to 1690 and 1620 cm^{-1}, respectively. This could imply either the formation of a hydrogen bond with the ester carbonyl of Carb that is weaker than that observed when the esterophilic subsite is unoccupied or the displacement of a counter ion upon Carb binding. The former interpretation of the data seems unlikely given that the nAChR has a stronger affinity for Carb than TMA. Alternatively, the shifts to higher frequency may reflect more complex vibrational couplings. Model compound studies are required to fully interpret the nature of the band shifts that occur upon the binding of Carb to the esterophilic subsite.

SUMMARY AND DISCUSSION

FTIR difference spectroscopy provides a spectral map of the vibrational changes that occur in the nAChR upon Carb binding. This map has been used extensively to investigate the conformational states of the nAChR stabilized by a variety of different ligands and upon reconstitution of the receptor into lipid bilayers of varying lipid compositions (123-126). Here we demonstrate that features in the Carb R→D difference spectrum also provide a vibrational map of the physical interactions that occur between the nAChR and Carb. The difference spectrum exhibits bands at frequencies potentially attributable to tyrosine, tryptophan, and aspartate/glutamate residues, which are all thought to play a role in agonist binding (see below). Several other protein vibrations suggest additional complexity to Carb-nAChR interactions.

We have developed a novel double ligand difference method that can be used to isolate the vibrational features from those residues in a large integral membrane receptor that interact physically either directly or indirectly with specific functional groups on a small molecule ligand. The difference between spectra of the nAChR recorded with either Carb or TMA bound to the neurotransmitter binding sites exhibits protein vibrations from only those residues in the esterophilic subsite that interact with the alkyl carbamylester portion of Carb (see below). Additional double ligand difference spectra show that these vibrations reflect residues that interact either directly or indirectly with the ester carbonyl functional group. Two main band shifts from 1690 and 1620 cm^{-1} to 1668 and 1605 cm^{-1}, respectively, are consistent with the formation of a hydrogen bond between the ester carbonyl of Carb and an arginine side chain. Significantly, these data highlight the utility of the double ligand difference method for dissecting the physical interactions that occur between a large integral membrane receptor and a bound ligand.

The relative simplicity of the resulting double ligand difference spectra is significant from a technical perspective. Band overlap in the Carb R→D difference spectrum prevents interpretation of the data in terms of both the identities of the amino acid side chains that are involved in Carb binding and the nature of the Carb-nAChR contacts. In fact, the two main band shifts observed from 1690 and 1620 cm^{-1} to 1668 and 1605 cm^{-1}, respectively, that occur upon interaction of the ester carbonyl of Carb with the esterophilic subsite are not discernable in either the Carb or TMA R→D difference spectra. The lack of band overlap in the double ligand difference spectrum permits a precise determination of the band frequencies of the protein side chains that interact with the ester carbonyl in both the Carb bound and TMA bound states.

The main conclusions regarding the nature of Carb-nAChR interactions derived from this study are the following: 1) The data show that the main physical interactions between Carb and the nAChR arise from interactions between the quaternary ammonium and the anionic subsite. This conclusion is based on the observation that the majority of features in the Carb R→D difference spectrum attributable to vibrational changes in residues that interact with Carb are also observed in the TMA R→D difference spectrum. Both the FTIR and fluorescence data show that TMA is capable of stabilizing the nAChR in the desensitized state (see "Results and Interpretation"). The demonstrated importance of the quaternary ammonium in both agonist-nAChR interactions and agonist-induced conformational change is in agreement with electrophysiological studies, which show that TMA is an agonist of the receptor (43, 128). 2) The difference spectra provide direct evidence that the quaternary ammonium of Carb interacts with tyrosine residues in the agonist-binding pocket. Carb binding to the nAChR leads to an increase in the vibrational intensity of a band near 1516 cm^{-1} indicating a change in the structure and/or local environment surrounding one or more tyrosine residues. This increase in tyrosine vibrational intensity is observed upon Carb binding to a desensitized nAChR suggesting that it reflects Carb-tyrosine physical interactions as opposed to a vibrational perturbation associated with the R→D conformational transition. The increase in intensity near 1516 cm^{-1} is also observed upon TMA binding, supporting the assignment of the band to one or more interactions between one or more tyrosines and the quaternary amine functional group. The relative strong intensity of the 1516 cm^{-1} band firmly establishes a key role for tyrosines in agonist binding in agreement with extensive data obtained using both chemical labeling and site-directed mutagenesis (43, 116-120, 128). 3) Vibrational features that are indicative of the interactions between the quaternary ammonium and several other amino acid side chains are

detected suggesting that a number of residues contribute to the anionic subsite. Bands potentially attributable to tryptophan and the carboxylate groups of aspartate and/or glutamate may reflect changes in structure and/or local environment surrounding both types of residues upon interaction with Carb, as has been proposed elsewhere (40, 121). Other vibrational features, most notably near 1620 cm^{-1}, suggest the involvement of additional amino acid side chains. 4) Finally, positive and negative bands near 1690/1668 cm^{-1} and 1620/1605 cm^{-1} detected in the Carb-minus-TMA, the Carb-minus-choline, the ACh-minus-TMA, and ACh-minus-choline difference spectra suggest the formation of a hydrogen bond between an esterophilic subsite residue and the ester carbonyl of Carb while the nAChR is in the desensitized state. Although other band assignments are possible, the frequencies are consistent with an arginine side chain interacting directly with the ester carbonyl. An arginine residue is likely located close to the agonist binding pocket (20).

The ability of the double ligand difference technique to detect specific ligand-receptor contacts highlights the potential of the technique for mapping subtle structural variations that exist between the binding sites of homologous ligand binding proteins. For example, Carb-TMA difference spectra recorded from both the nAChR and the homologous AChBP would reveal similarities and/or differences in amino acid side chains located in the esterophilic subsite. Given that the crystal structure of the AChBP has been solved, such information could prove valuable for modeling the binding site of the nAChR. A similar approach could also be used to investigate the structural basis for the different neuronal nAChR receptor pharmacologies.

The experimental approach used here is readily adaptable to almost any membrane-bound receptor. The main requirement is the ability to form a membrane film that adheres to the surface of an internal reflection element in the presence of flowing buffer. In our experience, most

biological membranes adhere to germanium internal reflection elements [see also (129)]. A variety of internal reflection element sizes, geometries, and materials allow one to tailor the experimental approach for a given application. Novel methods of recording difference spectra are continuously being developed for water-soluble proteins [reviewed in Ref. (122)]. The approaches described here should be applicable to a variety of both membrane-imbedded and water-soluble proteins.

CONCLUSIONS

The physical interactions that occur between the nicotinic acetylcholine receptor from *Torpedo* and the agonists carbamylcholine and tetramethylamine have been studied using both conventional infrared difference spectroscopy and a novel double-ligand difference technique. The latter was developed to isolate vibrational bands from residues in a membrane receptor that interact with individual functional groups on a small molecule ligand. The binding of either agonist leads to an increase in vibrational intensity at frequencies centered near 1663, 1655, 1547, 1430, and 1059 cm^{-1} indicating that both induce a conformational change from the resting to the desensitized state. Vibrational shifts near 1580, 1516, 1455, 1334, and between 1300 and 1400 cm^{-1} are assigned to structural perturbations of tyrosine and possibly both tryptophan and charged carboxylic acid residues upon the formation of receptor-quaternary amine interactions, with the relatively intense feature near 1516 cm^{-1} indicating a key role for tyrosine. Other vibrational bands suggest the involvement of additional side chains in agonist binding. Two side-chain vibrational shifts from 1668 and 1605 cm^{-1} to 1690 and 1620 cm^{-1}, respectively, could reflect the formation of a hydrogen bond between the ester carbonyl of carbamylcholine and an arginine residue. The results demonstrate the potential of the double-ligand difference technique for dissecting the chemistry of

membrane receptor-ligand interactions and provide new insight into the nature of nicotinic receptor-agonist interactions.

General Conclusions

The objective of the research presented in this thesis was to employ the Fourier transform infrared spectroscopy to examine the structural and orientational changes in the receptor and the nature of the physical interactions that form between the nAChR and the neurotransmitter analog carbamylcholine as it undergoes the resting to desensitized conformational change. FTIR spectroscopy exists as one of the few techniques capable of gleaning detailed structural information from large integral membrane proteins, such as the nAChR, by providing insight into the molecular vibrations of individual amino acids, which are extremely sensitive to changes in molecular structure and local environment. The principal results and conclusions of this project are summarized as follows.

TRANSMEMBRANE ORIENTATION

Under quiescent conditions, the nAChR exists in an equilibrium between the resting state (~80%) and the desensitized state (86). Upon exposure of the nAChR to ACh, it undergoes a conformational change to the open state, precipitating the conduction of cations into the post-synaptic cell. The open state is transient, however, and prolonged exposure of the nAChR to ACh induces an additional conformational change to the desensitized state.

Despite a considerable volume of research, our understanding of protein mechanisms is still in its infancy. Photoaffinity labeling studies have noted that the aromatic side chains of the neurotransmitter binding site appear to contract around the quaternary ammonium group of ACh, and the area of contact between the transmembrane helices increases upon desensitization. What happens in between ligand binding and channel opening remains a mystery.

One objective of this research was to investigate the orientation changes within the nAChR as it undergoes the resting to desensitized conformational transition by attenuated total reflectance

infrared spectroscopy. Since the quality of polarized ATR-FTIR spctroscopy is contingent on producing nice ordered membrane films, we began by characterizing the ordering of our nAChR membrane films on the IRE surface. We found that the order parameters for the nAChR reconstituted PC/PA/Chol 3:1:1 membranes were greater than the order parameter for the pure PC/PA/Chol 3:1:1 membranes, and concluded that the decrease in molecular order parameter of the acyl chain in the presence of the nAChR likely reflects an increased mosaic spread of the reconstituted nAChR membranes compared to the pure lipid bilayers. We proceeded to quantify the contribution of the nAChR-induced increase in mosaic spread in the membrane films and used it in the determination of the nAChR transmembrane helix orientation. Polarized ATR-FTIR spectra of the nAChR reconstituted into PC/PA/Chol membranes were recorded and significant dichroism in both the amide I and amide II bands was consistent with a perferential orientation of the nAChR transmembrane helices parallel to the membrane surface normal. Based on our characterization of the contribution of the mosaic spread to the order parameter, we computed the average tilt of the α-helix axis to be between 44° and 46°, relative to the bilayer normal. We then investigated the orientation changes in the nAChR upon receptor desensitization by polarized FTIR spectroscopy. No significant differences between the polarized absolute absorbance spectra of the nAChR in the resting state compared to the polarized spectra of the nAChR in the desensitized state were observed, leading us to conclude the orientation changes upon receptor desensitization were too small to be detected by this approach.

As more sensitive techniques are necessary to elucidate the subtle orientational changes within the nAChR as it undergoes the resting to desensitized conformational shift, we began collecting linear dichroism difference spectra of the nAChR (Fig. GC.1). Although the polarized

Figure GC.1

Polarized Carb R→D (top traces) and polarized Carb-TMA (bottom traces) difference spectra. FTIR spectra collected with perpendicular polarized light (dashed lines) were scaled by a factor of two to account for differences in the evanescent field strength. FTIR spectra collected with parallel polarized light are illustrated by the solid lines

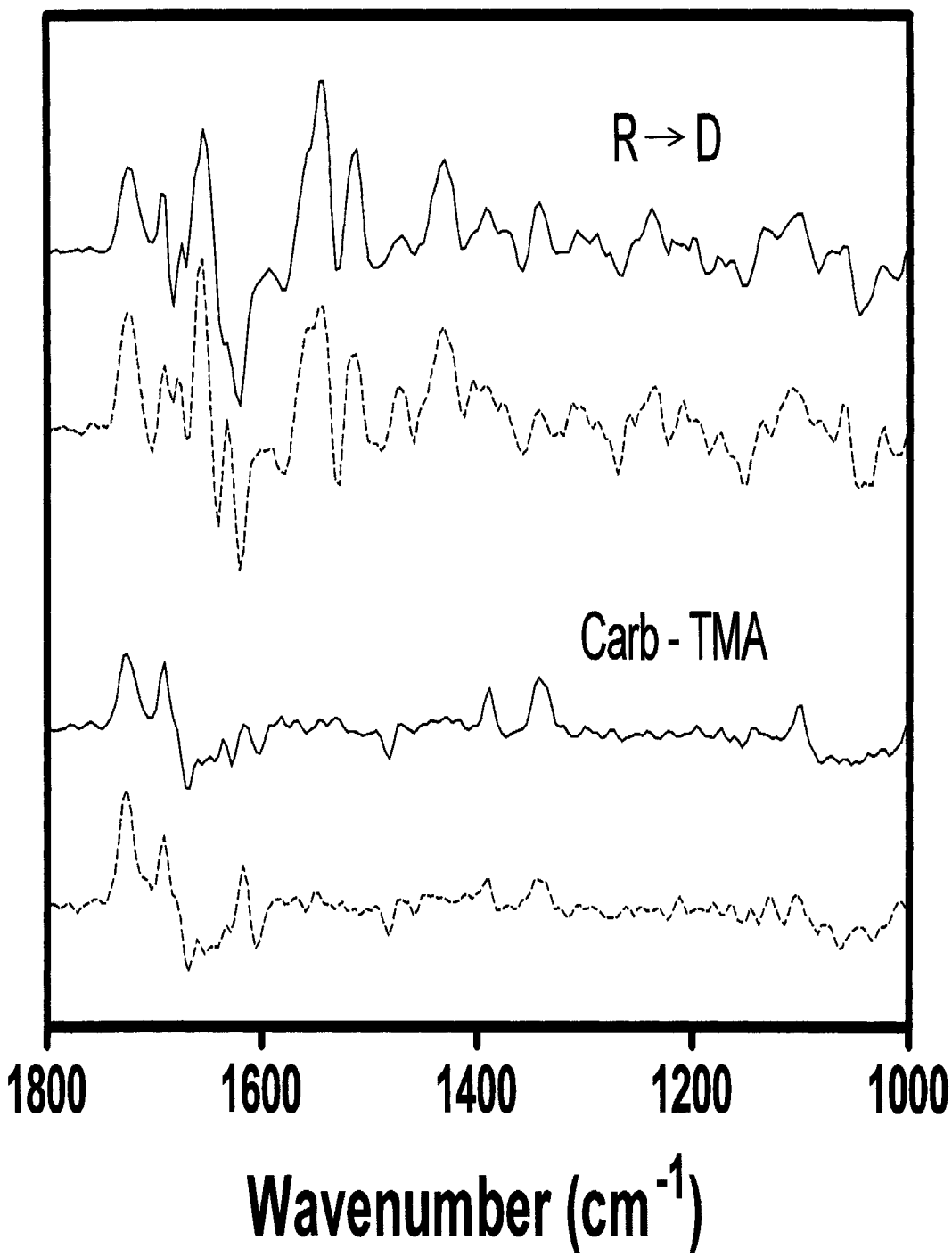
R→D
Carb - TMA
1800
1600
1400
1200
1000
Wavenumber (cm-1)

Carb R→D and Carb-TMA difference spectra illustrate significant dichroism in seveal of the vibrational bands, I exhausted my time at the University of Ottawa and was unable to analyze the spectra rigorously, unfortunately. A rigorous analysis of the orientation changes revealed by the linear dichroism difference spectra may provide crucial insight into the mechanism of desensitization.

NEUROTRANSMITTER BINDING

The nature of ACh binding to the nAChR has been studied extensively. Each of the two acetylcholine (ACh) binding sites on the nAChR consists of two subsites, an esterophilic subsite, that binds the ester functional group of ACh, and an anionic subsite that binds the quaternary ammonium cation (113). Sequence analysis, affinity labeling, and site-directed mutagenesis studies have identified predominately aromatic residues in the anionic subsite that are believed to interact with the quaternary ammonium of ACh via cation-pi electron interactions (115, 117-121). Moreover, the crystal structure of the homologous ACh binding protein confirms the essential role for tyrosine and tryptophan residues in the anionic subsite (20). However, the nature of the chemical interactions that occur between ACh and the esterophilic subsite, remain, have remained poorly understood.

A second objective of this research was to examine the physical interactions that occur between the nAChR and ACh, and to elucidate the physical interactions arising within the esterophilic subsite of the nAChR. We began by identifying vibrational features within the Carb R→D difference spectrum that reflect interactions within the anionic subsite and the quaternary ammonium of Carb. Difference spectra were recorded using the agonist analog TMA and compared to the Carb R→D difference spectrum. We found most of the bands in the Carb R→D difference spectrum that are potentially attributable to vibrational changes in residues interacting with Carb are

also present in the TMA difference spectrum, illustrating that the interactions between the nAChR and Carb are dominated by interactions with the quaternary ammonium functional group. However, we did find a few bands in the Carb R→D difference spectrum that are absent in the TMA R→D difference spectrum that could indicate of physical interactions between the alkyl carbamylester portion of Carb and residues in the esterophilic subsite. To explore this further and to simplify the difference spectrum, we devised a novel double ligand difference method which only exhibits positive and negative vibrational bands due to bound Carb and competitively displaced TMA, respectively, and bands from esterophilic subsite residues whose structures and/or environments are altered upon interaction with the alkyl carbamylester portion of Carb. The Carb-TMA difference spectrum revealed two sets of positive/negative protein vibrations located near 1690/1668 cm^{-1} and 1620/1605 cm^{-1} suggesting a potential hydrogen bond between an arginine residue of the esterophilic subsite and the alkyl carbamylester portion of Carb.

Although FTIR difference spectroscopy provides a spectral map of the vibrational changes that occur in the nAChR upon Carb binding, interpreting this map can be difficult. To fully extract all the mechanistic information contained in the difference spectrum, cells expressing side chain mutations or isotopically labeled residues is necessary.

REFERENCES

1. Karlin, A. (2002). Emerging structure of the nicotinic acetylcholine receptors. Nat Rev Neurosci : 3 (2), 102-14.
2. Reynolds, J. A., and Karlin, A. (1978). Molecular weight in detergent solution of acetylcholine receptor from *Torpedo californica*. Biochemistry : 17 (11), 2035-8.
3. Mishina, M., Takai, T., Imoto, K., Noda, M., Takahashi, T., Numa, S., Methfessel, C., and Sakmann, B. (1986). Molecular distinction between fetal and adult forms of muscle acetylcholine receptor. Nature : 321 (6068), 406-11.
4. Anand, R., Conroy, W. G., Schoepfer, R., Whiting, P., and Lindstrom, J. (1991). Neuronal nicotinic acetylcholine receptors expressed in *Xenopus* oocytes have a pentameric quaternary structure. J Biol Chem : 266 (17), 11192-8.
5. Cooper, E., Couturier, S., and Ballivet, M. (1991). Pentameric structure and subunit stoichiometry of a neuronal nicotinic acetylcholine receptor. Nature : 350 (6315), 235-8.
6. Elgoyhen, A. B., Johnson, D. S., Boulter, J., Vetter, D. E., and Heinemann, S. (1994). Alpha 9: an acetylcholine receptor with novel pharmacological properties expressed in rat cochlear hair cells. Cell : 79 (4), 705-15.
7. Vernallis, A. B., Conroy, W. G., and Berg, D. K. (1993). Neurons assemble acetylcholine receptors with as many as three kinds of subunits while maintaining subunit segregation among receptor subtypes. Neuron : 10 (3), 451-64.
8. Ramirez-Latorre, J., Yu, C. R., Qu, X., Perin, F., Karlin, A., and Role, L. (1996). Functional contributions of alpha5 subunit to neuronal acetylcholine receptor channels. Nature : 380 (6572), 347-51.
9. Lindstrom, J., Walter, B., and Einarson, B. (1979). Immunochemical similarities between subunits of acetylcholine receptors from *Torpedo*, *Electrophorus*, and mammalian muscle. Biochemistry : 18 4470-4480.
10. Raftery, M. A., Hunkapiller, M. W., Strader, C. D., and Hood, L. E. (1980). Acetylcholine receptor: complex of homologous subunits. Science : 208 (4451), 1454-6.
11. Sumikawa, K., Houghton, M., Smith, J. C., Richards, B. M., and Barnard, E. A. (1982). The molecular cloning and characterization of cDNA coding for the a subunit of the acetylcholine receptor. Nucleic Acid Res : 10 5809-22.
12. Noda, M., Takahashi, H., Tanabe, T., Toyosato, M., Furutani, Y., Hirose, T., Asai, M., Inayama, S., Miyata, T., and Numa, S. (1982). Primary structure of alpha-subunit precursor of *Torpedo californica* acetylcholine receptor deduced from cDNA sequence. Nature : 299 (5886), 793-7.
13. Devillers-Thiery, A., Giraudat, J., Bentaboulet, M., and Changeux, J.-P. (1983). Complete mRNA coding sequence of the acetylcholine binding a-subunit of *Torpedo marmorata* acetylcholine receptor: a model for the transmembrane organization of the polypeptide chain. Proc. Natl. Acad. Sci. U.S.A. : 80 2067-71.
14. Noda, M., Takahashi, H., Tanabe, T., Toyosato, M., Kikyotani, S., Furutani, Y., Hirose, T., Takashima, H., Inayama, S., Miyata, T., and Numa, S. (1983). Structural homology of *Torpedo californica* acetylcholine receptor subunits. Nature : 302 (5908), 528-32.

15. Claudio, T., Ballivet, M., Patrick, J., and Heinemann, S. (1983). Nucleotide and deduced amino acid sequences of *Torpedo californica* acetylcholine receptor gamma subunit. Proc Natl Acad Sci U S A : 80 (4), 1111-5.
16. Noda, M., Takahashi, H., Tanabe, T., Toyosato, M., Kikyotani, S., Hirose, T., Asai, M., Takashima, H., Inayama, S., Miyata, T., and Numa, S. (1983). Primary structures of beta- and delta-subunit precursors of *Torpedo californica* acetylcholine receptor deduced from cDNA sequences. Nature : 301 (5897), 251-5.
17. Unwin, N. (1993). Nicotinic acetylcholine receptor at 9 A resolution. J Mol Biol : 229 (4), 1101-24.
18. Miyazawa, A., Fujiyoshi, Y., Stowell, M., and Unwin, N. (1999). Nicotinic acetylcholine receptor at 4.6 A resolution: transverse tunnels in the channel wall. J Mol Biol : 288 (4), 765-86.
19. Unwin, N. (1995). Acetylcholine receptor channel imaged in the open state. Nature : 373 (6509), 37-43.
20. Brejc, K., van Dijk, W. J., Klaassen, R. V., Schuurmans, M., van Der Oost, J., Smit, A. B., and Sixma, T. K. (2001). Crystal structure of an ACh-binding protein reveals the ligand-binding domain of nicotinic receptors. Nature : 411 (6835), 269-76.
21. Corringer, P. J., Le Novere, N., and Changeux, J.-P. (2000). Nicotinic receptors at the amino acid level. Annu Rev Pharmacol Toxicol : 40 431-58.
22. West, A. P. J., Bjorkman, P. J., Dougherty, D. A., and Lester, H. A. (1997). Expression and circular dichroism studies of the extracellular domain of the alpha subunit of the nicotinic acetylcholine receptor. J Biol Chem : 272 (41), 25468-73.
23. Smit, A. B., Syed, N. I., Schaap, D., van Minnen, J., Klumperman, J., Kits, K. S., Lodder, H., van der Schors, R. C., van Elk, R., Sorgedrager, B., Brejc, K., Sixma, T. K., and Geraerts, W. P. (2001). A glia-derived acetylcholine-binding protein that modulates synaptic transmission. Nature : 411 (6835), 261-8.
24. Unwin, N., Miyazawa, A., Li, J., and Fujiyoshi, Y. (2002). Activation of the nicotinic acetylcholine receptor involves a switch in conformation of the alpha subunits. J Mol Biol : 319 (5), 1165-76.
25. Langenbuch-Cachat, J., Bon, C., Goeldner, M., Hirth, C., and Changeux, J.-P. (1988). Photoaffinity labelling by aryldiazonium derivatives of *Torpedo marmorata* acetylcholine receptor. Biochemistry : 27 2337-45.
26. Dennis, M., Giraudat, J., Kotzyba-Hibert, F., Goeldner, M., Hirth, C., Chang, J. Y., Lazure, C., Chretien, M., and Changeux, J. P. (1988). Amino acids of the *Torpedo marmorata* acetylcholine receptor alpha subunit labeled by a photoaffinity ligand for the acetylcholine binding site. Biochemistry : 27 (7), 2346-57.
27. Pedersen, S. E., and Cohen, J. B. (1990). d-Tubocurarine binding sites are located at alpha-gamma and alpha-delta subunit interfaces of the nicotinic acetylcholine receptor. Proc Natl Acad Sci U S A : 87 (7), 2785-9.
28. Oswald, R. E., and Changeux, J.-P. (1982). Crosslinking of alpha-bungarotoxin to the acetylcholine receptor from *Torpedo marmorata* by ultraviolet light irradiation. FEBS Lett. : 139 225-29.

29. Middleton, R. E., and Cohen, J. B. (1991). Mapping of the acetylcholine binding site of the nicotinic acetylcholine receptor: [3H]nicotine as an agonist photoaffinity label. Biochemistry : 30 6987-97.
30. Kao, P. N., Dwork, A. J., Kaldany, R.-R. J., Silver, M. L., Wideman, J., Stein, S., and Karlin, A. (1984). Identification of the a subunit half-cystine specifically labeled by an affinity reagent for the acetylcholine receptor binding site. J Biol Chem : 259 11662-5.
31. Galzi, J.-L., Revah, F., Black, D., Goeldner, M., Hirth, C., and Changeux, J.-P. (1990). Identification of a novel amino acid a-tyrosine 93 within the cholinergic ligands-binding sites of the acetylcholine receptor by photoaffinity labeling. Additional evidence for a three-loop model of the cholinergic ligands-binding sites. J Biol Chem : 265 10430-7.
32. Chiara, D. C., and Cohen, J. B. (1997). Identification of amino acids contributing to high and low affinity d- tubocurarine sites in the *Torpedo* nicotinic acetylcholine receptor. J Biol Chem : 272 (52), 32940-50.
33. Czajkowski, C., and Karlin, A. (1995). Structure of the nicotinic acetylcholine-binding site: identification of acidic residues in the d subunit within 0.9 nm of the a subunit binding site disulfide. J Biol Chem : 270 3160-4.
34. Blount, P., and Merlie, J. P. (1989). Molecular basis of the two nonequivalent ligand binding sites of the muscle nicotinic acetylcholine receptor. Neuron : 3 (3), 349-57.
35. Kao, P. N., and Karlin, A. (1986). Acetylcholine receptor binding site contains a disulfide cross-link between adjacent half-cystinyl residues. J Biol Chem : 261 (18), 8085-8.
36. Boulter, J., O'Shea-Greenfield, A., Duvoisin, R. M., Conolly, J. G., Wada, E., Jensen, A., Gardner, P. D., Ballivet, M., Deneris, E. S., McKinnon, D., Heinemann, S., and Patrick, J. (1990). alpha3, alpha5, and beta4: three members of the rat neuronal nicotinic acetylcholine receptor-related gene family form a gene cluster. J Biol Chem : 265 4472-82.
37. Galzi, J. L., Edelstein, S. J., and Changeux, J.-P. (1996). The multiple phenotypes of allosteric receptor mutants. Proc Natl Acad Sci U S A : 93 (5), 1853-8.
38. Dougherty, D. A., and Stauffer, D. A. (1990). Acetylcholine binding by a synthetic receptor: implications for biological recognition. Science : 250 (4987), 1558-60.
39. Sussman, J. L., Harel, M., Frolow, F., Oefner, C., Goldman, A., Toker, L., and Silman, I. (1991). Atomic structure of acetylcholinesterase from *Torpedo californica*: a prototypic acetylcholine-binding protein. Science : 253 (5022), 872-9.
40. Zhong, W., Gallivan, J. P., Zhang, Y., Li, L., Lester, H. A., and Dougherty, D. A. (1998). From ab initio quantum mechanics to molecular neurobiology: a cation-pi binding site in the nicotinic receptor. Proc Natl Acad Sci U S A : 72 (11), 9365-9.
41. Galzi, J. L., Revah, F., Bouet, F., Menez, A., Goeldner, M., Hirth, C., and Changeux, J. P. (1991). Allosteric transitions of the acetylcholine receptor probed at the amino acid level with a photolabile cholinergic ligand. Proc Natl Acad Sci U S A : 88 (11), 5051-5.
42. Martin, M. D., and Karlin, A. (1997). Functional effects on the acetylcholine receptor of multiple mutations of gamma Asp174 and delta Asp180. Biochemistry : 36 (35), 10742-50.
43. O'Leary, M. E., and White, M. M. (1992). Mutational analysis of ligand-induced activation of the Torpedo acetylcholine receptor. J Biol Chem : 267 (12), 8360-5.
44. Armstrong, N., and Gouaux, E. (2000). Mechanisms for activation and antagonism of an AMPA-sensitive glutamate receptor: crystal structures of the GluR2 ligand binding core. Neuron : 28 (1), 165-81.

45. Akk, G., Zhou, M., and Auerbach, A. (1999). A mutational analysis of the acetylcholine receptor channel transmitter binding site. Biophys J : 76 207-18.
46. Stauffer, D. A., and Karlin, A. (1994). Electrostatic potential of the acetylcholine binding sites in the nicotinic receptor probed by reactions of binding-site cysteines with charged methanethiosulfonates. Biochemistry : 33 (22), 6840-9.
47. Osaka, H., Sugiyama, N., and Taylor, P. (1998). Distinctions in agonist and antagonist specificity conferred by anionic residues of the nicotinic acetylcholine receptor. J Biol Chem : 273 (21), 12758-65.
48. Baenziger, J. E., and Methot, N. (1995). Fourier transform infrared and hydrogen/deuterium exchange reveal an exchange-resistant core of alpha-helical peptide hydrogens in the nicotinic acetylcholine receptor. J Biol Chem : 270 (49), 29129-37.
49. Corbin, J., Methot, N., Wang, H. H., Baenziger, J. E., and Blanton, M. P. (1998). Secondary structure analysis of individual transmembrane segments of the nicotinic acetylcholine receptor by circular dichroism and Fourier transform infrared spectroscopy. J Biol Chem : 273 (2), 771-7.
50. Methot, N., and Baenziger, J. E. (1998). Secondary structure of the exchange-resistant core from the nicotinic acetylcholine receptor probed directly by infrared spectroscopy and Hydrogen/Deuterium exchange. Biochemistry : 37 (42), 14815-22.
51. Charnet, P., Labarca, C., Leonard, R. J., Vogelaar, N. J., Czyzyk, L., Gouin, A., Davidson, N., and Lester, H. A. (1990). An open-channel blocker interacts with adjacent turns of alpha-helices in the nicotinic acetylcholine receptor. Neuron : 4 (1), 87-95.
52. Blanton, M. P., and Cohen, J. B. (1992). Mapping the lipid-exposed regions in the Torpedo californica nicotinic acetylcholine receptor [published erratum appears in Biochemistry 1992 Jun 30;31(25):5951]. Biochemistry : 31 (15), 3738-50.
53. Villarroel, A., and Sakmann, B. (1992). Threonine in the selectivity filter of the acetylcholine receptor channel. Biophys J : 62 196-205.
54. Akabas, M. H., Kaufmann, C., Archdeacon, P., and Karlin, A. (1994). Identification of acetylcholine receptor channel-lining residues in the entire M2 segment of the alpha subunit. Neuron : 13 (4), 919-27.
55. Blanton, M. P., and Cohen, J. B. (1994). Identifying the lipid-protein interface of the *Torpedo* nicotinic acetylcholine receptor: secondary structure implications. Biochemistry : 33 (10), 2859-72.
56. Miyazawa, A., Fujiyoshi, Y., and Unwin, N. (2003). Structure and gating mechanism of the acetylcholine receptor pore. Nature : 423 (6943), 949-55.
57. Heidmann, T., and Changeux , J.-P. (1984). Time-resolved photolabeling by the noncompetitive blocker chlorpromazine of the acetylcholine receptor in its transiently open and closed ion channel conformations. Proc Natl Acad Sci U S A : 81 (6), 1897-901.
58. Giraudat, J., Dennis, M., Heidmann, T., Chang, J. Y., and Changeux, J. P. (1986). Structure of the high-affinity binding site for noncompetitive blockers of the acetylcholine receptor: serine-262 of the delta subunit is labeled by [3H]chlorpromazine. Proc Natl Acad Sci U S A : 83 (8), 2719-23.
59. Giraudat, J., Gali, J., Revah, F., Changeux, J., Haumont, P., and Lederer, F. (1989). The noncompetitive blocker [(3)H]chlorpromazine labels segment M2 but not segment M1 of the nicotinic acetylcholine receptor alpha-subunit. FEBS Lett : 253 (1-2), 190-8.

60. Revah, F., Galzi, J. L., Giraudat, J., Haumont, P. Y., Lederer, F., and Changeux, J. P. (1990). The noncompetitive blocker [3H]chlorpromazine labels three amino acids of the acetylcholine receptor gamma subunit: implications for the alpha- helical organization of regions MII and for the structure of the ion channel. Proc Natl Acad Sci U S A : 87 (12), 4675-9.
61. Pedersen, S. E., Sharp, S. D., Liu, W. S., and Cohen, J. B. (1992). Structure of the noncompetitive antagonist-binding site of the *Torpedo* nicotinic acetylcholine receptor. [3H]meproadifen mustard reacts selectively with alpha-subunit Glu-262. J Biol Chem : 267 (15), 10489-99.
62. White, B. H., and Cohen, J. B. (1992). Agonist-induced changes in the structure of the acetylcholine receptor M2 regions revealed by photoincorporation of an uncharged nicotinic noncompetitive antagonist. J Biol Chem : 267 (22), 15770-83.
63. Hucho, F. L., Oberthür, W., and Lottspeich, F. (1986). The ion channel of the nicotinic acetylcholine receptor is formed by the homologous helices MII of the receptor subunits. FEBS Letters : 205 137-142.
64. Blanton, M. P., McCardy, E. A., Huggins, A., and Parikh, D. (1998). Probing the structure of the nicotinic acetylcholine receptor with the hydrophobic photoreactive probes [125I]TID-BE and [125I]TIDPC/16. Biochemistry : 37 (41), 14545-55.
65. Blanton, M. P., Dangott, L. J., Raja, S. K., Lala, A. K., and Cohen, J. B. (1998). Probing the structure of the nicotinic acetylcholine receptor ion channel with the uncharged photoactivable compound -3H-diazofluorene. Journal of Biological Chemistry : 273 (15), 8659-68.
66. Middleton, R. E., Strnad, N. P., and Cohen, J. B. (1999). Photoaffinity labeling the *Torpedo* nicotinic acetylcholine receptor with [(3)H]tetracaine, a nondesensitizing noncompetitive antagonist. Mol Pharmacol : 56 (2), 290-9.
67. Zhang, H., and Karlin, A. (1997). Identification of acetylcholine receptor channel-lining residues in the M1 segment of the beta-subunit. Biochemistry : 36 (30), 15856-15864.
68. Hucho, F. (1986). The nicotinic acetylcholine receptor and its ion channel. Eur J Biochem : 158 (2), 211-26.
69. Imoto, K., Busch, C., Sakmann, B., Mishina, M., Konno, T., Nakai, J., Bujo, H., Mori, Y., Fukuda, K., and Numa, S. (1988). Rings of negatively charged amino acids determine the acetylcholine receptor channel conductance. Nature : 335 (6191), 645-8.
70. Leonard, R. J., Labarca, C. G., Charnet, P., Davidson, N., and Lester, H. A. (1988). Evidence that the M2 membrane-spanning region lines the ion channel pore of the nicotinic receptor. Science : 242 (4885), 1578-81.
71. Labarca, C., Nowak, M. W., Zhang, H., Tang, L., Deshpande, P., and Lester, H. A. (1995). Channel gating governed symmetrically by conserved leucine residues in the M2 domain of nicotinic receptors. Nature : 376 (6540), 514-6.
72. Filatov, G. N., and White, M. M. (1995). The role of conserved leucines in the M2 domain of the acetylcholine receptor in channel gating. Mol Pharmacol : 48 (3), 379-84.
73. Revah, F., Bertrand, D., Galzi, J. L., Devillers-Thiery, A., Mulle, C., Hussy, N., Bertrand, S., Ballivet, M., and Changeux, J. P. (1991). Mutations in the channel domain alter desensitization of a neuronal nicotinic receptor. Nature : 353 (6347), 846-9.

74. Yakel, J. L., Lagrutta, A., Adelman, J. P., and North, R. A. (1993). Single amino acid substitution affects desensitization of the 5-hydroxytryptamine type 3 receptor expressed in *Xenopus* oocytes. Proc Natl Acad Sci U S A : 90 (11), 5030-3.
75. Pascual, J. M., and Karlin, A. (1998). State-dependent accessibility and electrostatic potential in the channel of the acetylcholine receptor. Inferences from rates of reaction of thiosulfonates with substituted cysteines in the M2 segment of the alpha subunit. J Genl Phys : 111 (6), 717-39.
76. Wilson, G., and Karlin, A. (2001). Acetylcholine receptor channel structure in the resting, open, and desensitized states probed with the substituted-cysteine-accessibility method. Proc Natl Acad Sci U S A : 98 (3), 1241-8.
77. Bertrand, D., Galzi, J. L., Devillers-Thiery, A., Bertrand, S., and Changeux, J.-P. (1993). Mutations at two distinct sites within the channel domain M2 alter calcium permeability of neuronal alpha 7 nicotinic receptor. Proc Natl Acad Sci U S A : 90 (15), 6971-5.
78. Kosolapov, A. V., Filatov, G. N., and White, M. M. (2000). Acetylcholine receptor gating is influenced by the polarity of amino acids at position 9' in the M2 domain. J Membr Biol : 174 (3), 191-7.
79. Ratnam, M., Sargent, P. B., Sarin, V., Fox, J. L., Nguyen, D. L., Rivier, J., Criado, M., and Lindstrom, J. M. (1986). Location of antigenic determinants on primary sequences of subunits of nicotinic acetylcholine receptors by peptide mapping. Biochemistry : 25 2621-32.
80. Ratnam, M., Manohar, Le Nguyen, D., Rivier, J., Sargent, P. B., and Lindstrom, J. (1986). Transmembrane topography of nicotinic acetylcholine receptor: immunochemical tests contradict theoretical predictions based on hydrophobicity profiles. Biochemistry : 25 2633-43.
81. Kordossi, A. A., and Tzartos, S. J. (1987). Conformation of cytoplasmic segments of acetylcholine receptor a- and b-subunits probed by monoclonal antibodies: sensitivity of the antibody competition approach. EMBO Journal : 6 1605-10.
82. LaRochelle, W. J., Wray, B. E., Sealock, R., and Froehner, S. C. (1985). Immunochemical demonstration that amino acids 360-377 of the acetylcholine receptor gamma-subunit are cytoplasmic. Cell Biol : 100 684-91.
83. Lei, S. J., Raftery, M. A., and Conti-Tronconi, B. M. (1993). Monoclonal antibodies against synthetic sequences of the nicotinic receptor cross-react fully with the native receptor, and reveal the transmembrane disposition of the epitopes. Biochemistry : 32 91-100.
84. Huganir, R. L. (1987). Regulation of the nicotinic acetylcholine receptor by protein phosphorylation. J Recept Res : 7 241-56.
85. Phillips, W. D., Maimone, M. M., and Merlie, J. P. (1991). Mutagenesis of the 43-kD postsynaptic protein defines domains involved in plasma membrane targeting and AChR clustering. J Cell Biol : 115 (6), 1713-23.
86. Boyd, N. D., and Cohen, J. B. (1980). Kinetics of binding of [3H]acetylcholine to *Torpedo* postsynaptic membranes: association and dissociation rate constants by rapid mixing and ultrafiltration. Biochemistry : 19 (23), 5353-8.
87. Stroud, R. M., McCarthy, M. P., and Shuster, M. (1990). Nicotinic acetylcholine receptor superfamily of ligand-gated ion channels. Biochemistry : 29 (50), 11009-23.
88. Katz, B., and Thesleff, S. (1957). A study of the desensitization produced by acetylcholine at the motor end-plate. Journal of Physiology : 138 63-80.

89. Weber, M., David-Pfeuty, M. T., and Changeux, J.-P. (1975). Regulation of binding properties of the nicotinic receptor protein by cholinergic ligands in membrane fragments from *Torpedo marmorata*. Proc. Natl. Acad. Sci. U.S.A : 72 3443-47.
90. Karlin, A. (1969). Chemical modification of the active site of the acetylcholine receptor. Journal of General Pysiology : 54 245S-262S.
91. Damle, V. N., and Karlin, A. (1980). Effects of agonists and antagonists on the reactivity of the binding site disulfide in acetylcholine receptor from *Torpedo californica*. Biochemistry : 19 (17), 3924-32.
92. Sine, S. M., Kreienkamp, H. J., Bren, N., Maeda, R., and Taylor, P. (1995). Molecular dissection of subunit interfaces in the acetylcholine receptor: identification of determinants of alpha-conotoxin M1 selectivity. Neuron : 15 (1), 205-11.
93. Hubner, W., and Mantsch, H. H. (1991). Orientation of specifically 13C=O labeled phosphatidylcholine multilayers from polarized attenuated total reflection FT-IR spectroscopy. Biophys J : 59 (6), 1264-72.
94. Gorne-Tschelnokow, U., Strecker, A., Kaduk, C., Naumann, D., and Hucho, F. (1994). The transmembrane domains of the nicotinic acetylcholine receptor contain alpha-helical and beta structures. Embo J : 13 (2), 338-41.
95. Hucho, F., Gorne-Tschelnokow, U., and Strecker, A. (1994). Beta-structure in the membrane-spanning part of the nicotinic acetylcholine receptor (or how helical are transmembrane helices?). Trends Biochem Sci : 19 (9), 383-7.
96. Ortells, M. O., and Lunt, G. G. (1996). A mixed helix-beta-sheet model of the transmembrane region of the nicotinic acetylcholine receptor. Protein Eng : 9 (1), 51-9.
97. Tamamizu, S., Todd, A. P., and McNamee, M. G. (1995). Mutations in the M1 region of the nicotinic acetylcholine receptor alter the sensitivity to inhibition by quinacrine. Cell Mol Neurobiol : 15 (4), 427-38.
98. Baenziger, J. E., Miller, K. W., McCarthy, M. P., and Rothschild, K. J. (1992). Probing conformational changes in the nicotinic acetylcholine receptor by Fourier transform infrared difference spectroscopy. Biophys J : 62 (1), 64-6.
99. Methot, N., McCarthy, M. P., and Baenziger, J. E. (1994). Secondary structure of the nicotinic acetylcholine receptor: implications for structural models of a ligand-gated ion channel. Biochemistry : 33 (24), 7709-17.
100. Methot, N., Ritchie, B. D., Blanton, M. P., and Baenziger, J. E. (2001). Structure of the pore-forming transmembrane domain of a ligand-gated ion channel. J Biol Chem : 276 23726-32.
101. Ochoa, E. L., Dalziel, A. W., and McNamee, M. G. (1983). Reconstitution of acetylcholine receptor function in lipid vesicles of defined composition. Biochim Biophys Acta : 727 (1), 151-62.
102. McCarthy, M. P., and Moore, M. A. (1992). Effects of lipids and detergents on the conformation of the nicotinic acetylcholine receptor from *Torpedo californica*. J Biol Chem : 267 (11), 7655-63.
103. Damle, V. N., and Karlin, A. (1978). Affinity labeling of one of two a-neurotoxin binding sites in acetylcholine receptor from *Torpedo californica*. Biochemistry : 17 2039-45.
104. Ellena, J. F., Blazing, M. A., and McNamee, M. G. (1983). Lipid-protein interactions in reconstituted membranes containing acetylcholine receptor. Biochemistry : 22 (24), 5523-35.

105. daCosta, C. J., and Baenziger, J. E. (2003). A rapid method for assessing lipid:protein and detergent:protein ratios in membrane-protein crystallization. Acta Crystallographica Section D-Biological Crystallography : 59 (1), 77-83.
106. Ludlam, C. F., Arkin, I. T., Liu, X. M., Rothman, M. S., Rath, P., Aimoto, S., Smith, S. O., Engelman, D. M., and Rothschild, K. J. (1996). Fourier transform infrared spectroscopy and site-directed isotope labeling as a probe of local secondary structure in the transmembrane domain of phospholamban. Biophys J : 70 1728-36.
107. daCosta, C. J., Ogrel, A. A., McCardy, E. A., Blanton, M. P., and Baenziger, J. E. (2002). Lipid-protein interactions at the nicotinic acetylcholine receptor. A functional coupling between nicotinic receptors and phosphatidic acid-containing lipid bilayers. J Biol Chem : 277 (1), 201-8.
108. Delange, F., Bovee-Geurts, P. H., Pistorius, A. M., Rothschild, K. J., and DeGrip, W. J. (1999). Probing intramolecular orientations in rhodopsin and metarhodopsin II by polarized infrared difference spectroscopy. Biochemistry : 38 13200-09.
109. Baenziger, J. E., Darsaut, T. E., and Morris, M. L. (1999). Internal dynamics of the nicotinic acetylcholine receptor in reconstituted membranes. Biochemistry : 38 (16), 4905-11.
110. Methot, N., Demers, C. N., and Baenziger, J. E. (1995). Structure of both the ligand- and lipid-dependent channel-inactive states of the nicotinic acetylcholine receptor probed by FTIR spectroscopy and hydrogen exchange. Biochemistry : 34 (46), 15142-9.
111. Baenziger, J. E., and Chew, J. P. (1997). Desensitization of the nicotinic acetylcholine receptor mainly involves a structural change in solvent-accessible regions of the polypeptide backbone. Biochemistry : 36 (12), 3617-24.
112. Baenziger, J. E., Miller, K. W., and Rothschild, K. J. (1993). Fourier transform infrared difference spectroscopy of the nicotinic acetylcholine receptor: evidence for specific protein structural changes upon desensitization. Biochemistry : 32 (20), 5448-54.
113. Michelson, M. J., and Zeimal, E. V. (1973) *Acetylcholine: An Approach to the Molecular Mechanisms of Action*, Pergamon Press, Oxford.
114. Luyten, W. H. (1986). A model for the acetylcholine binding site of the nicotinic acetylcholine receptor. J Neurosci Res : 16 (1), 51-73.
115. Peterson, G. (1989). Consensus residues at the acetylcholine binding site of cholinergic proteins. J Neurosci Res : 22 (4), 488-503.
116. Changeux, J. P., Galzi, J. L., Devillers-Thiery, A., and Bertrand, D. (1992). The functional architecture of the acetylcholine nicotinic receptor explored by affinity labelling and site-directed mutagenesis. Q Rev Biophys : 25 (4), 395-432.
117. Tomaselli, G. F., McLaughlin, J. T., Jurman, M. E., Hawrot, E., and Yellen, G. (1991). Mutations affecting agonist sensitivity of the nicotinic acetylcholine receptor. Biophys J : 60 (3), 721-7.
118. Aylwin, M. L., and White, M. M. (1994). Ligand-receptor interactions in the nicotinic acetylcholine receptor probed using multiple substitutions at conserved tyrosines on the alpha subunit. FEBS Lett : 349 (1), 99-103.
119. Nowak, M. W., Kearney, P. C., Sampson, J. R., Saks, M. E., Labarca, C. G., Silverman, S. K., Zhong, W., Thorson, J., Abelson, J. N., Davidson, N., and et al. (1995). Nicotinic receptor binding site probed with unnatural amino acid incorporation in intact cells. Science : 268 (5209), 439-42.

120. Kearney, P. C., Nowak, M. W., Zhong, W., Silverman, S. K., Lester, H. A., and Dougherty, D. A. (1996). Dose-response relations for unnatural amino acids at the agonist binding site of the nicotinic acetylcholine receptor: tests with novel side chains and with several agonists. Mol Pharmacol : 50 (5), 1401-12.
121. Czajkowski, C., Kaufmann, C., and Karlin, A. (1993). Negatively charged amino acid residues in the nicotinic receptor delta subunit that contribute to the binding of acetylcholine. Proc Natl Acad Sci U S A : 90 (13), 6285-9.
122. Zscherp, C., and Barth, A. (2001). Reaction-induced infrared difference spectroscopy for the study of protein reaction mechanisms. Biochemistry : 40 (7), 1875-83.
123. Ryan, S. E., and Baenziger, J. E. (1999). A structure-based approach to nicotinic receptor pharmacology. Mol Pharmacol : 55 (2), 348-55.
124. Ryan, S. E., Blanton, M. P., and Baenziger, J. E. (2001). A conformational intermediate between the resting and desensitized states of the nicotinic acetylcholine receptor. J Biol Chem : 276 (7), 4796-803.
125. Ryan, S. E., Demers, C. N., Chew, J. P., and Baenziger, J. E. (1996). Structural effects of neutral and anionic lipids on the nicotinic acetylcholine receptor. An infrared difference spectroscopy study. J Biol Chem : 271 (40), 24590-7.
126. Baenziger, J. E., Morris, M. L., Darsaut, T. E., and Ryan, S. E. (2000). Effect of membrane lipid composition on the conformational equilibria of the nicotinic acetylcholine receptor. J Biol Chem : 275 (2), 777-84.
127. Barth, A. (2000). The infrared absorption of amino acid side chains. Prog Biophys Mol Biol : 74 (3-5), 141-73.
128. Sine, S. M., Quiram, P., Papanikolaou, F., Kreienkamp, H. J., and Taylor, P. (1994). Conserved tyrosines in the alpha subunit of the nicotinic acetylcholine receptor stabilize quaternary ammonium groups of agonists and curariform antagonists. J Biol Chem : 269 (12), 8808-16.
129. Fahmy, K. (1998). Binding of transducin and transducin-derived peptides to rhodopsin studies by attenuated total reflection-Fourier transform infrared difference spectroscopy. Biophysical Journal : 75 (3), 1306-18.

CURRICULUM VITAE

NAME **Hill, Danny Grant**

DEGREES OBTAINED

B. Sc. (Honours), Biochemistry, University of Ottawa, 2001

RESEARCH EXPERIENCE

2001 - 2003	Masters thesis entitled: "Transmembrane Domain Orientation and Neurotransmitter Binding in the Nicotinic Acetylcholine Receptor." Carried out under the supervision of Dr. John Baenziger, University of Ottawa.
2001	Summer research student – Initiation of masters project.
2000 - 2001	Undergraduate honours project entitled: "Expression and Purification of the Ligand Binding Domain of MKP-3". Carried out under the supervision of Dr. Mary Alice Hefford, Health Canada.

SCHOLARSHIPS

2002	Ontario Graduate Scholarship - declined
2002 - 2003	University of Ottawa Excellence Scholarship
2002 - 2003	NSERC Post-Graduate Scholarship
2001	University of Ottawa Excellence Scholarship
2001	University of Ottawa Entrance Scholarship

PAPERS PUBLISHED IN REFEREED JOURNALS

Ryan, S.E., Hill, D.G., and Baenziger, J.E. Dissecting the Chemistry of the Nicotinic Acetylcholine Receptor. J. Biol. Chem. 277(12), 10420-10426.